2014

ANODE SOLID ELECTROLYTE INTERPHASE (SEI) OF LITHIUM ION BATTERY CHARACTERIZED BY MICROSCOPY AND SPECTROSCOPY

Mengyun Nie
University of Rhode Island, mnie@chm.uri.edu

ANODE SOLID ELECTROLYTE INTERPHASE (SEI) OF LITHIUM ION BATTERY CHARACTERIZED BY MICROSCOPY AND SPECTROSCOPY

BY

MENGYUN NIE

A DISSERTATION SUBMITTED IN PARTIAL FULFILLMENT OF THE

REQUIREMENTS FOR THE DEGREE OF

DOCTOR OF PHILOSOPHY

IN

CHEMISTRY

UNIVERSITY OF RHODE ISLAND

2014

DOCTOR OF PHILOSOPHY DISSERTATION

OF

MENGYUN NIE

APPROVED:

Dissertation Committee

Major Professor Brett Lucht

Arijit Bose

William Euler

Nasser H. Zawia
DEAN OF THE GRADUATE SCHOOL

UNIVERSITY OF RHODE ISLAND

2014

ABSTRACT

The surface reactions of electrolytes with the graphitic anode of lithium ion batteries have been investigated. The investigation utilizes two novel techniques, which are enabled by the use of binder-free graphite anodes. The first method, transmission electron microscopy (TEM) with energy dispersive X-ray spectroscopy, allows straightforward analysis of the graphite solid electrolyte interphase (SEI). The second method utilizes multi-nuclear magnetic resonance (NMR) spectroscopy of D_2O extracts from the cycled anodes. The TEM and NMR data are complemented by XPS and FTIR data, which are routinely used for SEI studies. Cells were cycled with $LiPF_6$ and ethylene carbonate (EC), ethyl methyl carbonate (EMC), and EC/EMC blends. This unique combination of techniques establishes that for EC/$LiPF_6$ electrolytes, the graphite SEI is ∼50 nm thick after the first full lithiation cycle, and predominantly contains lithium ethylene dicarbonate (LEDC) and LiF. In cells containing EMC/$LiPF_6$ electrolytes, the graphite SEI is nonuniform, ∼10−20 nm thick, and contains lithium ethyl carbonate (LEC), lithium methyl carbonate (LMC), and LiF. In cells containing EC/EMC/$LiPF_6$ electrolytes, the graphite SEI is ∼50 nm thick, and predominantly contains LEDC, LMC, and LiF. The novel techniques as combinations of binder free graphite electrodes with Transmission Electron Microscopy (TEM) grids and D_2O extraction allowed us to analyze SEI species efficiently and also can be applied in other systems. The investigation utilizes thoes novel techniques which are enabled by the use of binder free silicon (BF-Si) nano-particle anodes. The first method, Transmission Electron Microscopy (TEM) with Energy Dispersive X-ray Spectroscopy (EDX), allows straightforward analysis of the BF-Si solid electrolyte

interphase (SEI). The second method, utilizes Multi-Nuclear Magnetic Resonance (NMR) spectroscopy of D_2O extracts from the cycled anodes. The TEM and NMR data are complemented by XPS and FTIR data, which are routinely used for SEI studies. Coin cells (BF-Si/Li) were cycled in electrolytes containing $LiPF_6$ salt and ethylene carbonate (EC) or fluoroethylene carbonate (FEC) solvent. Capacity retention was significantly better for cells cycled with $LiPF_6$/FEC electrolyte than for cells cycled with $LiPF_6$/EC electrolyte. Our unique combination of techniques establishes that for $LiPF_6$/EC electrolyte, the BF-Si SEI continuously grows during the first 20 cycles and the SEI becomes integrated with the BF-Si nano-particles. The SEI predominantly contains lithium ethylene dicarbonate (LEDC), LiF, and Li_xSiO_y. BF-Si electrodes cycled with $LiPF_6$/FEC electrolyte have a different behavior; the BF-Si nano-particles remain relatively distinct from the SEI. The SEI predominantly contains LiF, Li_xSiO_y and an insoluble polymeric species.

The investigation of the interrelationship of cycling performance, solution structure, and electrode surface film structure has been conducted for electrolytes composed of different concentrations of $LiPF_6$ in propylene carbonate (PC) with a binder free (BF) graphite electrode. Varying the concentration of $LiPF_6$ changes the solution structure altering the predominant mechanism of electrolyte reduction at the electrode interface. The change in mechanism results in a change in the structure of the solid electrolyte interface (SEI) and the reversible cycling of the cell. At low concentrations of $LiPF_6$ in PC (1.2 M), electrochemical cycling and cyclic voltammetry (CV) of BF graphite electrodes reveal continuous electrolyte reduction and no lithiation/delithiation of the graphite. The solution structure is dominated by

solvent separated ion pairs ($Li^+(PC)_4//PF_6^-$) and the primary reduction product of the electrolyte is lithium propylene dicarbonate (LPDC). At high concentrations of $LiPF_6$ in PC (3.0 - 3.5 M), electrochemical cycling and CV reveal reversible lithiation/delithiation of the graphite electrode. The solution structure is dominated by contact ion pairs ($Li^+(PC)_3PF_6^-$) and the primary reduction product of the electrolyte is LiF.

ACKNOWLEDGMENTS

First of all, I would like to thank my major professor as well as my Ph.D advisor Prof. Brett Lucht for his guidance, help and providing me with great atmosphere and great opportunities for doing research about lithium ion battery. It was an honor to work in this lab. Also I appreciate all the help provided by Prof. William Euler as Chemistry Department Chair and the helps from my other committee members. I would like to thank Prof. Bose, Heskett and Yang for reviewing my dissertation. I also would like to thank Dr. Abraham in Argonne National Lab for offering me opportunity to visit his lab and teaching me great knowledge in research. I am grateful to many collaborators Dr. Yanjing Chen, Dr. Swapnil Dalavi and Dr.Cao Cuong Nygen for helping and encouraging me during my study. My deepest gratitude is for University of Rhode Island for giving me the opportunity to finish my Ph.D study.

I appreciate all people who company with me for almost five years in my lab. Finally, I would like to thank my mom and husband Guang to take care my life. I believe this achievement cannot complete without any one of you.

PREFACE

This dissertation is written in manuscript format. There are five chapters in this dissertation. The first chapter is the main introduction of Lithium ion battery. From the second chapter to the fifth chapter are the manuscripts I have completed. The second chapter is one article already published in the Journal of Physical Chemistry, C and this article is the most read article in that month. The third chapter is also made of my published paper in Journal of Physical Chemistry, C. The fourth chapter is come from my third publication in the same journal (JPCC). The last chapter, chapter 5, is written as a manuscript will be submitted to the Journal of Electrochemical Society.

TABLE OF CONTENTS

LIST OF TABLES

LIST OF FIGURES

CHAPTER 1

INTRODUCTION

Overview

Since the "Energy Crisis" becomes a big challenge for human society, energy exploration, renewable energy and energy storage have been mentioned worldwide. Except petrol, coal and natural gas, solar, wind and tidal energy are also very active in various areas. However, with the exploration and creation energy, tons of efforts are invested in order to improve of the effective energy storage--Battery one of the smartest inventions in people life. Among of all kinds of battery, lithium ion battery with its unique advantages such as high energy density, long service life (rechargeable battery), high working voltage and no memory effects.[1-4] And all of these benefits are almost cannot be achieved by traditional nickel-cadmium battery, thus as the past three decades, lithium ion battery received widely attentions and rapidly developments no matter in academic research or business market.

In a few years of lithium ion battery research study, the concept of lithium ion battery has been deeply understood.[5-7] Cathode, anodes, separator and electrolyte (additives) are necessary compositions for one lithium ion battery. In these compositions, electrolyte plays an important role in transport Li+ and solid electrolyte interface (SEI) formation. Solid electrolyte interface has attracted huge attention since it believed as one of primary factors in determining performance of battery. Thus in this chapter, I would like to give a general introductions of solid electrolyte interface (SEI) from what is SEI to why SEI is very important.[8-11]

It is well known that once the lithium ion battery start to work which companied by a certain moral Li^+ transporting from one electrode to another (cathode/anode). However in contact with liquid electrolyte with lithium salts, the solid electrodes are thermodynamic unstable, which means once the electrons pass through electrode, the highly reactive species in electrolytes will obtain electrons and various decompositions is going to happen. Therefore, it is actually an opportunity to generate multiple new components on the electrodes surface and offer a chance to control them as a passivation film to prevent electrolyte degradation or conductive layer which will promote further decomposition of electrolytes. Obviously, we need a stable worked electrolyte and a passivating film covered electrodes to let Li+ reversible diffusion without any consumption. In this condition, a good passivation film we want is able to block electron coming to surface of electrode but provide good "tunnels" for mobility of Li^+.

Solid Electrolyte Interphase in Lithium ion Battery

Nowadays, the lithium ion battery was used in a wide electrochemical open 4.2-3.0V vs.Li, but most aqueous system cannot be stable in this range. Thus, commercially used electrolytes are carbonates based, such as ethylene carbonate (EC), ethymethene carbonate (EMC), propylene carbonate(PC), dimenthle carbonate (DMC), etc. There are serveral literature mentioned the good candidates of electrolytes should meet some requirements:[12] 1) Retention of the electrode/electrolyte interface when volume expansion/shrink of electrode particles happened during cycling. 2) A Li^+ ion conductivity $\sigma_{Li} > 10^{-4}$ S/cm over the certain range of battery operation. 3) the electronic conductivity $\sigma e < 10^{-10}$ S/cm. 4) The transference number $\sigma_{Li}/\sigma_{total} \approx 1$,

σ total includes conductivities by other ions in the electrolyte as well as σ_{Li^+} σ e. 5) Chemical properties, including chemical stability in high/low temperature, moisture, oxygen, rapidly forming passiving film and non-toxic. 6) physical properties, including nonflammable and low cost, etc. The only commercial lithium ion salts is $LiPF_6$, although new types of salts are receiving huge intesetes, LiTFSI, LiFSI, LiBOB. LiFOB, etc are also popular in academic reaserch.[13-17] By far, cathodes and anodes of the state of art lithium ion battery are lithium transaction metal oxides and graphite. The major electrochemical reactions happened are:

Cathode: $Li_xMNO_y \rightarrow xLi^+ + Li_{1-x}\ MNO_y$

Anode: $Li^+ + 6C \rightarrow LiC_6$

So the lithium ions shuttle forth and back between those two electrodes according two cathodic and anodic reactions. However, in liquid state, lithium ions are not transporting along, due to the charge balance and the small size of Li^+, the carbonates solvent molecular will combine with Li+ and transfer together to the electrodes surface, which called “solvation”. As the first time the entire “solvation” groups try to intercalate into graphite, the thermodynamic unstable solvated Li+ group obtained electrons and formed a passivating film. Once the electrodes surface has been covered well, all related reductions/degradations will stop and the lithium ion battery is allowed to cycle reversible with good columbic efficiency. For example, Zhang,etc studied different lithaiton stage of first cycle, it clearly showed these are four stages lithiation state of graphite with different voltage plateaus. and typically, the ethlyenen carbonate is not preferd to decomposed below 1.5V to 0.8V. and other solvents also

will reduces before lithium ion intercalation to graphite. Thus, the passivation layer formed by electrolytes components scarified which can prevent further decomposition, let lithium ion efficiently transfer and electronic insolated is what we called solid electrolyte interphase in lithium ion battery.

Reactions proposed for SEI formation

As early as 1980', some research group already proposed several mechanisms of SEI formation including electrolytes degradation and lithium salts hydrolysis. Peled,etc and Auburch,etc research group[18,19] did related study on various metal electrodes surface, nickel, silver, platinum and HOPG or Li+ intercalated disordered carbon with Li+ salts contained electrolytes, under cyclic voltammetry scan which simulated the cycling conditions of real battery. The surface of those electrodes has been investigated by several new techniques: X-ray photoelectron spectroscopy (XPS), FTIR and surface-enhanced Raman spectroscopy (SERS). Gonbeau, etc also provided some ex-situ XPS evidence for the decomposition products including organic and inorganic species at each charging states. [20,21]

Proposed Reductions of Alkyl Carbonates on Lithium/ Lithiated Graphite:

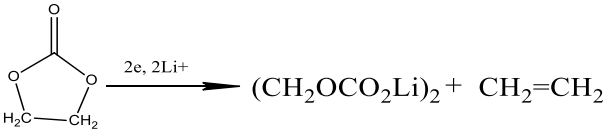

1.

(DMC) $CH_3OCO_2CH_3 + e + Li^+ \longrightarrow$ CH3OCO2Li + CH3· + CH3OLi 2.

$EC + 2e^- + 2Li^+ \longrightarrow Li_2CHO_3 + CH_2=CH$ 3.

4.

$$2ROCO_2Li + H_2O \rightarrow Li_2CO_3 + 2ROH + CO2$$ 5.

$$Li_2O + EC \rightarrow LiOCH_2CH_2OCO_2Li$$ 6.

$$Li_2CO_3 + HF \rightarrow LiF + CO2 + H_2O$$ 7.

$$ROCO_2Li + Li_2CO_3 + CH_3OLi + H^+ \rightarrow LiF + ROCO_2H + H_2CO_3 + CH3OH$$ 8.

Proposed Reductions Reactions about LiPF6 degradation:

$$LiPF_6 \rightarrow LiF + PF_5$$ 1.

$$PF_5 + H_2O \rightarrow 2HF + PF_3O$$ 2.

$$PF_3O + 2Li^+ + 2e \rightarrow Li_xPF_{3x}O + xLiF$$ 3.

$$PF_5 + 2Li^+ + 2e \rightarrow xLiF + Li_xPF_{5-x}$$ 4.

$$PF_5 + 2Li^+ + 2e \rightarrow xLiF + Li_xPF_{5-x}$$ 5.

$$PF_6^- + 3Li^+ + 2e \rightarrow 3LiF + PF_3$$ 6.

$$LiPF_6 + Li_2CO_3 \rightarrow 3LiF + POF_3 + CO_2$$ 7.

$$PF_5 + Li_2CO_3 \rightarrow 2LiF + POF_5 + CO_2$$ 8.

SEI Composition and Morphology

Since the importance of SEI has been widely recognized, the composition of it is always highly debated subject. Not only because the species mentioned above are very similar structure and quite limited amount are hard to measure by instruments.

Another reason is due to the formation of SEI is also highly dependent on location of electrodes. Zheng, etc found the type of graphite with various particle morphology exhibit different initial capacity losses. Some research groups: Ogumi, Farrington and Yamaguchi analyzed SEI formation and early stages of lithium intercalation on HOPG by STM, AFM and SPM. Based on these studies, people believed the carbon atoms have higher activity on the cross-section, zig-zag and armcharit planes than basal plane[22]. Later on, with more new technique, some group tried to build up novel functional microscopy by which allowed observing electrodes (SEI) morphology change with real time charging/discharging. Orgmuni, etc have designed in situ scanning probe microscopy planed into a HOPG/Li cell in order to observe the edge of electrodes change with voltage change during lithiation due to the edges of particles are mostly covered by SEI. Recently, In situ TEM got widely applied in lithium ion battery as well. At the same time, TEM combined with electron diffraction (EDX) are able to analyze elements concentration in nano-scale. Zhu, etc using TEM-EELS with in-situ X-ray diffraction to observe the silicon electrodes morphology changed and mapping the elemental distribution during each lithiated stages and determined crystal-amorphsed transformations.[23] With in-situ microscopy combining with elemental analyzer, it is possible to directly observe the process of SEI formation on different locations of electrode. It will help to fully understand interfacial reactions and supply information for better electrode design in the future.

Influence of SEI on battery performance

The importance and complication of SEI are well accepted by lithium ion battery research community, since every factor of SEI is crucial for real performance of

lithium ion battery. Now the researchers most focus on figure out SEI parameters from real cases. Typical lithium ion battery such as coin cells, punch cells and cylinder cells are fabricated with most used electrolytes with/without additives. The cycling performance usually will be tested consistent, for example CC and CV charging model, long time cycling (hundred cycles), various rate cycling and tempreture ambuse cycling. Then based on cycling performance, the surface analysis of electrodes with SEI are extremely important to indicate the differences showed up during cycling. Also, some reports mentioned SEI may dissolve/ pilled off/ or evolved during the following cycling and storage.[24,25] Thus, if the battery wants a decent and stable cycling performance during long time using, an effective and stable SEI is mandatory, which is also a goal for most commercial batteries. Actually, now the most attractive work is looking for novel SEI forming additives, large amount efforts are inputted on comparison of cycling performance with/without additives and ex-situ electrodes analysis, such as XPS, FTIR, and SEM (TEM) and try to find out the functional trigger in effecting performance change. Meanwhile, it is also important to mention the relationship of degradation of SEI with battery lift or stability. As discussed above, the lithium alkyl carbonates, lithium alkoxide, and PxOFy salts, etc are examined as components in SEI. However, most of them are not good thermally stable and moister sensitive or easily to be attacked by proton (HF, H_3O^+). Under these degradations, Li_2CO_3 from decomposition of lithium alkyl carbonates and LiF from $LiPF_6$ degradation are possible become the major products in SEI and result in a high internal resistance SEI layer on electrodes. Thus, as some research mentioned, once 25% of the active material inside of batteries has been reacted and changed to non-

active with high resistant precipitates, the batteries almost are useless and cannot offer normal cycling anymore.

Conclusion

Overall, the solid electrolyte interphase is emphasized as an ionic conductive and electronic insolate multi-species film special found on edge of electrodes particles in lithium ion battery. The main function is to allow reversible lithium ion shuttle back and forward between cathode and anode. A stable SEI prevents too much electrolytes to be consumed and protects electrodes to be exfoliated and damaged by solvent molecular co-intercalation. SEI also affects the internal resistant inside of battery in determining the capacity release during cycling. As well as the degradation and thermals instability of SEI are influent battery performance in long time using with various environmental. All of parameters of SEI are curial in practical applications, such as plug in electric vehicle (PIEV) and other lithium ion battery used portable devices.

Reference

1. Whittingham, M. S.,*Chemical Reviews* **2004,** *104* (10), 4271-4302.

2. M. Wakihara, O. Y., *Lithium Ion Batteries: Fundamentals and Performance*. Wiley-VCH: New York, 1998.

3. Yoda, S.; Ishihara, K.,*J. Power Sources* **1997,** *68* (1), 3-7.

4. Dahn, J.; Sleigh, A.; Shi, H.; Way, B.; Weydanz, W.; Reimers, J.; Zhong, Q.; Sacken, U., Lithium Batteries, New Materials and New Perspectives. Elsevier: North-Holland/New York: 1993.

5. Armand, M.; Tarascon, J.-M.,*Nature* **2008,** *451* (7179), 652-657.

6. Scrosati, B.; Garche, J.,*J. Power Sources* **2010,** *195* (9), 2419-2430.

7. Tarascon, J.-M.; Armand, M.,*Nature* **2001,** *414* (6861), 359-367.

8. Aurbach, D.,*J. Power Sources* **2000,** *89* (2), 206-218.

9. Benedek, R.; Thackeray, M. M.,*J. Power Sources* **2002,** *110* (2), 406-411.

10. Edström, K.; Herstedt, M.; Abraham, D. P.,*J. Power Sources* **2006,** *153* (2), 380-384.

11. Ein‐Eli, Y.,*Electrochem. Solid-State Lett.* **1999,** *2* (5), 212-214.

12. Goodenough, J. B.; Kim, Y.,*Chemistry of Materials* **2009,** *22* (3), 587-603.

13. Moumouzias, G.; Ritzoulis, G.; Siapkas, D.; Terzidis, D.,*J. Power Sources* **2003,** *122* (1), 57-66.

14. Philippe, B.; Dedryvère, R.; Gorgoi, M.; Rensmo, H.; Gonbeau, D.; Edström, K.,*Chemistry of Materials* **2013**.

15. Xu, K.; Zhang, S.; Jow, T. R.; Xu, W.; Angell, C. A.,*Electrochem. Solid-State Lett.* **2002,** *5* (1), A26-A29.

16. Zhang, S. S.; Xu, K.; Jow, T. R.,*Journal of the Electrochemical Society* **2002,** *149* (5), A586-A590.

17. Xu, M.; Xiao, A.; Li, W.; Lucht, B. L.,*Journal of the Electrochemical Society* **2010,** *157* (1), A115-A120.

18. Peled, E.; Menachem, C.; Bar‐Tow, D.; Melman, A.,*Journal of the Electrochemical Society* **1996,** *143* (1), L4-L7.

19. Aurbach, D.; Markovsky, B.; Shechter, A.; Ein‐Eli, Y.; Cohen, H.,*Journal of the Electrochemical Society* **1996,** *143* (12), 3809-3820.

20. Dedryvere, R.; Gireaud, L.; Grugeon, S.; Laruelle, S.; Tarascon, J. M.; Gonbeau, D.,*J. Phys. Chem. B* **2005,** *109* (33), 15868-15875.

21. Leroy, S.; Blanchard, F.; Dedryvere, R.; Martinez, H.; Carre, B.; Lemordant, D.; Gonbeau, D.,*Surf. Interface Anal.* **2005,** *37* (10), 773-781.

22. Domi, Y.; Ochida, M.; Tsubouchi, S.; Nakagawa, H.; Yamanaka, T.; Doi, T.; Abe, T.; Ogumi, Z.,*J. Phys. Chem. C* **2011,** *115* (51), 25484-25489.

23. Wang, F.; Wu, L.; Key, B.; Yang, X. Q.; Grey, C. P.; Zhu, Y.; Graetz, J.,*Advanced Energy Materials* **2013**.

24. Zheng, T.; Gozdz, A. S.; Amatucci, G. G.,*Journal of the Electrochemical Society* **1999,** *146* (11), 4014-4018.

25. Lucas, I. T.; Pollak, E.; Kostecki, R.,*Electrochemistry Communications* **2009,** *11* (11), 2157-2160.

CHAPTER 2

STRUCTURE OF THE GRAPHITE ANODE SOLID ELECTROLYTE INTERPHASE IN LITHIUM ION BATTERIES

Mengyun Nie[1], Dinesh Chalasani[1], Daniel P. Abraham[2], Yanjing Chen[1], Arijit Bose[1], and Brett L. Lucht[1]

[1]*University of Rhode Island, Kingston, Rhode Island 02881, United States*

[2]*Argonne National Laboratory, Argonne, Illinois 60439, United States*

The following was published in the Journal of the Physical Chemistry C, and is presented here in manuscript format

Introduction

Interest in lithium ion batteries (LIB) for consumer electronic devices has been steadily increasing over the last two decades. However, recent interest in electric vehicles (EV) has spawned a new wave of research and development on LIB.[1] The use of LIB in electric vehicles has created more stringent requirements on battery performance, especially related to calendar life (> 10 years) and temperature range (-30 to + 50 ^{o}C).[1] Commercial LIB use a graphite-based carbon anode. During the initial lithiation cycles a Solid Electrolyte Interphase (SEI) forms on the graphite anode surface due to the electrochemical instability of the electrolyte to lithiated graphite.[2-7] Ideally, the SEI allows Li ion conduction but is electrically insulating which inhibits further reduction of the electrolyte. SEI formation is one of the most important and fundamental reactions of LIB and is critical to reversible cycling performance. While the SEI in LIB has been under investigation for over thirty years, the composition, formation mechanism, and mechanism of function are still not fully understood.[2-6] Due to the importance of the SEI in cycle life, calendar life, safety, and low temperature performance, a better understanding of the SEI is required for the development of superior LIB for EV applications.

Ion transport at the electrode-electrolyte interface frequently represents the highest energy barrier for ion conduction in many electrochemical devices. The two most significant barriers for lithium ion transport from the bulk electrolyte to graphite anode are 1) desolvation of the lithium cation and 2) migration of the Li cation through the SEI.[8-10] A recent detailed computational investigation of ion transport through the anode SEI modeled a two phase boundary where the inner SEI was

Li_2CO_3 and the lowest energy pathway for ion diffusion was determined.[11] However, this investigation models ion transport through crystalline Li_2CO_3. Computational modeling of the anode SEI is limited by the knowledge of the composition of the anode SEI and models based on inaccurate compositions are unlikely to provide accurate models of ion transport.

The structure of the anode SEI of LIB has been investigated in great detail via many different analytical techniques over the last three decades. Ex-situ analysis of cycled anodes has been conducted most frequently with X-ray Photoelectron spectroscopy (XPS)[12-16] and Infrared spectroscopy (IR)[16-18]. However, characterization of the SEI components is difficult since the layer is thin (10 - 100 nm) and very sensitive to water and oxygen. In addition, the components of the SEI have structural similarity to the components of the electrolyte making spectroscopic discrimination difficult. The composition of the anode SEI generated in lithium ion cells containing a standard electrolyte, $LiPF_6$ in a mixture of carbonate solvents including ethylene carbonate (EC) and dialkyl carbonates,[19] has been reported to be a complex mixture of compounds including the reduction product of EC, lithium ethylene dicarbonate (LEDC, $(CH_2COCO_2Li)_2$).[4,6,20] Other frequently reported components include CH_3OCO_2Li (Lithium Methyl Carbonate, LMC), $CH_3CH_2OCO_2Li$ (lithium Ethyl Carbonate, LEC), Li_2CO_3, CH_3OLi, CH_3CH_2OLi, $LiOCH_2CH_2OLi$, Li_2O, LiF, and $Li_xPF_yO_z$.[2] Computational methods have been utilized to better understand the mechanism of formation of the SEI but are limited by the perceived complexity of the SEI.[21-27] The limited understanding of the SEI structure has resulted in difficulty in developing mechanistic insight into ion transport

and electrical insulation of the anode SEI. In order to develop a thorough understanding of the barrier for and mechanism of lithium ion transport through the SEI the structure and composition of the SEI must be better understood.

We have recently reported on the use of Binder Free (BF) graphite electrodes for the elucidation of the anode SEI.[28,29] In this manuscript, we report two novel methods to analyze the structure and composition of the SEI which have been enabled by the use of BF graphite anodes. The first is a novel Transmission Electron Microscopy (TEM) Energy Dispersive X-ray Spectroscopy (EDX) method with the TEM grid integrated into the electrode. While there have been limited TEM investigations of the SEI on graphite, most of these investigations have required significant sample preparation.[30-34] Most common sample preparation for ex-situ TEM analysis includes electrode dispersion, which could destroy the initial SEI structure. Alternatively, in-situ analysis is limited to specialized electrodes within nano-sized batteries. Knowledge of the morphology as well as the composition of the SEI is critical both from a battery performance as well as a modeling perspective. Our technique allows direct analysis of the graphite particles prepared in situ in an electron microscope grid. Reduced sample preparation steps limit structural changes to the SEI. The second method utilizes Multi-Nuclear Magnetic Resonance (NMR) spectroscopy of the D_2O extracts of the cycled anodes. Cycled electrodes are rinsed with D_2O in an Ar glovebox limiting changes to the SEI components in the presence of O_2. We have also investigated the reaction of EC with lithium naphthalenide to independently isolate and characterize the reduction products of EC. This unique combination of techniques

has allowed us to develop significant new insight into the structure and composition of the anode SEI.

Experimental Sections

Preparation of Binder-Free Electrodes

The binder-free electrodes are made by Electrophoretic Deposition (EPD).[26,27] In this method, graphite particles (SFG-6, TIMCAL, 5 g/L) are suspended in acetonitrile solution by ultrasonication followed by the addition of Triethylamine (1mL/L). A copper current collector is immersed in the EPD bath and a DC potential of 50 V was applied for 2 minutes. Graphite particles were deposited evenly on the copper surface to yield a Binder-Free (BF) Graphite Electrode[26]. The electrode is placed in a vacuum oven at ~120 ℃ overnight to dry the electrode and stored in an Ar-filled gloved box.

Preparation of Electrolytes

Carbonate solvents are used to dissolve 1.2 M lithium hexafluorophosphate ($LiPF_6$): Ethylene Carbonate (EC), Ethyl Methyl Carbonate (EMC) and mixture of Ethylene Carbonate (EC) and Ethyl Methyl Carbonate (EMC) in a 3:7 volume ratio. These solvents were used to better understand differences in the reduction reactions for each electrolyte during SEI formation.

Coin cell assembly and cycling

Special coin cells were designed in order to meet the requirements for analysis. First binder-free graphite electrodes were assembled with copper TEM grids (Figures 1-2). Cell assembly was conducted in an Ar-atmosphere glove box (<1 ppm H_2O,). All cells underwent one galvanostatic lithiation/delithiation cycle at C/20 rate with an Arbin BT2000 battery cycler. Four voltages: 1.3 V, 0.6 V, 0.1 V and 0.05 V vs.Li

were selected as cut-off points for analysis of surface film formation. All samples were investigated in the delithiated state.

TEM Imaging and EDX

Cycled cells were disassembled in an Ar-atmosphere glove box (< 1 ppm H_2O). TEM grids were extracted from cycled coin cells and rinsed with anhydrous dimethyl carbonate (DMC, Acros) to remove residual electrolyte and dried overnight in a vacuum. The TEM grids were quickly transferred into the TEM. Imaging was contacted using a JEOL JEM-2100F TEM (Peabody, MA) at 160 kV. Size analysis was performed using Image J software. Energy-dispersive X-ray spectroscopy or EDX (Model INCAx-act, Oxford Instrument, UK) was used to detect the element composition at various points in the SEI as well as on the anode; three spots from the edge to the center of particles were examined by EDX during imaging. The diameter of beam was 5 nm and low-dose imaging was employed to minimize the electron beam induced changes to the organic components of SEI layers.

XPS, FTIR and NMR samples preparation

XPS and FTIR were conducted on the same anodes extracted from cycled coin cells after rinsing by DMC and drying overnight in a vacuum. The X-ray photo-electron spectroscopy (XPS) was obtained on a PHI 5500 system using Al, Kradiation (hv= 1486.6 eV) under ultrahigh vacuum conditions; the XPS data were collected at multiple locations on graphite anodes. The C 1s, O 1s, F 1s, P 2p spectra were calibrated based on the C1s graphite peak binding energy at 284.5ev. The spectra obtained were analyzed by Multipak 6.1 A software. Line syntheses of elemental spectra were conducted using Gaussian–Lorentzian (70:30) curve fitting. Element

concentration was calculated based on the equation:Cx = (Ix/Sx)/(Ii/Si), where Ix is the intensity of the relative element, and Si is the sensitivity number of the element. The FTIR data were acquired on a Bruker TENSOR 27 spectrometer inside of an Ar purged chamber. 64 scans were acquired on all samples.

Multinuclear and multidimensional NMR analyses were conducted on a Bruker Avance III 300 MHz NMR spectrometer. All NMR samples were extracted from cycled graphite anodes with D_2O, the extraction was conducted after the samples were lightly rinsed with anhydrous DMC and dried overnight in a vacuum oven. Then ^{1}H, ^{13}C, xx define DEPT-135, HSQC,HMBC,COSY NMR were acquired for samples with different cut-off voltages. The data is processed with Mestronova and TOPSPIN.

Synthesis of Lithium-Naphthalenide

Naphthalene (4.0 g, 0.031 moles) and lithium metal (0.20 g, 0.028 moles) are added to a 100 mL round bottom flask containing 50 mL of Tetrahydrfuran (THF). The reaction mixture is stirred over night at room temperature. A dark green color solution of Lithium-naphthalenide is obtained (Scheme 1).

Reaction of Li-naphthalnelide with ethylene carbonate

To a round bottom flask containing a THF solution of Li-naphthalenide (0.0283moles, 25ml) ethylene carbonate (EC) is added in 1:1 mole ratio. The solution immediately turns reddish brown and precipitation occurs. The reaction is allowed to stir overnight. The solvent is removed by high vacuum and the resulting reddish brown solid is washed with diethyl ether to remove the naphthalene and any residual organic carbonate solvent. The solid is dried under vacuum to remove the solvent. The gas analysis is performed by evacuating the head space of the reaction flask

containing Li naphthalenide in THF followed by carbonate solvent addition. The evolved gases are then sampled using a 10 µL GC syringe. The analysis of evolved gases during the reaction is performed on Thermo trace GC-Ultra equipped with mass selective detector-ISQ. Helium is used as carrier gas with a flow rate of 1.5ml/min. The Intial column temperature is 50^{o}C and the temperature ramped at 10 ^{o}C/min to 220 ^{o}C and held at that temperature for 20 min. the total run time is 37 min. An Agilent poroplot Amines column is used. The mass spectra obtained on these gases are compared with NIST library to determine the molecular structure.

Results and Discussion

Cycling behavior

The voltage versus capacity plots for cells cycled with three different electrolytes are shown in Figure 3. The lithiation-delithiation cycles are conducted over 40 h as is typical for formation cycles in lithium ion batteries and possess the expected shoulders for electrolyte reduction (OCV~2.8 – 0.6V) and plateaus for lithium ion intercalation (0.3 – 0.05 V).[26-27] Cells were lithiated to four different cut-off voltages (1.3, 0.6, 0.1, and 0.05 V). The voltages selected coincide with the plateaus present during the first lithiation cycle of the $LiPF_6$/EC electrolytes. The same cutoff potentials were used for the $LiPF_6$/EC/EMC (3/7, v/v) and the $LiPF_6$/EMC electrolytes. The cycling performance (time and capacity) of cells prepared with BF graphite anodes was comparable to standard coin cells and previous reports of cells containing BF graphite.[28,29]

TEM and EDX analysis of graphite cycled with $LiPF_6$ in EC

TEM analysis shows the presence of an SEI on graphite anodes. SEI formation is especially apparent on the edge planes of graphite cycled with $LiPF_6$ in EC during first lithiation (Figure 4 A-B), as previously reported.[2,7] The edge sites are the primary location for lithium intercalation and thus also the primary location of solvent reduction. TEM images of graphite anode lithiated to 1.3 V display smooth edges of graphite (Figure 4 C-D) with a very thin SEI (~5-10 nm). The EDX data show the element compositions from the center to the edge of the graphite particle (insets of Figure 4 D, F, H, J). The carbon concentration is high and constant upon moving from location 1 to 2 but is significantly lower upon moving to location 3 at the edge of the particle. The concentrations of O and F are significantly higher at the edge. When cells are lithiated to 0.6 V, the SEI film on the edge of the graphite has an increased thickness (~20 nm). The changes in elemental concentration as determined by EDX are also more significant. The C concentration decreases from 98.6 % in the center of the particle to 91.7 % at the edge. The O and F concentrations increase to 3.2 and 4.2 %, respectively. Upon further lithiation to 0.1 V, the TEM images indicate that the SEI thickness at the graphite edges increases further. The formation of an SEI on the edges is also supported by an increase in the concentration of F and O. At the 0.05 V cutoff potential, the TEM images indicate that the SEI completely covers the particle, the O and F surface concentration show a small increase. In general, the data supports formation of a thicker anode SEI when cells are cycled to lower potential and the SEI prefers to grow along the graphite edges.

The TEM images of a graphite anode cycled to 0.05 V for one cycle in $LiPF_6$/EC and then extracted with D_2O are depicted in Figure 5. The surface film observed on the

graphite particles before D_2O extraction is no longer present. The TEM images are very similar to uncycled graphite particles. The element composition as detected by EDX is similar from the edge of graphite to the center of graphite further supporting removal of the SEI. XPS and FTIR analysis of the samples after D_2O extraction, as discussed below, are also consistent with removal of the SEI.

NMR analysis of graphite cycled with $LiPF_6$ in EC

Binder free graphite electrodes were extracted with D_2O in and Ar glove box for ^{1}H, ^{13}C, and ^{19}F NMR analysis (Figure 6). ^{1}H NMR spectra of the D_2O extract of an anode after one cycle to 0.05 V with $LiPF_6$/EC electrolyte contains a single peak at 3.51 ppm (singlet) consistent with a C-O species. ^{13}C NMR spectra of the samples revealed two carbon resonances at 62.5 and 161.2 ppm characteristic of the C-O and C=O functional groups respectively. In order to further characterize the SEI component, a direct C—H correlation experiment (HSQC) and long range C—H correlation experiment (HMBC) were used to analyze the simples (supporting information, where?). HSQC spectrum indicated the ^{1}H resonance at 3.51 ppm is coupled to the carbon peak at 62.5 ppm while the HMBC spectrum indicated the existence of a symmetric structure which consists of two carbons with the same ^{13}C NMR chemical shift which are directly connected. The NMR spectral data is consistent with the presence of Lithium Ethylene Dicarbonate (LEDC). There is no evidence for the presence of Li_2CO_3 (168.1 ppm) in the ^{13}C NMR spectrum. The spectral data is also consistent with previously reported spectral information for independently synthesized LEDC further supporting this assignment.[18] Analysis of the D_2O extract with ^{19}F NMR spectroscopy reveals the presence of a doublet at -72.2

ppm, characteristic of $LiPF_6$ and a singlet at -123.0 ppm characteristic of LiF.[36] No other significant peaks were observed by ^{1}H, ^{13}C, ^{19}F NMR spectroscopy suggesting that LEDC and LiF are the primary components of the anode SEI generated with $LiPF_6$/EC electrolyte. The characterization of LEDC is difficult due to the sensitivity of LEDC to atmospheric O_2. When cycled electrodes were extracted with D_2O after exposure to air the NMR spectra contained a complicated mixture of resonances suggesting the LEDC readily decomposes in the presence of O_2.

BF graphite anodes with $LiPF_6$/EC electrolyte were extracted and analyzed by ^{1}H NMR spectroscopy after cycling to different cut-off voltages during the lithiation process in order to investigate SEI formation during the initial stages of lithiation process (Figure 7). A gradual increase of LEDC was observed as the cells were cycled to lower potential (1.3 V to 0.05 V, Figure 8) compared to the internal standard. The increases in the concentration of LEDC correlate well with the increased thickness of the surface film observed by TEM. In order to determine at which potential LEDC begins to form, a sample was lithiated to 2.0 V (vs Li). Upon extraction of the cell with D_2O, resonances characteristic of LEDC are observed. This suggests that the reduction of the EC to generate LEDC begins at ~2.0 V (vs Li) and continues during the lithiation process on the first cycle. Binder free anodes were also extracted with D_2O after cells completed five cycles (one C/20, two C/10 and two C/5). Again, the only products observed by ^{1}H, ^{13}C, and ^{19}F NMR spectroscopy are LEDC and LiF (See supporting information) and the concentrations do not appear to increase significantly after the first cycle suggesting that little reduction occurs on subsequent

cycles The NMR spectra contained no other peaks suggesting that LEDC and LiF are the predominant species in the anode SEI.

Reaction of lithium naphthalenide with EC

Lithium naphthalenide is a well know single electrode reductant, with structural similarity and reduction potential (0.34 V vs Li) to lithiated graphite.[37] In order to better understand the reduction reaction of EC at surface of the graphite anode, the reaction of lithium naphthalenide with EC was investigated. Addition of EC to a solution of lithium naphthalenide in THF results is a rapid color change and precipitation. The THF was removed by high vacuum leaving a residual solid which was extracted with diethyl ether to remove the naphthalene. The solid was then analyzed via a combination of ^{1}H, ^{13}C NMR and FTIR. The solid was dissolved in D_2O for analysis by ^{1}H and ^{13}C NMR spectroscopy. The ^{1}H NMR spectrum contains a singlet at 3.51 ppm while the ^{13}C NMR spectrum contains two singlets at 62.5 ppm and 161.1 ppm (Figure 8 a-b). The spectra are identical to those described above for the extracts of BF graphite cycled with $LiPF_6$ in EC and previously reported for independently synthesized LEDC.[35] The residual solid was also analyzed with FT-IR spectroscopy (Figure 8c). The IR spectrum contains absorptions at ~ 1650, 1395, 1305, 1080 and 820 cm^{-1} and are similar to the IR spectra of the BF graphite cycled with $LiPF_6$ in EC and the IR spectra of independently synthesized LEDC.[35] Interestingly, LEDC is isolated in nearly quantitative yields (>95 %). There are no other observed products is the solid or wash solvent. Since gas evolution was observed during the reduction reaction of carbonates with lithium naphthalenide, the gasses evolved during reaction were analyzed by GC-MS. A single gaseous product is

observed by GC and the MS matches to the NIST library spectrum of ethylene. Thus, the only observed products of the reduction of EC by the one electron reluctant, lithium naphthalenide, are LEDC and ethylene. The mechanism for this reaction was proposed by Aurbach and co-workers (Scheme 2).[38] Interestingly, addition of $LiPF_6$ to THF solutions of lithium naphthalenide does not result in a reaction. $LiPF_6$ is not reduced to LiF. In addition, when a 1:1 mixture of $LiPF_6$ and EC is added to a THF solution of lithium naphthalenide, the only observed product is LEDC. There is not reaction of $LiPF_6$ with lithium naphthalenide.

XPS analysis of graphite cycled with $LiPF_6$ in EC

XPS spectra of electrodes extracted from cells cycled with 1.2 M $LiPF_6$ in EC to the specified cut-off voltages are depicted in Figure 9 and the elemental concentrations are provided in Table1. The fresh un-cycled BF graphite electrode is dominated by the C1s peak characteristic of graphite (284.5 eV). A weak peak is observed in the O1s spectrum centered at 534 eV suggesting the presence of surface oxidation of the graphite, as typically observed.[27,28] The ex-situ XPS spectra of all cycled binder free graphite electrodes have peaks with similar bonding energies but different relative intensities. The C1s spectra of anodes cycled with 1.2 M $LiPF_6$/EC, contain peaks at 284.5 eV (graphite), 285.5 eV (C-H), 287.5 eV (C-O) and 290 eV (C=O). Cells lithiated to 1.3 V vs Li are dominated by the peak for graphite, but have significant new peaks characteristic of C-H, C-O, and C=O containing species. Related peaks are observed in the O1s spectrum at 534 and 532.5 eV consistent with the presence of C-O and C=O containing species. New peaks are also observed in the F1s spectrum at 688, 687 and 685 eV characteristic of $LiPF_6$, $Li_xPF_yO_z$ and LiF, respectively. The related

peaks for $LiPF_6$ and $Li_xPF_yO_z$ are observed in the P2p spectrum at 138 and 135 eV. The new peaks are accompanied by changes in the elemental concentrations. A decrease in the concentration of C is observed while the concentrations of O, F, and P are all increased. The changes to the anode surface are consistent with the deposition of electrolyte reduction products including LEDC and LiF on the anode surface. As the potential of the cells is sequentially decreased to 0.6, 0.1 and 0.05 V, the peaks characteristic of electrolyte reduction products increase while the intensity of the graphite peak is decreased. The intensity for the graphite peak on the surface of the electrode cycled to 0.05 V is almost negligible suggesting complete coverage of the graphite surface by the electrolyte reduction products. While there is some fluctuation in the element concentrations as the cell potentials are decreased a clear trend is observed with a decreasing concentration of C and increasing concentrations of O and F.

The anodes cycled with 1.2 M $LiPF_6$ in EC were also analyzed by XPS after extraction with D_2O (Figure 9B). The elemental concentration as determined by XPS is 90.3% C and 9.7% O which is similar to the fresh graphite. The C1s XPS spectrum of the anode after D_2O extraction is dominated by the graphite peak (284.5eV). Small peaks characteristic of C-O (533.5 eV, O1s; 287 eV, C1s) are also observed, but the spectra are very similar to XPS spectra of the fresh anode. The results suggest that all of the anode SEI components were dissolved in the D_2O and removed from the electrode surface. Similar results were observed with the EMC and EC/EMC electrolytes. Analysis of the D_2O extracts by NMR spectroscopy is described above.

FTIR analysis of graphite cycled with $LiPF_6$ in EC

FTIR spectra were collected for fresh anodes and anodes extracted from cells cycled with 1.2 M $LiPF_6$ in EC to 1.3 V, 0.6 V, 0.1 V, and 0.05 V, respectively. The fresh electrodes contain absorptions at 1560 and 1050 cm^{-1} characteristic of oxygenated impurities on the graphite surface.[27,28] There are only small changes to the IR spectra of the electrodes cycled to higher potentials (1.3 V, 0.6 V, and 0.1 V): compared with fresh uncycled graphite electrode (Figure 10). New absorptions are observed at 1416 and 870 cm^{-1} for cells cycled to 0.6 or 0.1 V and are consistent with the formation of Li_2CO_3 and $LiPF_6$, respectively. However, the electrode cycled to 0.05 V exhibits additional absorptions at 1650, 1395, 1305, 1080, and 820 cm^{-1} as depicted in Figure 14. This supports a thickening of the anode SEI as the potential of the graphitic anode is decreased. The observed absorptions are similar to those observed for lithium ethylene dicarbonate as described above. The presence of Li_2CO_3 by FT-IR spectroscopy may be due to the longer exposure of samples to air during transfer into the Ar filled IR chamber compared to the NMR and XPS analysis. The surfaces of the anodes cycled with 1.2 M $LiPF_6$ in EC were investigated by IR spectroscopy after extraction with D_2O (Figure 14). After D_2O extraction the IR spectra of the anode surface is nearly identical to the fresh anode surface suggesting that of all of the SEI components were removed by D_2O extraction. Similar results were observed for the IR spectra of the anodes cycled with EMC and EC/EMC

TEM and EDX analysis of graphite cycled with $LiPF_6$ in EMC or EC/EMC

Graphite anodes lithiated to various potentials with $LiPF_6$ in EMC were also analyzed by TEM (Figure 11, supporting information). The formation of an SEI at 1.3 V is unclear, but upon decreasing the potential to 0.6 V the SEI is clearly evident.

The surface films were found to be very thin and non-uniform (10-20 nm) suggesting little deposition of electrolyte decomposition products on the surface of the anode. Analysis of the edge of the particles by EDX support increases in the concentration of O, F, and P supporting the generation of reduction products on the surface of cells cycled to 0.6 V or below.

Graphite anodes were cycled with $LiPF_6$ in EC/EMC (3:7, vol) under similar conditions to those reported above for $LiPF_6$ in EC. A similar morphology and elemental composition is observed on the surface of graphite particles cycled with a mixed EC/EMC (Figure 11, Supporting Information). The surface films are thin for cells cycled to 1.3 V and have low concentrations of O and F while cells cycled to lower potential (0.1 or 0.05 V) have thicker surface films with higher concentrations of O and F. The results are very similar to those observed for $LiPF_6$ in EC.

Graphite removed from cells after five cycles to 0.05 V was also analyzed (supporting information). The surface morphology of the graphite after five cycles is very similar to graphite after one cycle. The elemental analysis as determined by EDX also supports a similar increase in the concentration of O and F in the surface film on the graphite. The results suggest that the structure and composition of the SEI does not change significantly upon increasing the cycle number from 1 to 5.

NMR analysis of graphite cycled with $LiPF_6$ in EMC and EC/EMC

Similar D_2O extractions were conducted on binder free graphite electrolytes after one cycle with $LiPF_6$ in EMC electrolyte. Three sets of peaks were observed in the ^1H NMR spectrum; a triplet (J=7.0 Hz) at 1.03 ppm, a quartet (J=7.0 Hz) at 3.50 ppm, and a singlet at 3.19 ppm (Figure 12). This triplet and quartet are consistent with an

ethoxy group and the singlet is consistent with a methoxy group. The corresponding peaks were observed in the ^{13}C 135-DEPT NMR spectrum at 17.0 (CH_2) and 57.4 (CH_3) ppm for the ethoxy group and at 48.9 (CH_3) ppm for the methoxy group (supporting information). Thus based on the NMR spectral data and comparison to previously reported spectra, the two primary reduction products of EMC are Lithium methyl carbonate (LMC) and Lithium ethyl carbonate (LEC).[35] However, due to low concentrations of the species and a lack of the nuclear Overhauser effect the carbonyl resonances were not detected despite long acquisition times. The ^{19}F NMR spectrum is very similar to that observed for $LiPF_6$ in EC. LiF and residual $LiPF_6$ are the only observed species.

Experiments to investigate the SEI components as a function of cut-off voltage were conducted with $LiPF_6$ in EMC. Cells were cycled to the same potentials as cells containing $LiPF_6$ in EC (1.3, 0.6, 0.1, and 0.05 V vs Li). The cells were dismantled, rinsed with DMC and then extracted with D_2O. The ^1H NMR spectra were acquired of the extracted anodes (supporting information), and indicate that the reduction products of the electrolyte, LEC and LMC, are not present on the anode surface for cells cycle to 1.3 V and 0.6 V. When cells were lithiated to 0.1 V, the resonances of LEC (t, 3.50 ppm and quart, 1.03 ppm) are observed along with very low concentrations of LMC (s, 3.19 ppm). Cells cycled to 0.05 V vs Li have high concentrations of both LEC and LMC (Figure 13). The difference in ratios of the LEC and LMC could be due to differences in reactivity or differences in solubility of the different lithium alkyl carbonates in the DMC wash solvent, but is not easily determined due to the non-quantitative nature of this procedure. Extraction of cycled

binder free graphite electrodes allowed the unambiguous characterization of the components of the anode SEI by ^{1}H, ^{13}C, and ^{19}F NMR spectroscopy. The observation of LEDC and LiF on the anode surface for cells cycled with $LiPF_6$ in EC and LEC, LMC, and LiF on the anode for cells cycled with $LiPF_6$ in EMC is in agreement with the less definitive characterization via XPS and IR spectroscopy, as described below. Similar experiments on binder free graphite anodes were conducted with $LiPF_6$ in EC/EMC mixed electrolyte. The D_2O extract was analyzed by NMR spectroscopy. The ^{1}H NMR spectrum contains a dominant singlet at 3.51 ppm, and a second smaller singlet at 3.20 ppm, characteristic of LEDC and LMC, respectively (Figure 10). The ratio of the two compounds is approximately 2:1. The corresponding peaks were observed in the ^{13}C NMR spectrum at 62.5 and 48.9 ppm. The ^{19}F NMR spectrum contains a singlet characteristic of LiF (-123 ppm) along with residual $LiPF_6$. The NMR spectra suggest that LEDC, LMC, and LiF are the major reduction products of cells cycled with $LiPF_6$ in a mixture of EC/EMC.

Extraction of cells cycled with $LiPF_6$ in EC/EMC at various potentials was also conducted (supporting information). The ^{1}H NMR spectrum of the D_2O extract from a cell cycled to 1.3 V contained a very weak singlet at 3.51ppm assigned to LEDC. The D_2O extract from cells cycled to 0.6 V, contain two singlets in the ^{1}H NMR spectrum at 3.20 and 3.51 ppm consistent with the presence of LEDC and LMC spectrum. The concentration of the LEDC resonances is significantly greater than that for the LMC resonance. The ^{1}H NMR spectrum of D_2O extract from the anode cycled to 0.1 V contained the same resonances, but with slightly greater intensity suggesting the quantity of LEDC and LMC are increasing as the cells are lithiated to lower potential.

The ^{19}F NMR spectrum of the D_2O extract from an anode cycled to 0.05 V contains peaks for LiF (-123 ppm) and residual $LiPF_6$ (-73.4 ppm). The major products observed on the surface are LEDC and LiF with low concentrations of LMC. The absence of LEC may be related to greater solubility in the DMC wash solvent. To examine this possibility the wash DMC was removed by rotary-evaporation, the reside was extracted with C_6D_6 and D_2O and analyzed by ^1H and ^{13}C NMR spectroscopy. There were no products observed by NMR spectroscopy, indicating that other compounds are absent or present in very small quantities.

XPS analysis of graphite cycled with $LiPF_6$ in EMC and EC/EMC

XPS spectra of anodes extracted from cells cycled with 1.2 M $LiPF_6$/EMC electrolyte contain peaks with similar bonding energies to those observed for cells cycled with $LiPF_6$/EC (Figure 14, supporting information). The cells lithiated to 1.3 V and 0.6 V have nearly identical C1s spectra with a dominant graphite peak (284.5 eV) and a weak peak characteristic of C-H (286 eV). The O1s spectrum contains a single broad peak at 534 eV corresponding to C-O containing species from residual surface oxidation of fresh graphite. Weak signals are also observed in the F1s and P2p spectra consistent with residual $LiPF_6$ on the surface. Thus there is no evidence the electrolyte reduction is occurring at these potentials. As the potential is decreased to 0.1 and 0.05 V, new peaks are observed in the C1s spectra at 287.8 eV and 290 eV which are attributed to presence of C-O and C=O containing species, from the reduction of carbonate electrolytes. Related peaks in the O1s spectra are observed at 534 eV (C-O) and 532.5 eV (C=O). A similar trend is seen in the F1s and P2p spectra. As the

potential is reduced to 0.1 and 0.05 V and increase in the concentrations of LiF (685 eV, F1s) and $Li_xPF_yO_z$ (687 eV, F1s; 134 eV, P2p) is observed.

The XPS spectra of BF graphite anodes cycled with 1.2 M $LiPF_6$ in EC/EMC (3:7 v/v) are very similar to the spectra of samples with 1.2 M $LiPF_6$ in EC (Figure 14, supporting information). The C1s spectra of cells lithiated to 1.3 V are dominated by graphite (284.5 eV) but have additional small peaks characteristic of C-H, C-O, and C=O containing species. The O1s, F1s and P2p spectra are consistent with the presence of lithium alkyl carbonates, LiF and $LiPF_6$. As the potential of the cells are decreased to 0.6, 0.1 and 0.05 V, the changes to the XPS spectra are nearly identical to those observed for $LiPF_6$ in EC. Intensities of C1s peaks at 286 eV (C-H), 287 eV (C-O) and 290 eV (C=O) increase while the graphite peak is decreased. Similar trends are also observed in the O1s, F1s, and P2p spectra consistent with the generation of lithium alkyl carbonates, LiF and $Li_xPF_yO_z$. The similarity of the XPS spectra suggest that the anode SEI is dominated by the reduction products of EC and $LiPF_6$ and that the reduction products of EMC are lesser contributors to the composition of the SEI.

FTIR analysis of graphite cycled with $LiPF_6$ in EMC and EC/EMC

The IR spectra of anodes cycled with 1.2 M $LiPF_6$/EMC were collected for samples lithiated to the same four cut-off voltages (Figure 15, supporting information). Lithiation to 0.6 V results in the appearance of new absorptions at 1160 and 1260 cm^{-1} there are no additional changes for cells cycled to 0.1 V. These two peaks may result from the generation of C-O or P-O containing species on the anode surface. Cells cycled to 0.05 V result in the appearance of several new absorption peaks at 1640 ,

1450, 1090 and 820 cm^{-1} which are consistent with the generation of lithium ethyl carbonate and lithium methyl carbonate.[28]

Similar investigations were conducted on anodes cycled with 1.2 M $LiPF_6$ in EC/EMC (3:7) (Figure 15, supporting information). The IR results indicate the similar trend of the formation of SEI, the absorption peaks are weak for cells cycled to 1.3, 0.6, and 0.1 V but become more intense at 0.05V. The anode extracted from the cell cycled to 0.05 V contains multiple absorptions at 1650, 1450, 1395, 1305, 1080 and 820 cm^{-1}. The spectra suggest that the anode SEI is dominated by LEDC but likely contains some LEC and LMC. For all samples investigated there does not appear to be a significant quantity of Li_2CO_3 (1426 cm^{-1}) in the anode SEI.

Summary

While the literature reports that the Solid Electrolyte Interphase (SEI) is a very complicated mixture of components, a combination of solution NMR spectroscopy, XPS, and FT-IR suggest that when an electrolyte composed of $LiPF_6$ in EC is utilized the SEI is predominantly a mixture of lithium ethylene dicarbonate (LEDC) and lithium fluoride (LiF) (Figure 15) with a low concentration of lithium oxyfluorophosphates ($Li_xPF_yO_z$). The composition of the anode SEI is constant during the entire charging process suggesting that the initially formed SEI close to the graphite surface is identical to the SEI at the interface with the electrolyte. The SEI composition is also unchanged upon increasing the number of cycles from one to five. All of the extracted electrodes contain the same two components LEDC and LiF. While some IR spectra suggest low concentrations of Li_2CO_3 may be present, no Li_2CO_3 was observed by ^{13}C NMR spectroscopy for any samples, suggesting that if

Li_2CO_3 is present in the graphite anode SEI the concentration is very low compared to LEDC and LiF.

A relatively consistent ratio of F to O is observed in the anode SEI during formation and after multiple cycles implying a consistent mixture of LEDC and LiF during all stages of formation of the SEI. Furthermore , the ratio of F to O is also constant at the surface and interior positions of the SEI as determined by EDX, further supporting a constant composition throughout the entire anode SEI. The thickness of the anode SEI gradually increases as the cell is cycled to lower potentials but the thickness does not significantly increase between the first and fifth cycles. The SEI is primarily located on the edges of the graphite and is relatively thin ~ 50 nm.

Independent investigations of the reaction of EC with the single electron reductant lithium naphthalenide confirm that the reaction mechanism follows two sequential one electron transfer reactions to generate LEDC and ethylene as proposed by Aurbach and co-workers (Scheme 2).[38] The mechanism of $LiPF_6$ reduction is less clear although the dominant product is LiF with low concentrations of $Li_xPF_yO_z$.

Conclusions

The structure and composition of the anode Solid Electrolyte Interphase (SEI) on the graphite anode of lithium ion batteries was investigated via a unique combination of TEM, solution NMR, XPS, and FT-IR spectroscopy. The analysis was conducted with novel binder free graphite electrodes and simple two or three component electrolytes to simplify analysis. A TEM grid was embedded in a BF graphite electrode which allowed TEM analysis of the cycled graphite particles without

dispersion. NMR samples were prepared by D_2O extraction of the SEI in and Ar glovebox to prevent SEI component decomposition.

The composition of the SEI generated with an electrolyte composed of 1.2 M $LiPF_6$ in EC is predominantly a mixture of lithium ethylene dicarbonate (LEDC) and lithium fluoride (LiF). Upon increasing the complexity of the electrolyte, 1.2 M $LiPF_6$ in 3:7 EC/EMC, a slight change in the composition is observed. In addition to high concentrations of LEDC and LiF, low levels of LEC and LMC are observed in the SEI. However, the slight change in composition does not result in a significant change in the thickness or function of the anode SEI. The SEI is ~50 nm thick and predominantly located on the edges of the graphite particles. The results suggests that a interfacial film of LEDC and LiF can function as an effective passivation layer on graphite preventing further electrolyte reduction. While there are many results that suggest upon additional cycling and aging the structure, composition and thickness of the anode SEI changes,[12,13] the initial composition is relatively simple. This should allow computational investigators an improved basis for modeling this critical structure.

ACKNOWLEDGMENTS

The authors gratefully acknowledge funding from Department of Energy Office of Basic Energy Sciences EPSCoR Implementation award (DE-SC0007074).

Reference

(1) Armand, M.; Tarascon, J.-M. Nature 2008, 451, 652.

(2) Verma, P.; Maire, P.; Novak, P. Electrochim. Acta 2010, 55, 6332.

(3) Peled, E. J. Electrochem. Soc. 1979, 126, 2047.

(4) Aurbach, D. J. Power Sources 2000, 89, 206.

(5) Edstro¨m, K.; Herstedt, M.; Abraham, D. P. J. Power Sources 2006,153, 380.

(6) Aurbach, D.; Markovsky, B.; Shechter, A.; Ein-Eli, Y.; Cohen, H. J. Electrochem. Soc. 1996, 143, 3809.

(7) Xu, K.; von Cresce, A. J. Mater. Chem. 2011, 21, 9849.

(8) Andersson, A. M.; Abraham, D. P.; Haasch, R.; MacLaren, S.; Liu, J.; Amine, K. J. Electrochem. Soc. 2002, 149, A1358.

(9) Herstedt, M.; Abraham, D. P.; Kerr, J. B.; Edstrom, K. Electrochim. Acta 2004, 49, 5097.

(10) Bodenes, L.; Dedryvere, R.; Martinez, H.; Fischer, F.; Tessier, C.; Peres, J.-P. J. Electrochem. Soc. 2012, 159, A1739.

(11) Andersson, A. M.; Edstrom, K. J. Electrochem. Soc. 2001, 148, A1100.

(12) Li, W.; Xiao, A.; Lucht, B. L.; Smart, M. C.; Ratnakumar, B. V. J. Electrochem. Soc. 2008, 155, A648.

(13) Zhuang, G. V.; Ross, P. N. Electrochem. Solid-State Lett. 2003, 6, A136.

(14) Zhuang, G. V.; Yang, H.; Blizanac, B.; Ross, P. N. Electrochem. Solid-State Lett. 2005, 8, A441.

(15) Xu, K. Chem. Rev. 2004, 104, 4303.

(16) Xu, K.; Zhuang, G. V.; Allen, J. L.; Lee, U.; Zhang, S. S.; Ross, P.N.; Jow, T. R. J. Phys. Chem. B 2006, 110, 7708.

(17) Wang, Y.; Nakamura, S.; Ue, M.; Balbuena, P. B. J. Am. Chem.Soc. 2001, 123, 11708.

(18) Wang, Y.; Nakamura, S.; Tasaki, K.; Balbuena, P. B. J. Am. Chem.Soc. 2002, 124, 4408.

(19) Tasaki, K. J. Phys. Chem. B 2005, 109, 2920−2933.

(20) Tasaki, K.; Harris, S. J. J. Phys. Chem. C 2010, 114, 8076.

(21) Borodin, O.; Smith, G. D. J. Phys. Chem. B 2006, 110, 22773.

(22) Kim, S.-P.; van Duin, A. C. T.; Shenoy, V. B. J. Power Sources 2011, 196, 8590.

(23) Leung, K.; Budzien, J. L. Phys. Chem. Chem. Phys. 2010, 12,6583−6586.

(24) Kang, S. H.; Abraham, D. P.; Xiao, A.; Lucht, B. L. J. Power Sources 2008, 175, 526.

(25) Vatamanu, J.; Borodin, O.; Smith, G. D. J. Phys. Chem. C 2012, 116, 1114.

(26) Yamada, Y.; Iriyama, Y.; Abe, T.; Ogumi, Z. Langmuir 2009, 25,12766.

(27) Xu, K.; von Cresce, A.; Lee, U. Langmuir 2010, 26, 11538.

(28) Shi, S.; Lu, P.; Liu, Z.; Qi, Y.; Hector, L. G.; Li, H.; Harris, S. J. J.Am. Chem. Soc. 2012, 134, 15476.

(29) Aurbach, D.; Markovsky, B.; Rodkin, A.; Cojocaru, M.; Levi, E.;Kim, H.-J. Electrochim. Acta 2002, 47, 1899.

(30) Zhuang, G. R.; Ross, P. N. Electrochem. Solid-State Lett. 2003, 6,A136.

(31) Xiao, A.; Lucht, B. L.; Kang, S.-H.; Abraham, D. P. J.Electrochem. Soc. 2009, 156, A318.

(32) Naji, A.; Ghanbaja, J.; Willmann, P.; Billaud, D. J. Power Sources1999, 81, 207.

(33) Dolle, M.; Grugeon, S.; Beaudoin, B.; Dupont, L.; Tarascon, J.-M. J. Power Sources 2001, 97, 104.

(34) Wang, F.; Graetz, J.; Moreno, M. S.; Ma, C.; Wu, L.; Volkov, V.;Zhu, Y. ACS Nano 2011, 9, 1190.

(35) Brazier, A.; Dupont, L.; Dantras-Laffont, L.; Kuwata, N.;Kawamura, J.; Tarascon, J. M. Chem. Mater. 2008, 20, 2352.

(36) Campion, C. L.; Li, W.; Lucht, B. L. J. Electrochem. Soc. 2005,152, A2327.

(37) Connelly, N. G.; Geiger, W. E. Chem. Rev. 1996, 96, 877.

(38) Zhuang, G. V.; Yang, H.; Ross, P. N.; Xu, K.; Jow, T. R.Electrochem. Solid-State Lett. 2006, 9, A64.

(39) Aurbach, D.; Daroux, M. L.; Faguy, P. W.; Yeager, E. J.Electrochem. Soc. 1987, 134, 1611.

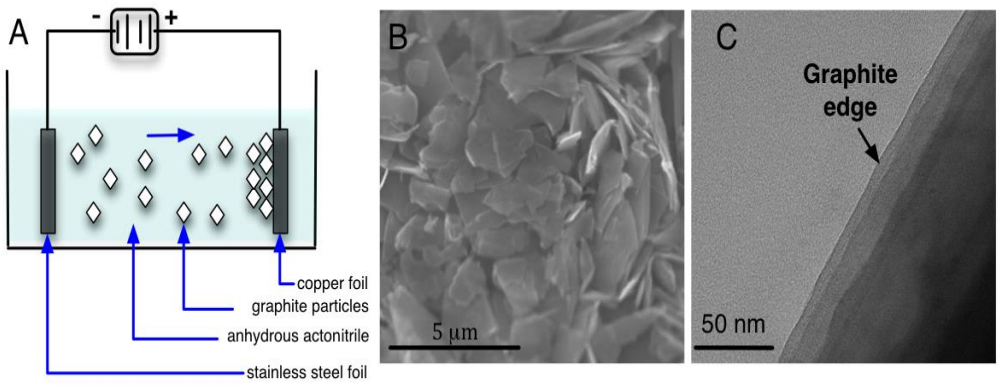

Figure 2-1. Schematic diagram of preparation of binder-free (BF) graphite electrode by electrophoretic deposition (EPD) (A) and SEM (B) and TEM (C) images of graphite in the as-prepared electrode.

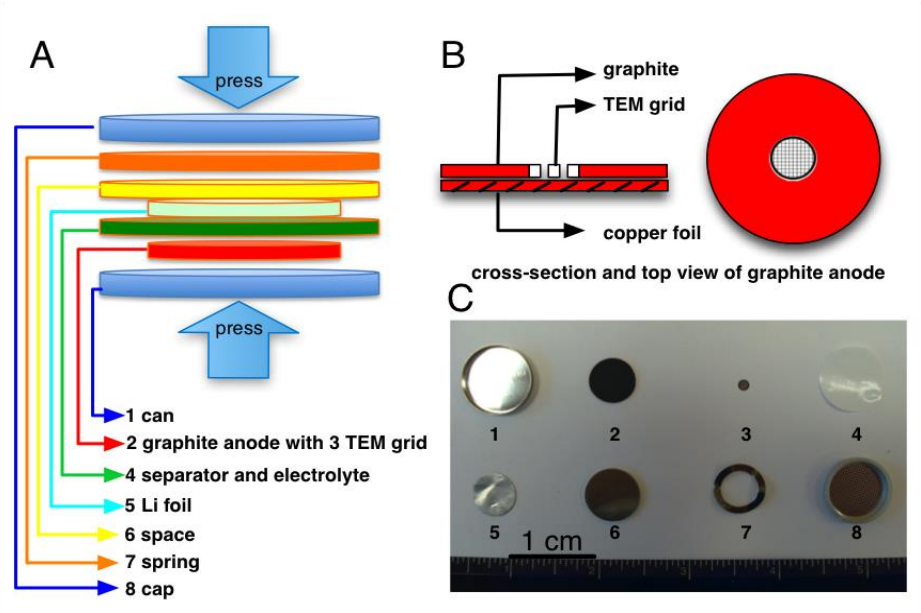

Figure 2-2. Schematic diagram and picture showing (a) the assembly of a Li/Graphite half-cell (b) TEM-grid embedded graphite electrode and (c) the parts of a Li/Graphite half-cell.

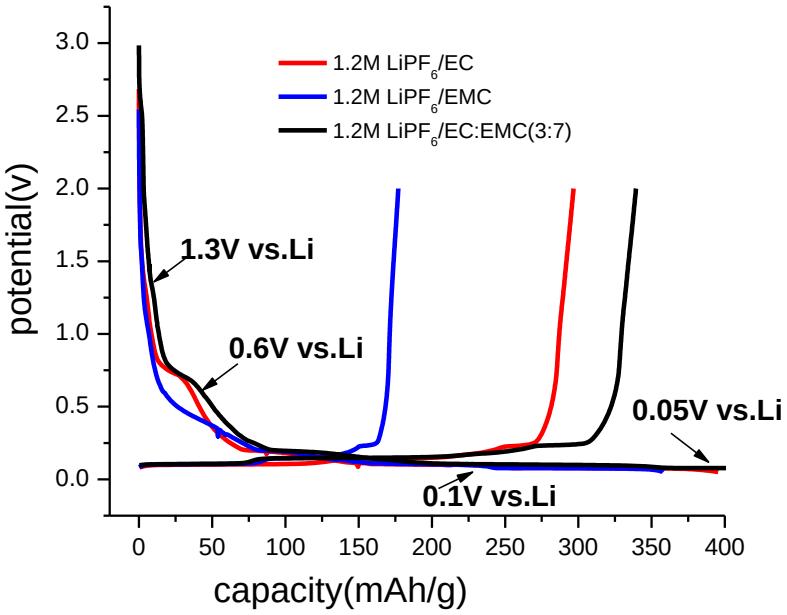

Figure 2-3. Voltage versus capacity plots for coin cells with $LiPF_6$ in EC, EMC and EC/EMC (3:7v/v) electrolytes.

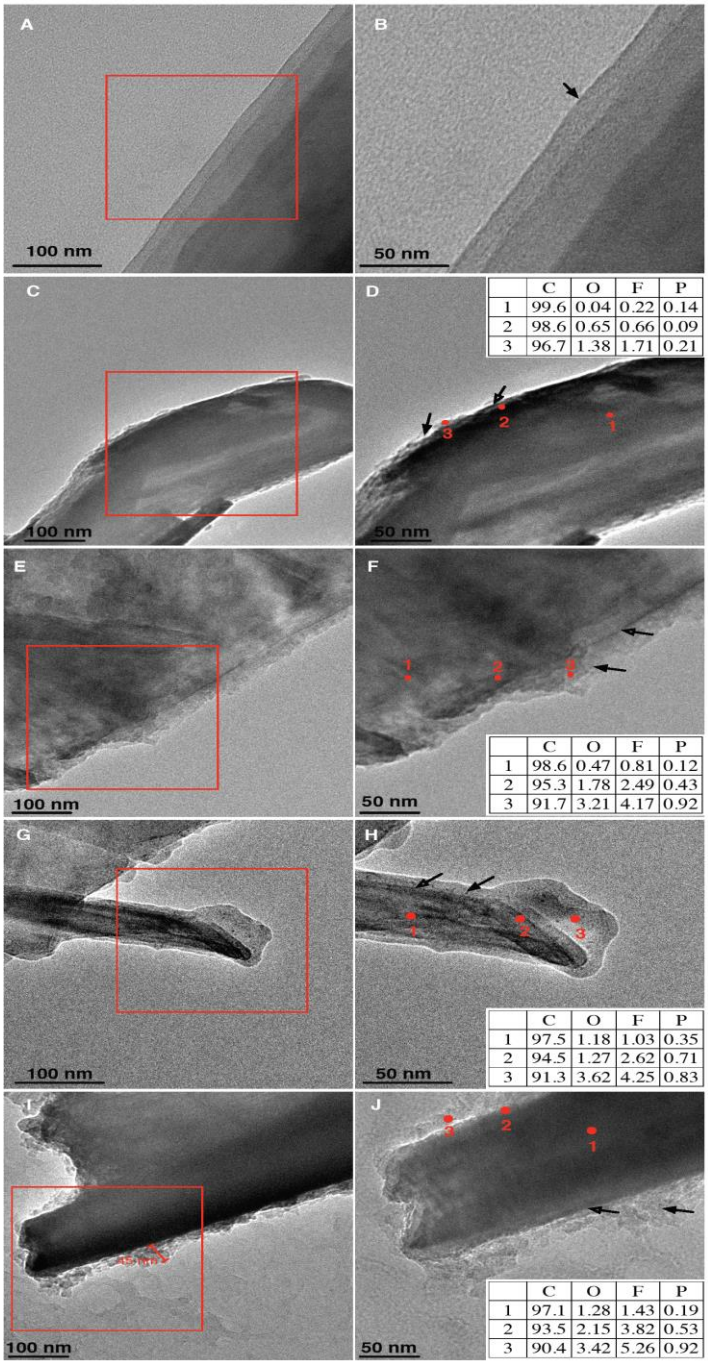

	C	O	F	P
1	99.6	0.04	0.22	0.14
2	98.6	0.65	0.66	0.09
3	96.7	1.38	1.71	0.21

	C	O	F	P
1	98.6	0.47	0.81	0.12
2	95.3	1.78	2.49	0.43
3	91.7	3.21	4.17	0.92

	C	O	F	P
1	97.5	1.18	1.03	0.35
2	94.5	1.27	2.62	0.71
3	91.3	3.62	4.25	0.83

	C	O	F	P
1	97.1	1.28	1.43	0.19
2	93.5	2.15	3.82	0.53
3	90.4	3.42	5.26	0.92

Figure 2-4. TEM bright-field images of fresh graphite and graphite anodes cycled to four cut-off voltages during first lithiation containing 1.2 M $LiPF_6$/EC. (a) Fresh graphite electrode, (C) 1.3 V, (E) 0.6 V, (G) 0.1 V and (I) 0.05. The inset of D, F, H, J show element composition detected by EDX. The solid and empty arrows indicate the SEI layer and the edge of graphite, and the red spots indicate locations probed by EDX.

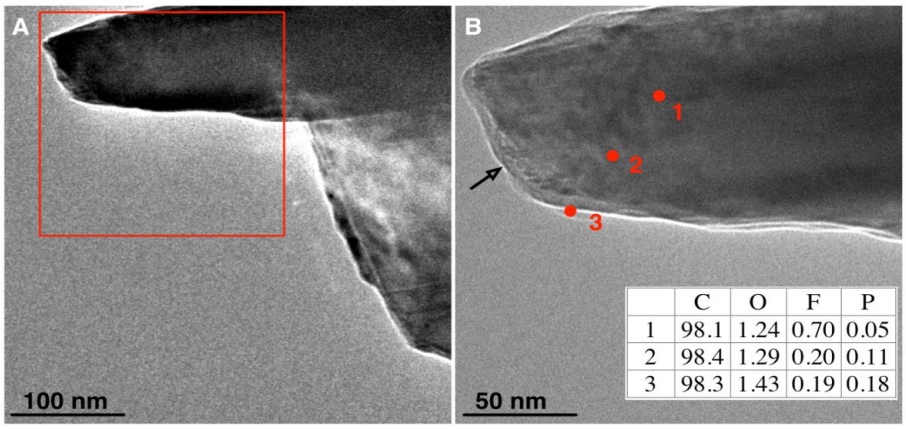

	C	O	F	P
1	98.1	1.24	0.70	0.05
2	98.4	1.29	0.20	0.11
3	98.3	1.43	0.19	0.18

Figure 2-5. TEM images of BF graphite anodes cycled with 1.2 M $LiPF_6$/EC to 0.05 V after D_2O extraction. The red spots indicate the areas performed by EDX

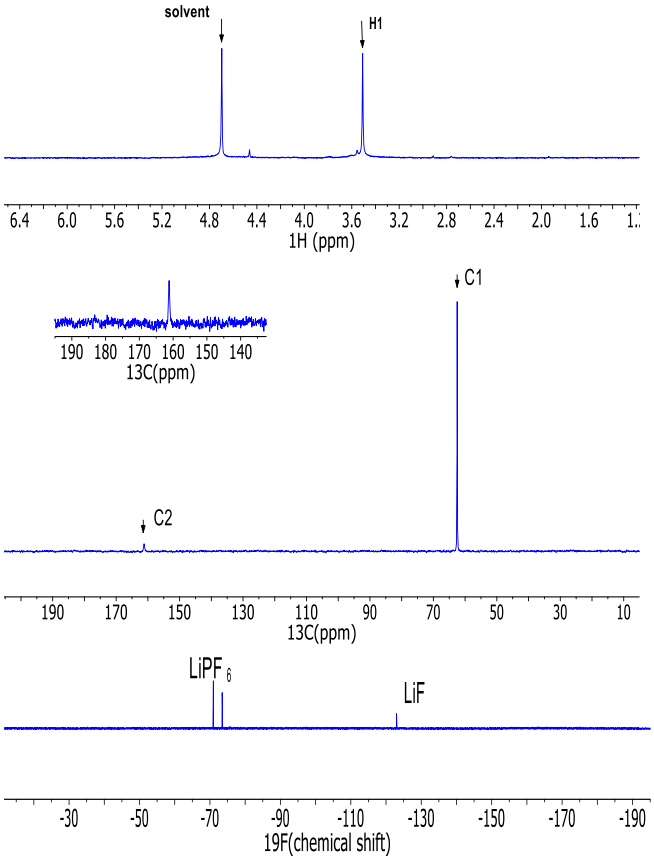

Figure 2-6. (a) ^{1}H NMR spectrum (b) ^{13}C NMR spectrum (c) ^{19}F NMR spectrum of the D_2O extract of a graphite anode cycled to 0.05 V with $LiPF_6$/EC.

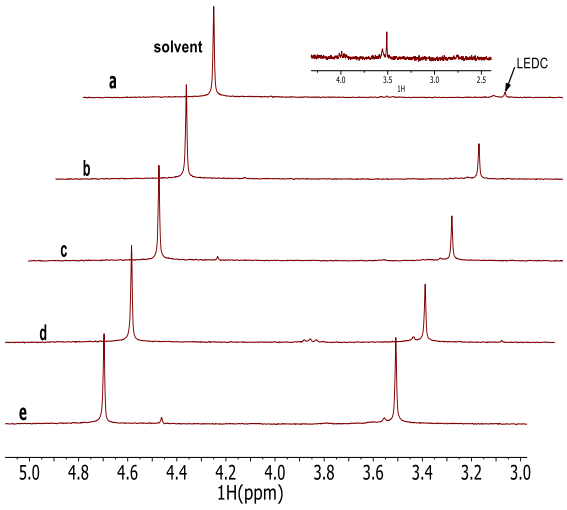

Figure 2-7: ^{1}H NMR spectra of the D_2O extract of graphite anodes cycled to four cut-off voltages (a) 2.0 V (b) 1.3 V, (C) 0.6 V, (d) 0.1 V, and (e) 0.05 V.

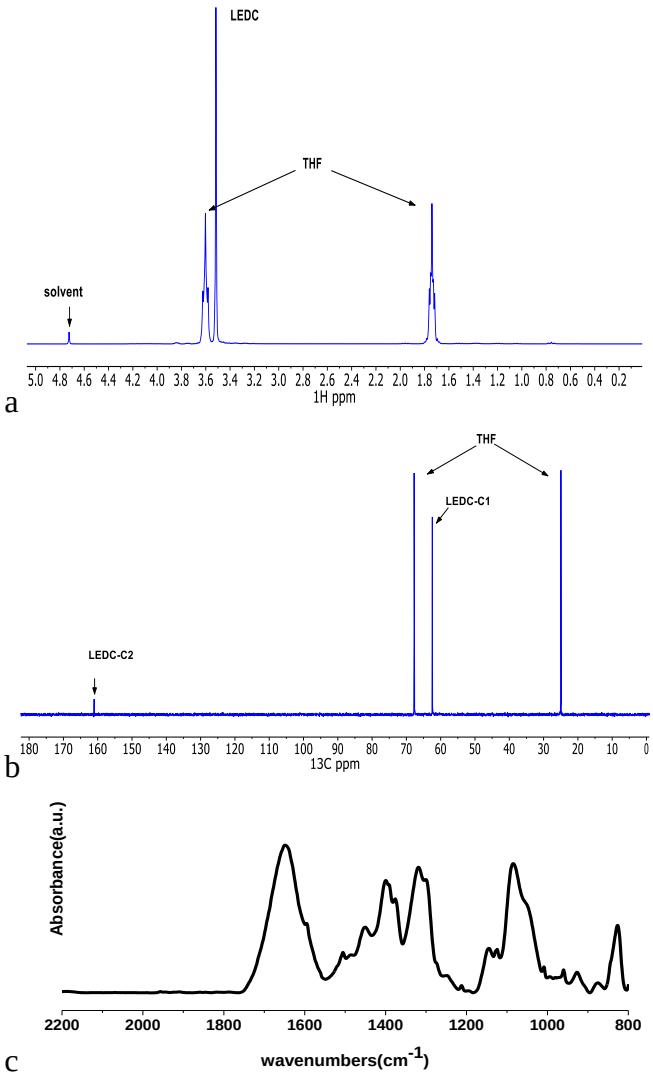

Figure 2-8. (a) ^{1}H and (b) ^{13}C NMR spectra and (c) FT-IR spectra of the reduction product of EC.

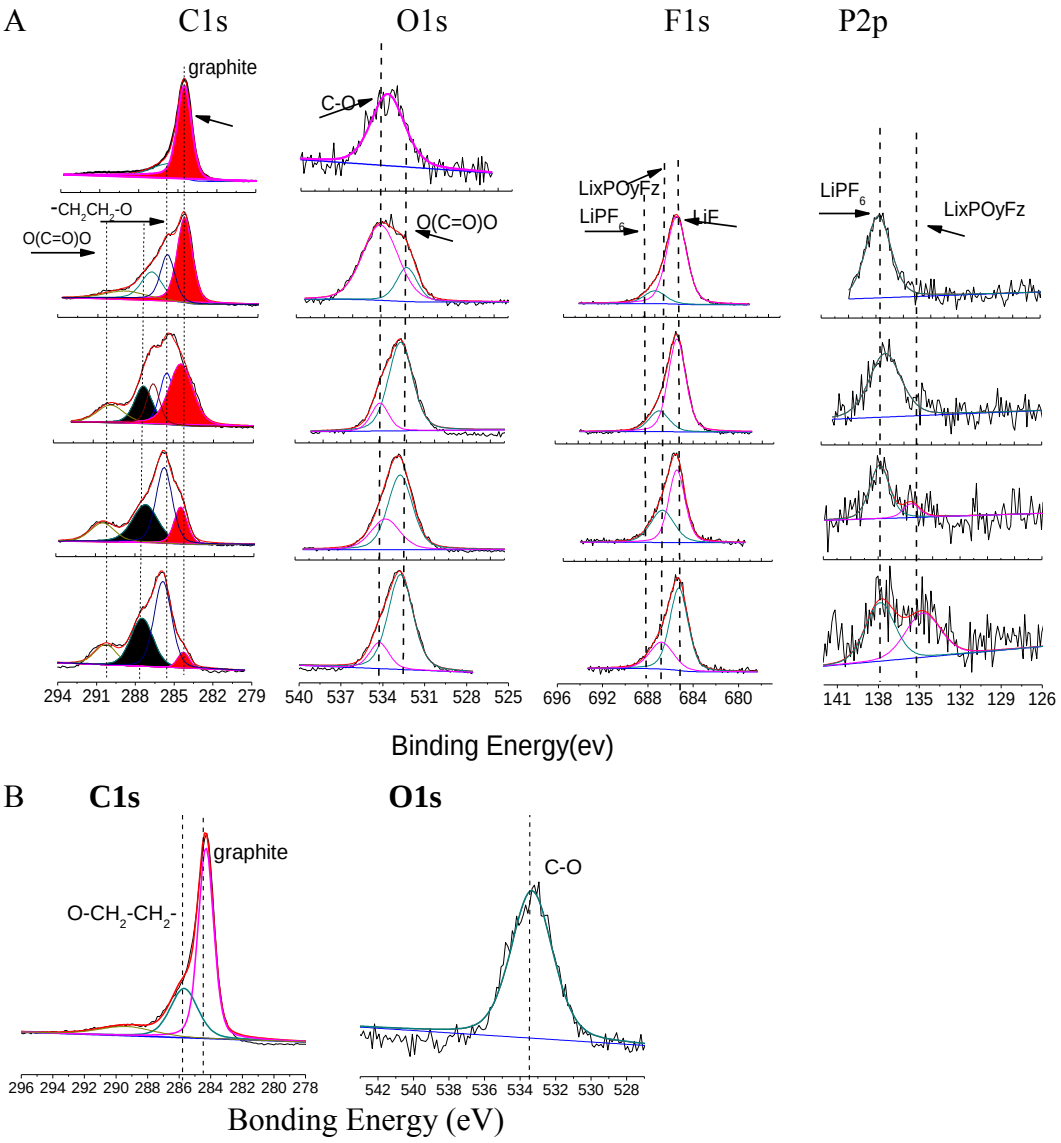

Figure 2-9. (A) XPS spectra of Fresh BF graphite electrodes and BF graphite anodes extracted from coin cells cycled to different cut-off voltages, from top: 1.3 V, 0.6 V, 0.1 V and 0.05 V vs.Li. (B) XPS spectra of BF graphite anode after D_2O extraction.

Element precentage	C1s	O1s	F1s	P2p
Fresh electrode	**94.5**	**5.5**		
1.3V	**57.1**	**14.9**	**27.3**	
0.6V	**46.7**	**25.5**	**27.0**	**0.7**
0.1V	**41.9**	**24.9**	**32.2**	**0.8**
0.05V	**37.8**	**35.1**	**26.0**	**0.9**
After D_2O rinse	**90.3**	**9.7**		**1.1**

Table 2-1: element percentage from BF graphite anodes cycled with 1.2M $LiPF_6$/EC

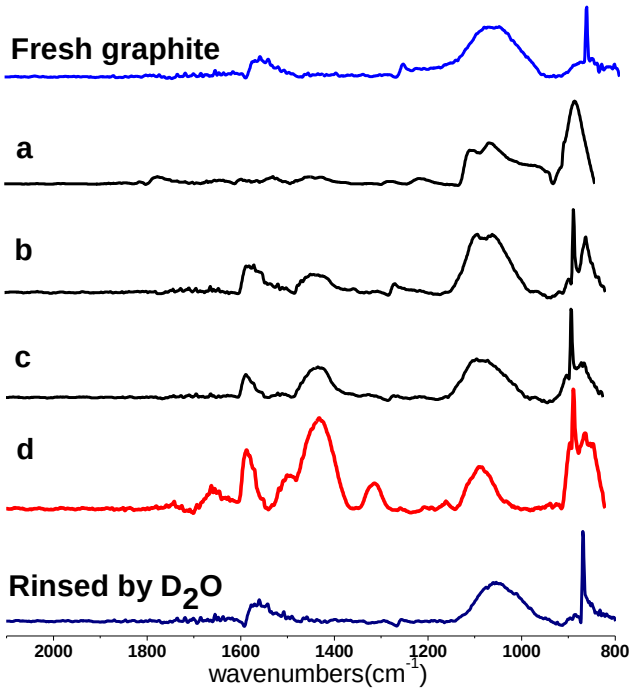

Figure 2-10. IR spectra of 1.2M $LiPF_6$/EC cycled BF graphite anodes (a) 1.3 V, (b) 0.6 V,(c) 0.1 V and (d) 0.05 V vs. Li. Top and bottom spectra are fresh graphite electrode and cycled graphite after D_2O extraction.

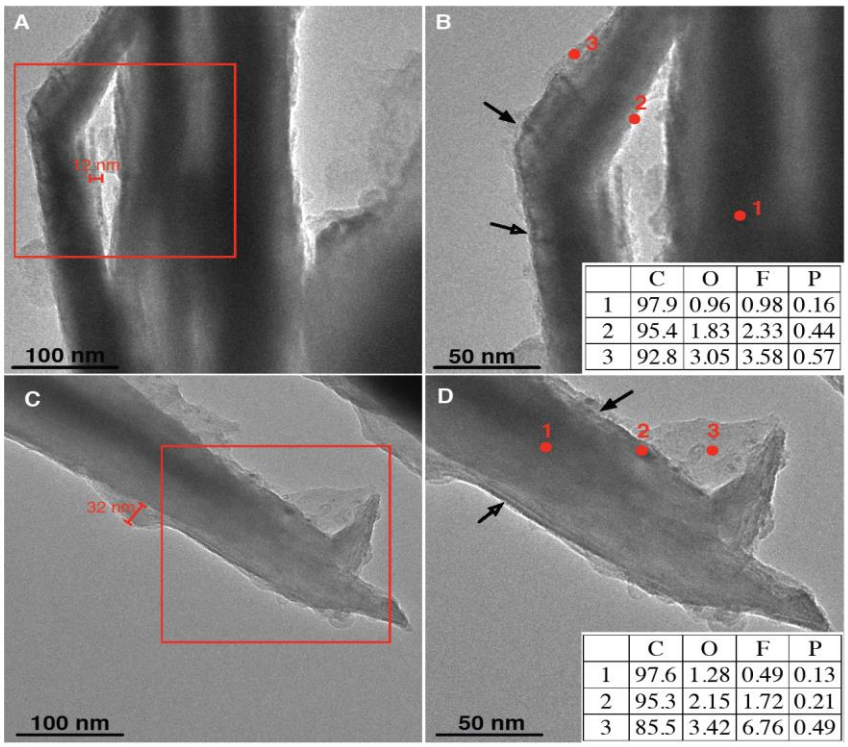

	C	O	F	P
1	97.9	0.96	0.98	0.16
2	95.4	1.83	2.33	0.44
3	92.8	3.05	3.58	0.57

	C	O	F	P
1	97.6	1.28	0.49	0.13
2	95.3	2.15	1.72	0.21
3	85.5	3.42	6.76	0.49

Figure 2-11. TEM bright-field images of the BF graphite anodes cycled to 0.05 V vs Li with (A,B), 1.2 M $LiPF_6$/EMC or (C,D), 1.2 M $LiPF_6$/EC:EMC (3:7v/v). The red spots indicate the areas performed by EDX.

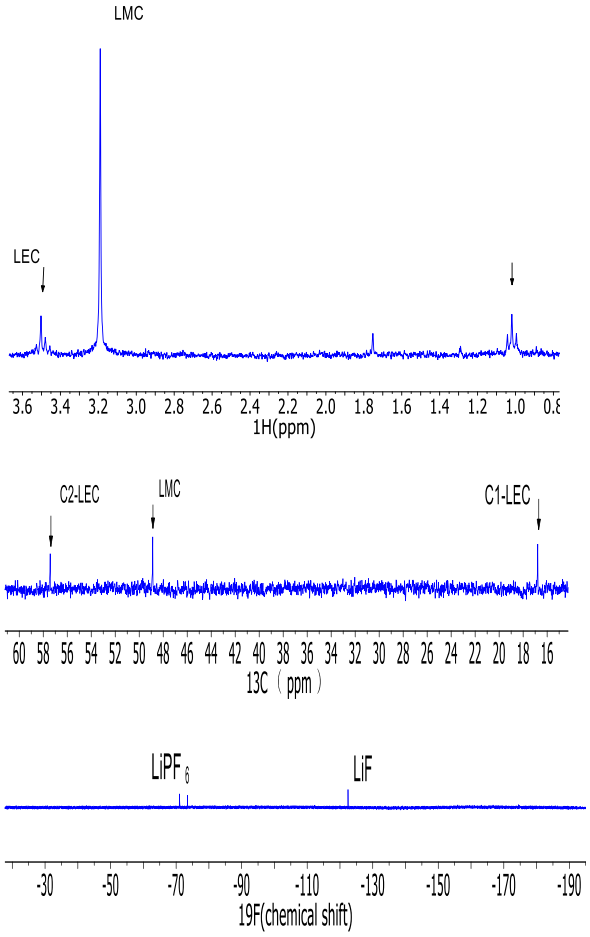

Figure 2-12. (a) ^{1}H NMR spectrum, (b) ^{13}C NMR spectrum and (c) ^{19}F NMR spectrum of the D_2O extract of graphite anode cycled to 0.05 V with $LiPF_6$/EMC.

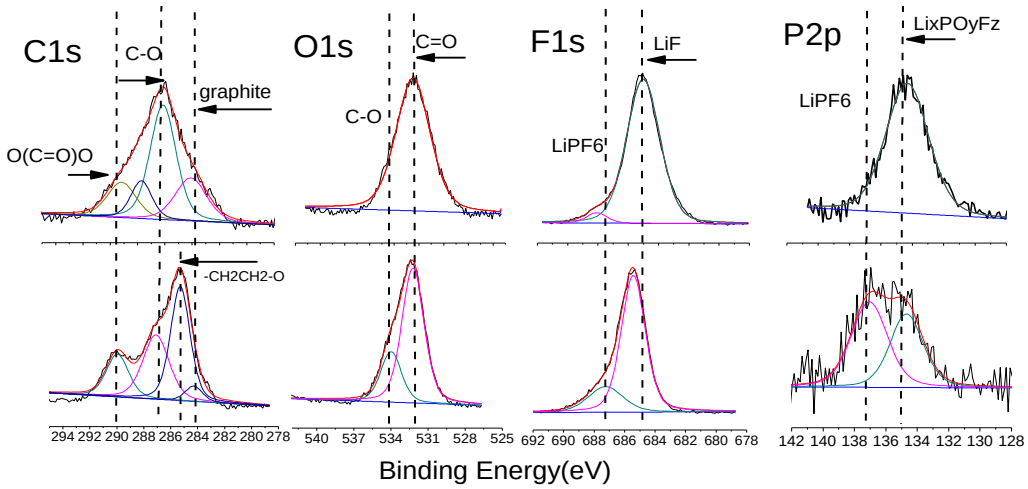

Figure 2-13. XPS spectra of BF graphite anodes after one cycle to 0.05 V vs.Li with (a) 1.2 M $LiPF_6$/EMC and (b) 1.2M $LiPF_6$/EC:EMC(3:7 v/v).

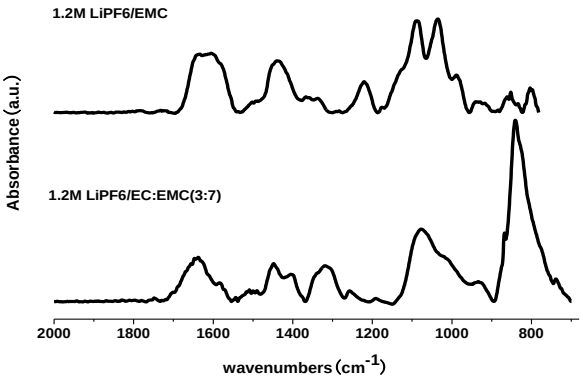

Figure 2-14. IR spectra of BF-anodes cycled to 0.05 V with (a) 1.2 M $LiPF_6$/EMC (b) $LiPF_6$/EC:EMC (3:7 v/v).

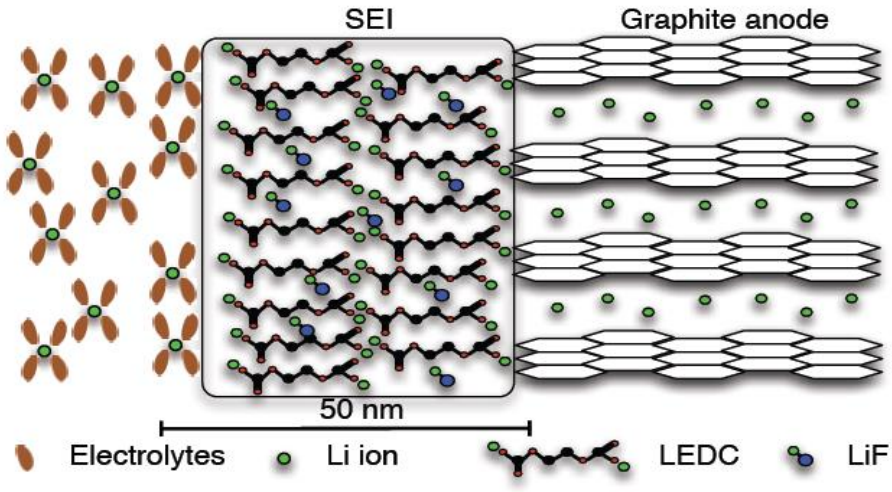

Figure 2-15: Schematic figure of SEI formed on graphite anodes during first cycle.

CHAPTER 3

SILICON SOLID ELECTROLYTE INTERPHASE (SEI) OF LITHIUM ION BATTERY CHARACTERIZED BY MICROSCOPY AND SPECTROSCOPY

Mengyun Nie[1], Daniel P. Abraham[2], Yanjing Chen[1], Arijit Bose[1], and Brett L. Lucht[1]

[1]*University of Rhode Island, Kingston, Rhode Island 02881, United States*

[2]*Argonne National Laboratory, Argonne, Illinois 60439, United States*

The following was published in the Journal of the Physical Chemistry C, and is presented here in manuscript format

Introduction

There has been significant interest in the development of lithium ion batteries due to the high energy density of these secondary batteries. However, meeting the requirements of electric vehicles (EV) requires the development of anode and cathode materials with higher energy density than the anode and cathode materials used in traditional lithium ion batteries. Silicon is one of the most promising candidates for an anode material in LIBs due to the high theoretical capacity, 3580 mAh/g, when fully lithiated.[1] This theoretical capacity is ~10 times that of commercial graphite (372 mAh/g) currently used in lithium ion batteries. However the silicon electrodes have a very large volume expansion (300–400%) during lithiation resulting in large stresses, mechanical damage, and surface area changes.[2-3] The problems associated with the large volumetric changes have prompted the design and application of nano-structured silicon materials. [4-5] It is well known that during the first charging cycles a solid electrolyte interphase (SEI) is generated on the surface of the graphite anode in lithium ion batteries. Significant research has been conducted on the structure and composition of the graphite SEI.[6-7] The structure and stability of the graphite SEI has been reported to be dependent upon the composition of the electrolyte, salt, solvent, and additives.[8-9] A related SEI has been reported to be generated on the surface of silicon electrodes in lithium ion batteries as well.[10] However, the instability of the solid electrolyte interphase (SEI) silicon electrodes is a significant problem leading to poor capacity retention.

Analysis of the SEI generated on silicon anodes has been conducted by several research groups with standard $LiPF_6$/ethylene carbonate (EC) based electrolytes. One

investigation of SEI formation on silicon nanoparticles was conducted via a combination of hard and soft X-ray photoelectron spectroscopy, suggesting that the SEI on the silicon electrodes at the electrolyte interface is similar to the SEI formed on carbonaceous electrodes and is dominated by lithium alkyl carbonates, while the SEI at the interface of the silicon interface is dominated by the conversion of the surface SiO_2 layer to Li_xSiO_y.[11] Another investigation of SEI formation on silicon in EC-based electrolytes was conducted via a combination of XPS, IR and Raman spectroscopy. The analysis was conducted as a function of electrochemical potential during the first charge and revealed an SEI composed primarily of LiF, Li_xPF_y, lithium alkyl carbonates, and lithiated fluorosilicates Li_xSiF_y.[12] In addition, the presence of ionic species including LiF or Li_2CO_3 at the silicon anode electrolyte interface was supported by *ex-situ* ^{7}Li MAS-NMR spectra.[13]

In order to improve the cycling behavior of silicon anodes in lithium ion batteries, the electrolyte formulation has been modified via the addition of reactive additives or co-solvents designed to generate a more stable SEI. One of the most frequently investigated additives is fluoroethylene carbonate (FEC). The addition of FEC has been investigated in low concentrations (1-5 %) as an additive and in high concentrations (10-50 %) as a co-solvent in $LiPF_6$/carbonate electrolytes. The addition of FEC has been reported to significantly improve the capacity retention of many silicon electrodes.[14] Surface analysis of silicon electrodes, via SEM, XPS and IR, cycled with electrolyte containing a low concentration of FEC (3% wt) suggests that the SEI contains LiF, lithium alkyl carbonates, and fluorinated silicon species (Si-F) and has many similarities to the SEI generated with $LiPF_6$ in carbonates without

FEC.[15-16] Investigation of the surface of silicon anodes cycled with higher concentrations of FEC provided different results. Analysis of the electrode surface via a combination of XPS, TEM, TOF-SIMS, and IR spectroscopy suggests that the surface has a high concentration of LiF and a polymer which may be a polyalkene or polycarbonate.[17-18] However lithium alkyl carbonates are also observed due to the presence of EC and dialkyl carbonates in the electrolyte. The presence of FEC is believed to generate a thinner SEI, with a lower impedance, on the silicon surface.[17, 19] However, even in the presence of FEC, the SEI on the silicon anode is not as stable as the SEI on graphite anodes. The SEI instability contributes to the poor cycling performance of silicon anodes. Therefore, a better understanding of the SEI on silicon anodes in EC and FEC based electrolytes is necessary.

We have developed novel binder free silicon (BF-Si) nano-particle electrodes and investigated the cycling performance in $LiPF_6$/EC and $LiPF_6$/FEC electrolytes. The absence of binder and presence of a single solvent electrolyte simplifies the analysis of the SEI components. After cycling, ex-situ analysis of the silicon electrodes has been conducted via a combination of TEM, solution NMR spectroscopy of electrode extracts, FT-IR, and XPS. The specially designed TEM experiment allows direct imaging of the silicon nano-particles after cycling, while analysis of the D_2O extracts provides the molecular structure of the SEI components.[20] The analysis provides information about the components of the SEI resulting from electrolyte (salt and solvent) decomposition on silicon anodes, and insights into the difference in cycling performance for electrolytes containing FEC.

Experimental

Preparation of binder-free Silicon Electrodes and Coin Cells Fabrication

Binder free silicon (BF-Si) electrodes were prepared by Electrophoretic Deposition (EPD) methods in a similar manner to our previously reported preparation of binder free graphite electrodes[21-22] The EPD bath was prepared with silicon nano-particles (~50 nm, Alfa Aesar) dissolved in acetonitrile (anhydrous, Fisher). Utilizing this method, results in the preparation of electrodes without polymer binders (PVDF, CMC, SBR, etc) or conductive carbon. The electrodes are composed exclusively of silicon nano-particles with a theoretical capacity ~3580 mAh/g.[1] BF-Si electrodes were coated on copper foil with a surface density of ~0.37 mg/cm^2. The BF-Si electrodes were vacuum dried for 24 h at 120^{o}C. Coin cells (CR2032) were fabricated with BF-Si electrodes, polypropylene separator (Celgard 3501), and lithium foil in a high purity Ar-filled glove box. Two different electrolytes were used: 1.2 M $LiPF_6$ in ethylene carbonate (EC) (BASF) and 1.2 M $LiPF_6$ in fluorethlyene carbonate (FEC) (BASF). Each coin cell contains 30 uL of electrolyte.

Special coin cells, containing binder-free silicon electrodes with copper TEM grids (Figure 1), were assembled [20]. Silicon was removed from the center of the BF-Si electrode to allow placement of the copper TEM grid. During cell construction some of the silicon nano-particles shifted from the BF-Si electrode and adhered to the copper TEM grid enabling TEM visualization of cycled Si particles. Cell assembly was conducted in an Ar-atmosphere glove box (<1 ppm H_2O).

Electrochemical cycling

Coin cells undergo a constant-current charge and discharge between 2.0 to 0.05 V on a ARBIN BT 2000 cycler with a current density of ~50 A/cm^2 which is approximately a C/20 rate. The cells were cycled with the following procedures: first cycle at C/20, second cycle at C/10, and remaining cycles at C/5 at 25^oC. Cells cycled comparably with and without the integrated TEM grids.

XPS, FTIR, and NMR

X-ray photoelectron spectroscopy (XPS) of BF-Si electrodes was conducted on a PHI 5500 system using Al K_α radiation source ($h\nu$=1486 eV). The binding energies of all elements were calibrated based on the C-H binding energy at 285 eV. The spectra were analyzed and fitted by Multipack 6.1 and XPS peak software (version 4.1). Line syntheses of elemental spectra were conducted using Gaussian–Lorentzian (70:30) curve fitting. Element concentration was calculated based on the equation: $Cx = (I_x/S_x)/(\sum I_i/S_i)$, where I_x is the intensity of the relative element, and S_i is the sensitivity number of the element[23]. Scanning electron microscopy was conducted on a JEOL-5900 SEM. FTIR-ATR spectra were acquired on a Bruker-2700 with Ge crystal detector; the data were collected in an Ar-purged chamber. All NMR samples were prepared via extraction from cycled BF-Si electrodes by D_2O in an Ar-filled glove box; the BF-Si electrodes were rinsed with anhydrous DMC to remove residual electrolyte and dried overnight under vacuum prior to D_2O extraction. Multinuclear NMR analyses were conducted on a Bruker Avance III 300 MHz NMR spectrometer.

Results

Electrochemical Cycling

The first cycle plots for $LiPF_6$/EC and $LiPF_6$/FEC electrolytes have similar lithiation capacities (~3000 mAh/g) and delithiation capacities (~1800 mAh/g) (Figure 2a). Thus, both electrolytes also have large first cycle irreversible capacity, 38% and 36% for $LiPF_6$/EC and $LiPF_6$/FEC, respectively. The first cycle discharge capacity and cycling efficiency are in agreement with previous reports.[24-25] The capacity retention for BF-Si electrodes cycled for 20 cycles with $LiPF_6$/EC and $LiPF_6$/FEC electrolytes are depicted in Figure 2b. Due to the nature of binder-free electrodes and silicon anode materials, the electrodes suffer more rapid capacity fading than other silicon electrodes. However, better capacity retention (~1000 mAh/g after 20 cycles) and more stable cycling efficiency (~98 %) are observed for cells cycled with the $LiPF_6$/FEC electrolyte.

Good reversible cycling of graphite or silicon anodes in lithium ion batteries requires the generation of a stable solid electrolyte interface (SEI).[26-27] Thus the differences in cycling performance between EC and FEC suggest that there may be differences in the SEI generated in the presence of different solvents. In order to develop a better understanding of the different cycling behavior, the $LiPF_6$/EC and $LiPF_6$/FEC containing cells were disassembled and ex-situ analysis of the BF-Si electrodes was conducted after the 1^{st}, 5^{th} and 20^{th} cycle.

TEM analysis of BF-Si electrode

Integration of TEM grids into the BF-Si anode allows the acquisition of images of cycled silicon nano-particles directly from cells after cycling. The morphology of BF-Si anode particles has been monitored after the 1^{st}, 5^{th}, and 20^{th} cycle. The morphology of BF-Si anodes cycled with $LiPF_6$/EC electrolyte compared to fresh BF-

Si anode nano-particles is depicted in 3 while the elemental concentrations of the surface, as determined by EDX, are provided in the Figure 3 insets. After 1 cycle the sharp edges of the fresh silicon nano-particles are converted to a rough inhomogeneous layer consistent with the generation of an SEI. However, the individual Si nano- particles remain discrete. EDX analysis indicates the presence of C, O, F, and P (5.9, 9.6, 0.9, and 0.5 %, respectively) consistent with the deposition of electrolyte decomposition products. After five cycles the Si nano-particles are covered and connected by a thick SEI and the silicon particles are no longer discrete (Figure 3c). The surface EDX concentrations of C, O, F, and P (13.2, 18.1, 1.5, and 0.5, respectively) are higher and consistent with a thicker SEI. The integration of the SEI with the BF-Si nano-particles is more apparent after 20 cycles. The C and O concentrations are comparable to the concentration of Si (26.2, 33.4, and 36.2 %, respectively) suggesting a very high concentration of electrolyte decomposition products on the surface of the BF-Si nano-particles and incorporation of Si containing species into the SEI. The repeated volume expansion and contraction of the nano-particle leads to significant increases in the concentration of electrolyte decomposition products and results in significant change to the silicon nano-particles.[28-29]

Analysis of the BF-Si electrode cycled with the $LiPF_6$/FEC electrolyte suggests different and less severe morphological changes to the nano-particles (Figure 4). After the first cycle, the BF-Si particles retain a spherical shape and have clear edges. A thinner SEI is observed with grainy particles (5-10 nm) on the surface of the silicon nano-particles. The elemental concentrations of C and O are similar to those observed for BF-Si cycled with $LiPF_6$/EC electrolyte, but the concentration of F is much higher

(5.2 % compared to 0.9 % for the electrode cycled with $LiPF_6$/EC). After additional cycling, the SEI becomes thicker and very grainy. However, the Si nano-particles remain largely intact and the SEI and Si nanoparticles appear more distinctly separate than that observed for BF-Si cycled with $LiPF_6$/EC electrolyte. Thus the deposition of the electrolyte decomposition products appears to be occurring on the surface of the Si nano-particles with the $LiPF_6$/FEC electrolyte. The composition of the SEI generated from the $LiPF_6$/FEC electrolyte is also quite different than the SEI generated from the $LiPF_6$/EC electrolyte. Analysis of the elemental concentration at the surface with EDX after 20 cycles suggests that the SEI generated from $LiPF_6$/FEC has a much higher concentration of F than the SEI generated from $LiPF_6$/EC, 32.8 and 3.5 %, respectively.

The cycled BF-Si electrodes were also analyzed by TEM after extraction with D_2O (Figure 5). The cycled BF-Si electrodes were extracted with D_2O to allow the characterization of SEI components via solution NMR spectroscopy, as described below.[20] After extraction, the residual silicon nanoparticles were deposited onto a TEM grid and vacuum dried. The silicon nanoparticles cycled with EC or FEC have very different morphology after D_2O extraction. The thick integrated SEI formed on the BF-Si electrode after cycling with $LiPF_6$/EC is no longer observed. Some distinct silicon nanoparticles are observed but most of the material is agglomerated into fused particles. Analysis of the particles by EDX reveals a significant decrease in the concentration of C and F (14.6 and 0.7%, respectively) after extraction suggesting that most of the C and F containing species are dissolved in the D_2O. The residual nanoparticles are dominated by Si and O (14.6 and 58.5 %, respectively) consistent

with the presence of SiO_2. The silicon nanoparticles cycled with $LiPF_6$/FEC are also significantly modified upon D_2O extraction. Analysis of the silicon nanoparticles by EDX reveals a large decrease in the concentration of F (32.8 to 0.3 %) and a large increase in the concentration of C (26.5 to 70.5 %) suggesting that most of the F containing species are soluble in D_2O while most of the C containing species are D_2O insoluble. Thus the C containing SEI components generated from $LiPF_6$/EC and $LiPF_6$/FEC have significantly different structures and properties.

XPS analysis of BF-Si electrodes

The XPS spectra of BF-Si electrodes extracted from cells cycled with $LiPF_6$/EC electrolyte after the 1^{st}, 5^{th} and 20^{th} cycle are presented in Figure 6 and the elemental concentrations are summarized in Table I. The absence of binder in the BF-Si electrodes allows more straight forward analysis of the SEI. The spectra suggest changes to the electrodes surface as a result of cycling. The fresh BF-Si electrode is dominated by Si and O due to the presence of SiO_2 on the surface of the nano-particles, and contains a weak C peak associated with universal carbon contamination. Upon cycling with $LiPF_6$/EC electrolyte, the concentration of Si decreases significantly, the concentration of O also decreases, but the concentrations of C and F increase. The largest changes are observed after the first cycle, but the elemental concentrations continue to have small fluctuations with increased cycling, which suggests that the SEI continues to evolve.

The element spectra of the fresh BF-Si electrode contain two clearly separated peaks in the Si 2p spectrum characteristic of SiO_2 (103.5 eV) and Si (99.5 eV). Upon cycling, the two strong peaks are converted to a weak broad peak centered at ~102 eV

which is assigned to Li_xSiO_y.[11] For the fresh electrode the major C1s peak at 285 eV is consistent with alkane species and the universal hydrocarbon contamination. Upon cycling, new C1s peaks are observed at 286.5 and 290 eV consistent with the presence of species containing C-O and O-(C=O)-O, respectively. A single broad peak is observed in the O1s spectra consistent with the presence of C-O and O-(C=O)-O containing species at 533–534 and 532–533 eV, respectively. The peaks observed in the C1s and O1s spectra are consistent with the presence of LEDC, from the reduction of EC. The F1s spectrum contains a single peak at 685 eV supporting the presence of LiF.[16] The XPS results are similar to those previously reported for thin film silicon, silicon nano-wires, and silicon nanopatricles, and consistent with the generation of a SEI composed of LEDC, LiF and some Si containing species.[11, 17-18] The concentration of silicon is low, suggesting that the SEI is primarily composed of electrolyte reduction products and is similar to that observed on graphite electrodes.[20] The XPS element spectra of BF-Si electrodes extracted from cells cycled with the $LiPF_6$/FEC electrolyte are provided in Figure 7 and the element concentrations are summarized in Table II. Upon cycling with $LiPF_6$/FEC electrolyte the concentrations of Si and O decrease significantly while the concentrations of C and F increase, consistent with the generation of an SEI. Concentrations of Si, C, O, and F for BF-Si electrodes extracted after 1 cycle with $LiPF_6$/FEC electrolyte are similar to BF-Si electrodes extracted after 1 cycle with $LiPF_6$/EC electrolyte. However, upon additional cycling the concentration of F is significantly higher while the concentration of O is significantly lower for cells cycled with $LiPF_6$/FEC compared to cells cycled with $LiPF_6$/EC electrolyte, consistent with a change in the SEI structure.

The element spectra of the BF-Si electrode extracted from a cell after one cycle with $LiPF_6$/FEC contains two peaks in the Si_2p spectrum at 99.5eV and 103.5eV, characteristic of Si and SiO_2 respectively. However, after 20 cycles the peaks for Si and SiO_2 are diminished and a peak at ~102 eV is observed consistent with the formation of Li_xSiO_y.[11] The results are similar to that observed for BF-Si electrodes cycled with $LiPF_6$/EC electrolyte, although a larger number of cycles are required to bring about comparable changes. The other element spectra (C, O, and F) are changed significantly after the first cycle but increased cycling results in only small changes. The C1s spectra contain three peaks at 285, 286.5 and 290 eV, characteristic of C-H, CH_2-O, and O-(C=O)-O containing species, and are similar to the C1s spectra of BF-Si electrodes cycled with $LiPF_6$/EC electrolytes although the peaks characteristic of O-(C=O)-O containing species are weaker for electrodes cycled with the $LiPF_6$/FEC electrolyte. The O1s spectra contain a broad peak centered at ~533 eV consistent with the presence of (CO(O)C]O*) (532.5 eV) and (CO*(O)C]O) (533.5 eV) containing species.[15] The F1s spectra contain a dominant peak for LiF at 685eV and a small peak at 687 eV suggesting the presence of $Li_xPF_yO_z$. The P2p XPS spectra are not included because of weak signal intensities. The XPS results support the TEM-EDX results suggesting that the SEI is composed of LiF, Li_xSiO_y and a polymeric species containing C-O and O-(C=O)-O bonds.[17-18] The concentration of LiF is much higher in the SEI generated from $LiPF_6$ in FEC than the SEI generated from $LiPF_6$ in EC.

FTIR analysis of BF-Si Electrodes

FTIR spectra were collected from BF-Si electrodes extracted from cells cycled with $LiPF_6$/EC electrolyte after the 1^{st}, 5^{th} and 20^{th} cycle, respectively (Figure 8a). The Fresh electrodes contain a broad absorbance with peaks at 1220 and 1100 cm^{-1}

due to the Si-O_x functional group on the surface of the Si nano-particles of the BF-Si electrodes. The IR spectrum of BF-Si electrode after the first cycle contains more absorption peaks located at 1655, 1416, 1305, 1145, and 845cm-1 characteristic of LEDC, as previously reported,[30] along with overlapping absorptions associated with Li_2CO_3 at 1420 cm^{-1} and O-Si-O with lithium silicates (LixSiOy) at 1070 cm^{-1}. Close to 845cm-1, another small peak at 865 is from P-F contained salts. Continued cycling results in increases in the intensity of the peaks associated with LEDC and decreases in the intensity of the Li_2CO_3 and O-Si-O absorptions consist with an increase in the concentration of LEDC with increased cycling and the generation of a thicker SEI. The major peak at 985cm^{-1} is assignable to Li_XsiOy as displaed in IR spectrum of electrode with five cycles. Comparing with peak at 1070 cm on IR spectrum of electrode after first cycle, the peak shifted to 985 due to upon cycling lithiated state of silicon nanoparticles changed and dominated by lithium silicates as displayed in XPS Si_2p spectra. The same shift also found on IR spectrum of BF-silicon electrodes after 20 cycles. The shift of si-o and LixSiOy resulted from the lithiaed and delithiaed state change during cycling. A similar trend is observed for the IR spectra of BF-Si electrodes extracted from cells cycled with $LiPF_6$/FEC electrolyte, Figure 8b. Upon cycling the peaks characteristic of Si-O bonds at 1220 and 1100 cm^{-1} are diminished consistent with the deposition of electrolyte decomposition products on the surface. The spectrum of the BF-Si electrode after one cycle contains weak absorption bands at: 1640, 1450, 1090, and 847 cm^{-1}. The strong absorption at 870 cm^{-1} is from residual $LiPF_6$.[22] Additional cycling of the BF-Si electrodes with $LiPF_6$/FEC electrolyte results in an increase in the intensity of the absorptions observed after one

cycle, 1640, 1450, 1090 cm^{-1}, along with the appearance of a new absorption at 1810 cm^{-1}. The absorptions are very similar to those reported for polymeric decomposition product of FEC.[17] Peaks at 1640,1312 and 1075(overlapping with silicate)are attributed to the −C=O, C-O and O-C-C stretching of $-CO_2$-R, which is the possible structure of polymeric products. A small peak at 1261cm-1 is due to possible functional group P-O from LixPOF with very low concentration consistent with XPS F1s spectra suggested. The IR spectra are different from those observed for the BF-Si anode cycled with $LiPF_6$/EC supporting a change in the composition of the SEI.

NMR multinuclear analysis of BF-Si electrodes extracted with D_2O

In order to further characterize the structure of the SEI on BF-Si anodes, ^{1}H, ^{13}C, ^{19}F, and ^{29}Si NMR spectroscopy of D_2O extracts of the BF-Si electrodes has been conducted. The ^{1}H NMR spectra of extracts of BF-Si electrodes cycled with $LiPF_6$/EC electrolyte contain a single peak at 3.51 ppm (s) consistent with lithium ethylene dicarbonate (LEDC) (Figure 9a).[31] LEDC is the only reduction product of EC observed on graphite electrodes and thus the same reduction product of EC is observed on both silicon and graphite electrodes. The ^{13}C NMR spectrum contain a peak at 62.5 ppm, characteristic of LEDC.[20, 32] However, unfortunately due to the low concentration of the LEDC and the lack of hydrogen atoms directly attached to carbonyl carbon (lack of nuclear Overhauser effect) the resonance for the C=O is too weak to be observed. The intensity the LEDC resonance continually increases with increased cycling suggesting that the $LiPF_6$/EC electrolyte reduction continues and the BF-Si anode is not passivated during the first 20 cycles. The results are consistent with previous reports of continuous electrolyte reduction on Si electrodes due to the large volume changes. The lack of passivation is one of the most severe problems for

Si electrodes and is the main contributor to poor cycling performance [30]. The ^{19}F NMR spectra of extracts of BF-Si electrodes cycled with $LiPF_6$/EC electrolyte contain a single peak at 123 ppm (s), characteristic of LiF. The concentration of LiF increases with increasing cycle number suggesting that both EC and $LiPF_6$ continue to be reduced throughout the cycling process (Figure 10). The ^{29}Si NMR spectra of the D_2O extracts contain no observable resonances suggesting that the silicon species are either not soluble in water or the concentrations are below our detection limits.

The ^{1}H NMR spectra of D_2O extracts from BF-Si electrodes cycled with $LiPF_6$/FEC electrolyte contain no observable peaks even after 20 cycles (Figure 9b). The lack of any observable peaks in the ^{1}H NMR spectra is consistent with the presence of an insoluble organic polymer on the BF-Si anode surface.[17-18] The ^{19}F NMR spectra of the BF-Si extracts contain a single peak at 123 ppm (s), characteristic of LiF. The concentration of LiF increases with increasing cycle number. (Figure 10b) Moreover, the concentration of LiF is much greater for extracts of BF-Si electrodes cycled with $LiPF_6$/FEC than is observed for BF-Si electrodes cycled with $LiPF_6$/EC suggesting that FEC may be an additional source of LiF. In order to confirm that FEC can be a source of LiF, BF-Si/Li cells were cycled with 1.2 M $LiClO_4$/FEC. Analysis of the D_2O extracts of BF-Si electrodes cycled (one cycle) with $LiClO_4$/FEC electrolyte by ^{19}F NMR spectroscopy reveal a single resonance at -123 ppm consistent with the presence of LiF (Figure 11c). Thus the reduction reaction of FEC generates LiF along with an unstable organic radical species which is polymerized on the BF-Si electrodes (Scheme 1). The polymeric species has been proposed to be either a poly(alkene)[17] or a poly(carbonate).[18] However, due to the poor solubility of the

polymerized organic material, characterization via solution NMR spectroscopy is not possible.

Discussion

The SEI on BF-Si anodes was investigated for two different electrolytes, $LiPF_6$/EC and $LiPF_6$/FEC, via a combination of analytical techniques, TEM with EDX, solution NMR, XPS and FT-IR. The SEI generated from $LiPF_6$/EC is thick and becomes integrated with the silicon nano-particles after 20 cycles. The SEI is primarily composed of LEDC, LiF, and Li_xSiO_y. The concentrations of LEDC and LiF are high at the surface of the cycled particles, as detected via XPS (top ~5 nm). The concentration of the bulk SEI, as determined by TEM/EDX, contains high concentrations of Si, C, and O and a low concentration of F, consistent with an inner SEI composed primarily of Li_xSiOy and LEDC. The IR spectra and D_2O extracts of the cycled BF-Si electrodes reveal that LEDC is the single predominant organic component in the SEI. Thus the data are in qualitative agreement with the results of Edstrom and co-workers supporting an inner SEI primarily composed of Li_xSiO_y and LEDC and an outer SEI primarily composed of LEDC and LiF [10, 11]. The layered SEI is different than the homogeneous SEI generated on BF graphite anodes. The differences are likely due to the differences in the nature of Li-Si alloying and lithium intercalation into graphite. However, the primary decomposition products of the electrolyte are the same, LEDC and LiF. The SEI generated from $LiPF_6$/FEC after 20 cycles is quite different than the SEI generated from $LiPF_6$/EC. The SEI is primarily composed of LiF, Li_xSiO_y, and an insoluble organic polymer species. The concentration of LiF and the organic polymer are high at the surface of the cycled

particles as detected by XPS. However, the bulk SEI, as determined by TEM/EDX, has a much higher LiF content than that observed for the SEI generated from $LiPF_6$/EC. The Si concentration is lower (21.4 %) and the concentrations of C, O, and F of the bulk SEI (EDX, 26.5, 18.6, and 32.8 %, respectively) are similar to the surface SEI (XPS, 35.8, 29.5, and 29.4 %, respectively). The TEM images also depict a clearer demarcation between the silicon nano-particles and the SEI. This feature suggests that the SEI generated from $LiPF_6$/FEC is less layered and contains less Li_xSiO_y. The IR spectra reveal the presence of an organic polymer which likely contains some polycarbonate. The D_2O extractions reveal a high concentration of LiF, but no soluble organic components. An SEI composed of a high concentration of LiF and an organic polymer leads to better capacity retention of BF-Si anodes, but it is not clear which component, the high concentration of LiF or the organic polymer, is more important to SEI stability and capacity retention.

Conclusions

The cycling performance of BF-Si electrodes with $LiPF_6$/EC and $LiPF_6$/FEC electrolytes was investigated. The surfaces of BF-Si electrodes were examined via a unique combination of TEM with EDX, solution NMR, SEM, XPS, and FT-IR to understand the differences in cycling performance. Ex-situ TEM analysis suggests that there are significant changes to the silicon nano-particles upon cycling. Electrodes cycled with $LiPF_6$/EC electrolyte have poor cycling performance. The BF-Si nano-particles form a continuous amorphous phase with the SEI after 20 cycles. BF-Si electrodes cycled with $LiPF_6$/FEC have better capacity retention and clearer separation of the Si nano-particle and the SEI. The composition of the SEI was

characterized via NMR spectroscopy of the D_2O extracts of the BF-Si electrode. The primary components of the SEI formed with $LiPF_6$/EC electrolyte are LEDC, LiF and Li_xSiO_y. The predominant products of SEI formed with $LiPF_6$/FEC electrolyte are LiF, an insoluble polymeric species, and Li_xSiO_y. The concentration of LiF is much higher for BF-Si electrodes cycled with $LiPF_6$/FEC than with $LiPF_6$/EC and FEC is an additional source of LiF. The SEI formed with the $LiPF_6$/FEC electrolyte provides superior passivation of the BF-Si electrodes leading to better capacity and structure retention.

Acknowledgement

The authors gratefully acknowledge funding from Department of Energy Office of Basic Energy Sciences EPSCoR Implementation award (DE-SC0007074).

References

1. Obrovac, M. N.; Christensen, L.,Electrochem. Solid State Lett. 2004, 7 (5), A93-A96.

2. Chon, M. J.; Sethuraman, V. A.; McCormick, A.; Srinivasan, V.; Guduru, P. R.,Physical Review Letters 2011, 107 (4), 045503.

3. Benedek, R.; Thackeray, M. M.,J. Power Sources 2002, 110 (2), 406-411.

4. Ren, Y. R.; Ding, J. N.; Yuan, N. Y.; Jia, S. Y.; Qu, M. Z.; Yu, Z. L.,J. Solid State Electrochem. 2012, 16 (4), 1453-1460.

5. Wu, H.; Cui, Y.,Nano Today 2012, 7 (5), 414-429.

6. Aurbach, D.,Journal of Power Sources 2000, 89 (2), 206-218.

7. Verma, P.; Maire, P.; Novák, P.,Electrochim. Acta 2010, 55 (22), 6332-6341.

8. Li, S. Y.; Xu, X. L.; Shi, X. M.; Li, B. C.; Zhao, Y. Y.; Zhang, H. M.; Li, Y. L.; Zhao, W.; Cui, X. L.; Mao, L. P.,J. Power Sources 2012, 217, 503-508.

9. Xu, K.,Chemical Reviews 2004, 104 (10), 4303-4418.

10. Philippe, B.; Dedryvère, R.; Gorgoi, M.; Rensmo, H.; Gonbeau, D.; Edström, K.,Chemistry of Materials 2013.

11. Philippe, B.; Dedryvere, R.; Allouche, J.; Lindgren, F.; Gorgoi, M.; Rensmo, H.; Gonbeau, D.; Edstrom, K.,Chemistry of Materials 2012, 24 (6), 1107-1115.

12. Arreaga-Salas, D. E.; Sra, A. K.; Roodenko, K.; Chabal, Y. J.; Hinkle, C. L.,J. Phys. Chem. C 2012, 116 (16), 9072-9077.

13. Trill, J. H.; Tao, C. Q.; Winter, M.; Passerini, S.; Eckert, H.,J. Solid State Electrochem. 2011, 15 (2), 349-356.

14. Elazari, R.; Salitra, G.; Gershinsky, G.; Garsuch, A.; Panchenko, A.; Aurbach, D.,Journal of the Electrochemical Society 2012, 159 (9), A1440-A1445.

15. Choi, N. S.; Yew, K. H.; Lee, K. Y.; Sung, M.; Kim, H.; Kim, S. S.,J. Power Sources 2006, 161 (2), 1254-1259.

16. Dalavi, S.; Guduru, P.; Lucht, B. L.,Journal of the Electrochemical Society 2012, 159 (5), A642-A646.

17. Etacheri, V.; Haik, O.; Goffer, Y.; Roberts, G. A.; Stefan, I. C.; Fasching, R.; Aurbach, D.,Langmuir 2011, 28 (1), 965-976.

18. Nakai, H.; Kubota, T.; Kita, A.; Kawashima, A.,Journal of the Electrochemical Society 2011, 158 (7), A798-A801.

19. Lin, Y. M.; Klavetter, K. C.; Abel, P. R.; Davy, N. C.; Snider, J. L.; Heller, A.; Mullins, C. B.,Chemical Communications 2012, 48 (58), 7268-7270.

20. Nie, M.; Chalasani, D.; Abraham, D. P.; Chen, Y.; Bose, A.; Lucht, B. L.,The Journal of Physical Chemistry C 2013, 117 (3), 1257-1267.

21. Kang, S. H.; Abraham, D. P.; Xiao, A.; Lucht, B. L.,J. Power Sources 2008, 175 (1), 526-532.

22. Xiao, A.; Yang, L.; Lucht, B. L.; Kang, S. H.; Abraham, D. P.,Journal of the Electrochemical Society 2009, 156 (4), A318-A327.

23. Benoit, R.,Vide-Sci. Techn. Appl. 2003, 58 (308), 219-+.

24. Ng, S.-H.; Wang, J.; Wexler, D.; Konstantinov, K.; Guo, Z.-P.; Liu, H.-K.,Angewandte Chemie International Edition 2006, 45 (41), 6896-6899.

25. Wen, Z. S.; Yang, J.; Wang, B. F.; Wang, K.; Liu, Y.,Electrochemistry Communications 2003, 5 (2), 165-168.

26. Song, J. W.; Nguyen, C. C.; Song, S. W.,RSC Adv. 2012, 2 (5), 2003-2009.

27. Nguyen, C. C.; Song, S. W.,Electrochim. Acta 2010, 55 (8), 3026-3033.

28. Sethuraman, V. A.; Srinivasan, V.; Bower, A. F.; Guduru, P. R.,Journal of the Electrochemical Society 2010, 157 (11), A1253-A1261.

29. Bettge, M.; Li, Y.; Sankaran, B.; Rago, N. D.; Spila, T.; Haasch, R. T.; Petrov, I.; Abraham, D. P.,Journal of Power Sources 2013, 233 (0), 346-357.

30. Zhuang, G. R. V.; Xu, K.; Yang, H.; Jow, T. R.; Ross, P. N.,J. Phys. Chem. B 2005, 109 (37), 17567-17573.

31. Xu, K.; Zhuang, G. R. V.; Allen, J. L.; Lee, U.; Zhang, S. S.; Ross, P. N.; Jow, T. R.,J. Phys. Chem. B 2006, 110 (15), 7708-7719.

32. Chan, C. K.; Ruffo, R.; Hong, S. S.; Cui, Y.,J. Power Sources 2009, 189 (2), 1132-1140.

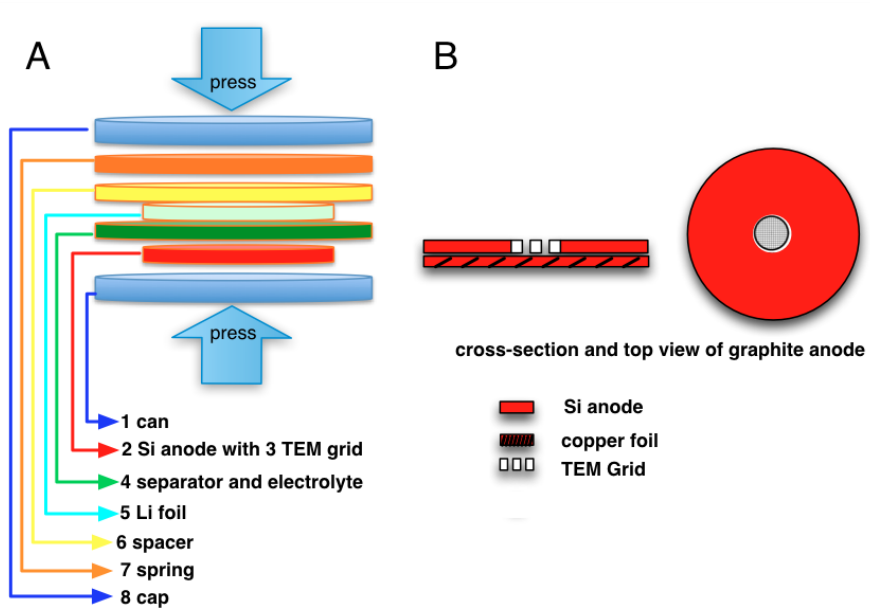

Figure 3-1. Schematic diagram and picture showing (A) the assembly of a Li/BF-Si half-cell (B) TEM-grid embedded BF-Si electrode.

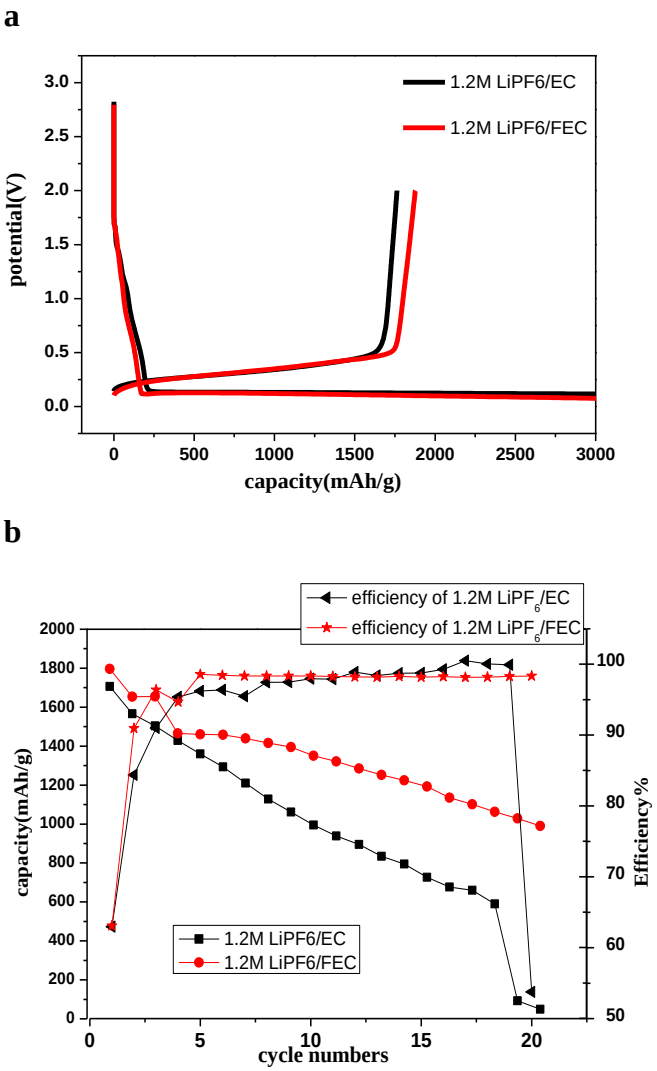

Figure 3-2. (a) first cycle charge/discharge profiles of BF-Si electrodes half cells with two electrolytes (b) cycling performance of EC and FEC-containing electrolytes in BF-Si cells at 20 cycles.

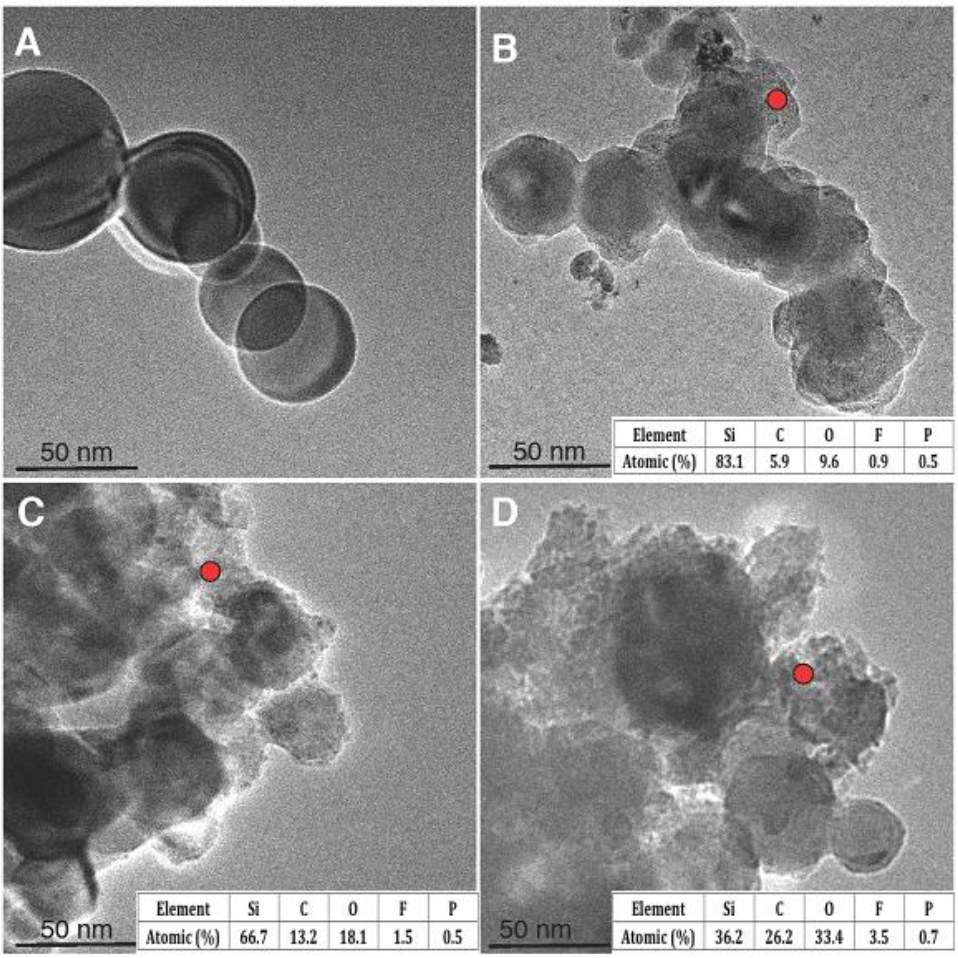

Figure 3-3. TEM images of BF-Si electrodes cycled with 1.2M $LiPF_6$/EC (right): A Fresh BF-Si, B BF-Si after 1^{st} cycle, C BF-Si with 5^{th} cycle and D BF-Si after 20^{th} cycle.

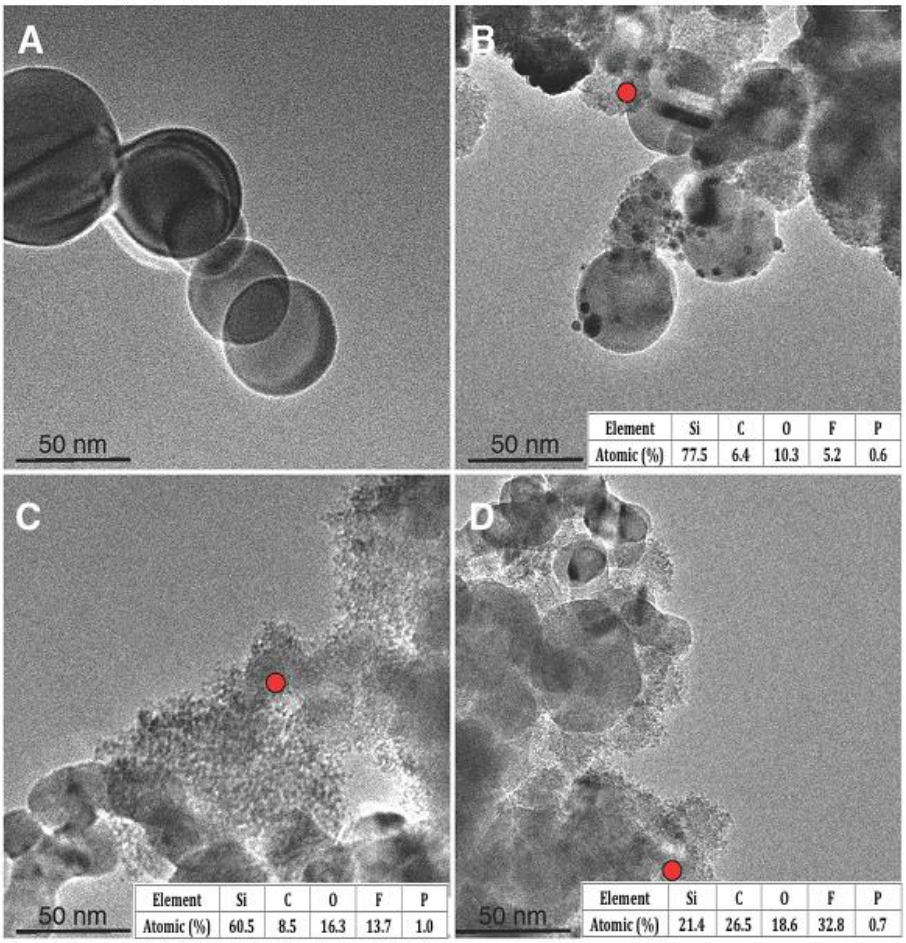

Figure 3-4. TEM images of BF-Si electrodes cycled with 1.2M $LiPF_6$/FEC (right): A, Fresh BF-Si, B, BF-Si after 1st cycle, C, BF-Si with 5th cycle and D, BF-Si after 20th cycle.

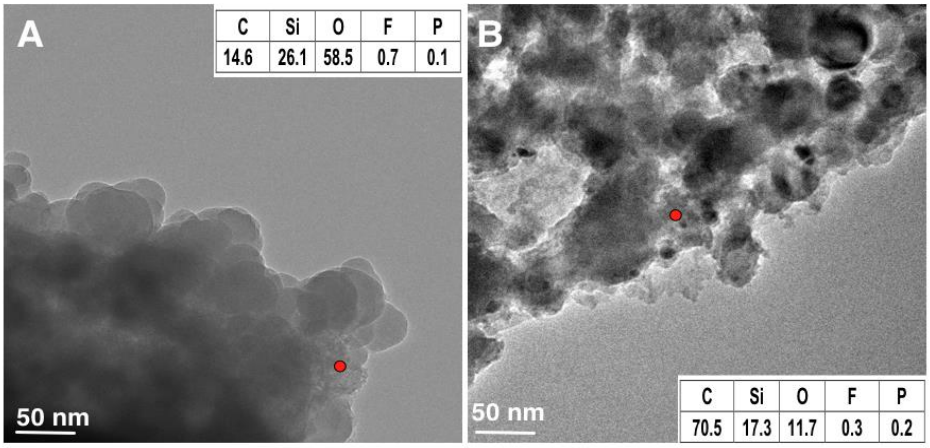

Figure 3-5. TEM images of BF-Si electrodes after 20 cycles followed by D_2O extraction. (A) 1.2 M $LiPF_6$/EC; (B) 1.2 M $LiPF_6$/FEC

Element	C	O	Si	F
Fresh	19.0	45.7	35.3	
1st	31.6	33.4	8.3	26.7
5th	36.1	35.9	4.6	23.4
20th	40.1	35.7	3.5	20.7

Table 3-1: Elemental concentration on fresh and cycled BF-Si electrodes for different cycle numbers in EC-electrolyte.

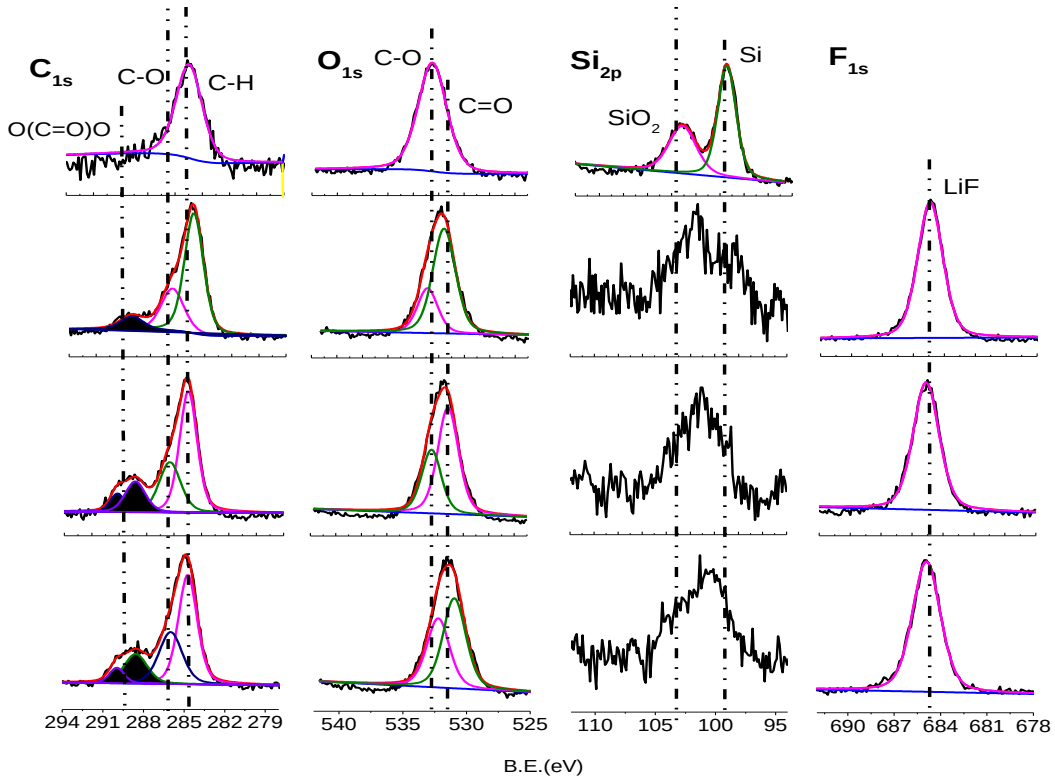

Figure 3-6. XPS spectra of BF-Si electrode cycled with EC-electrolyte from top: Fresh electrode, 1st cycle, 5th cycle and 20th cycle.

Element	C	O	Si	F
Fresh	19.0	45.7	35.3	
1st	32.7	28.7	15.2	23.4
5th	35.5	29.7	6.5	28.3
20th	35.8	29.5	5.3	29.4

Table 3-2: Elemental concentration on cycled BF-Si electrodes for different cycle numbers in FEC-electrolyte.

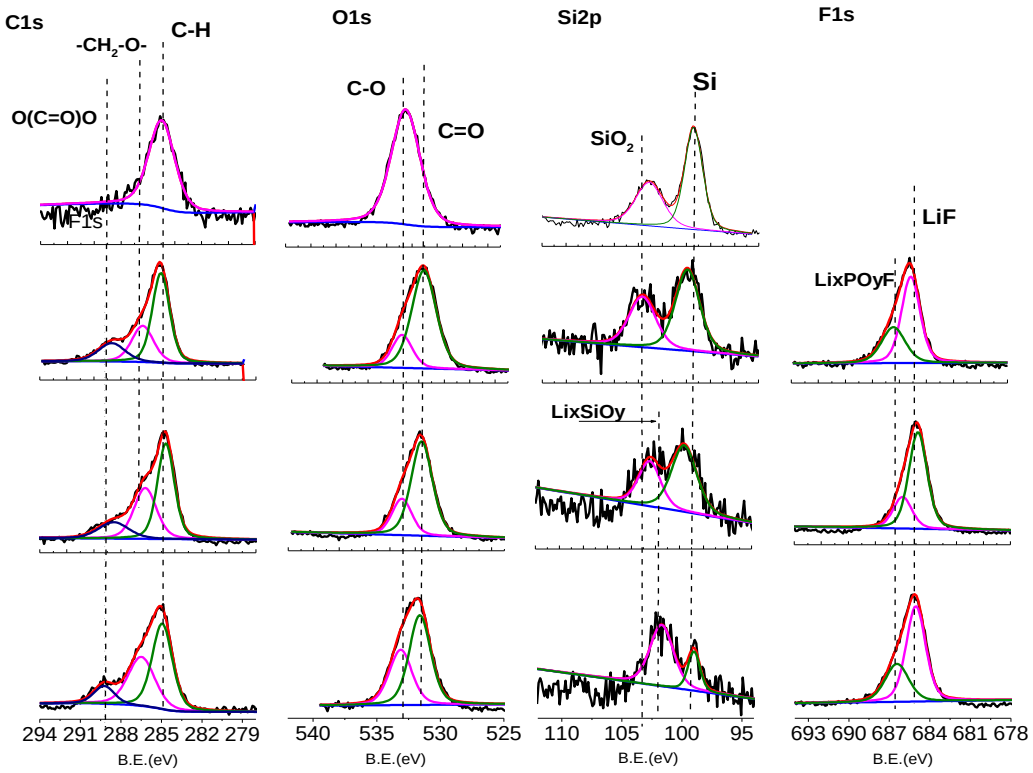

Figure 3-7. XPS spectra of BF-Si electrode cycled with FEC-electrolyte from top: Fresh electrode, 1st cycle, 5th cycle and 20th cycle.

a

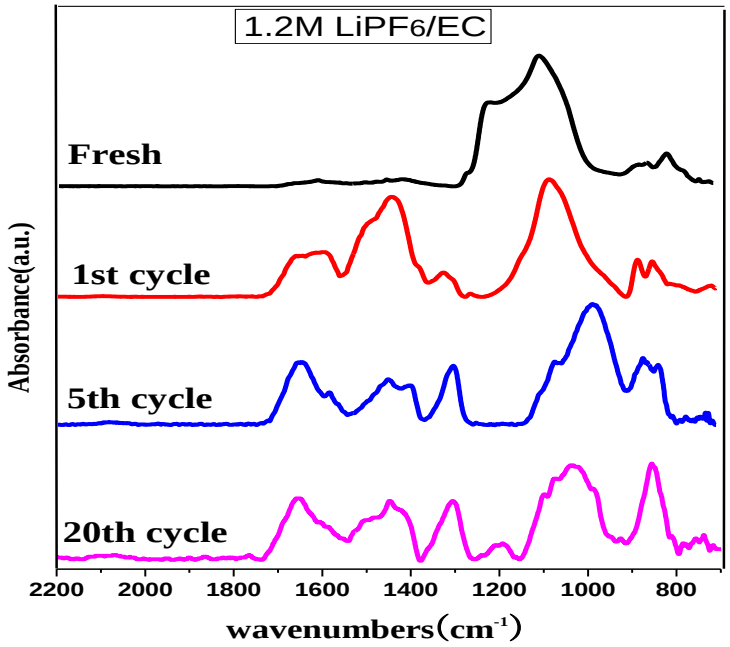

b

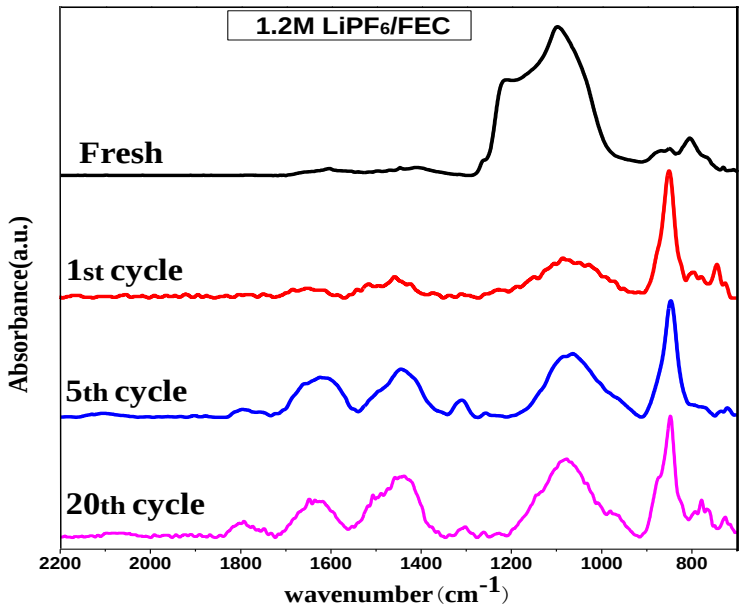

Figure 3-8. (a) IR spectra of BF-Si electrodes cycled with EC-electrolyte from top: Fresh electrode, 1st, 5th and 20th cycle. (b) BF-Si electrodes cycled with FEC-electrolyte from top: 1st, 5th and 20th cycle.

a

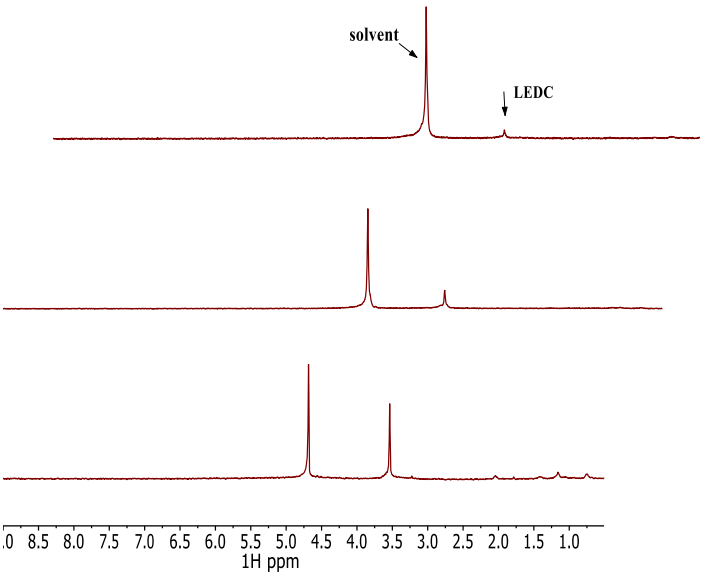

b

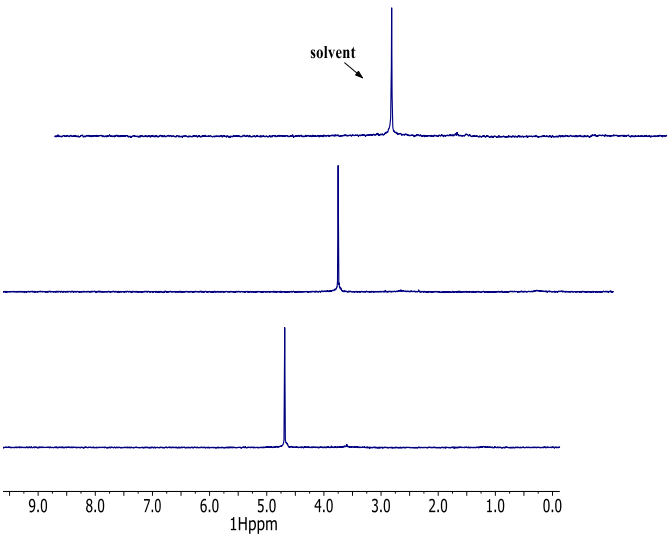

Figure 3-9. (a) ^{1}H NMR spectra of BF-Si electrode cycled in EC-electrolyte and exacted by D_2O from top: first cycle, fifth cycle and 20^{th} cycle. (b) ^{1}H NMR spectra of BF-Si electrode cycled in FEC-electrolyte and exacted by D_2O from top: 1^{st} cycle, 5^{th} cycle and 20^{th} cycle.

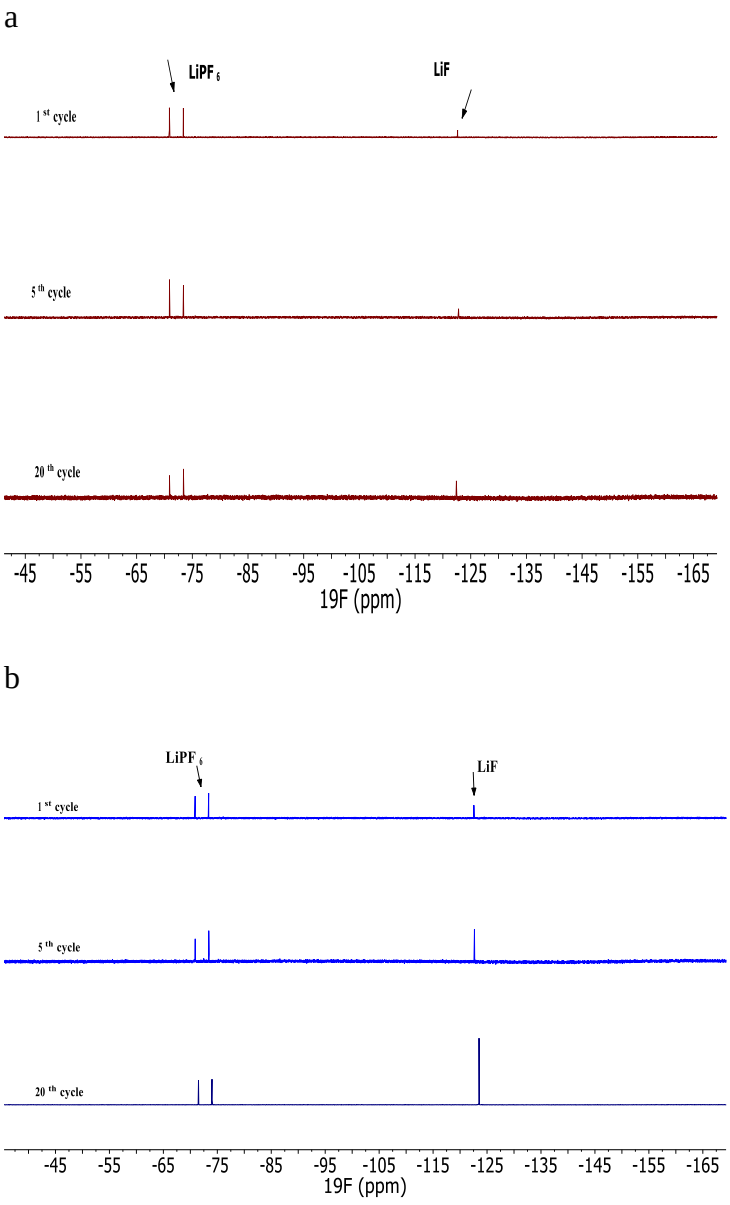

Figure 3-10. (a) ^{19}F NMR spectra of BF-Si electrode cycled in EC-electrolyte and exacted by D2O from top: 1st cycle, 5th cycle and 20th cycle. (b) ^{19}F NMR spectra of BF-Si electrode cycled in FEC-electrolyte and exacted by D_2O from top: 1st cycle, 5th cycle and 20th cycle.

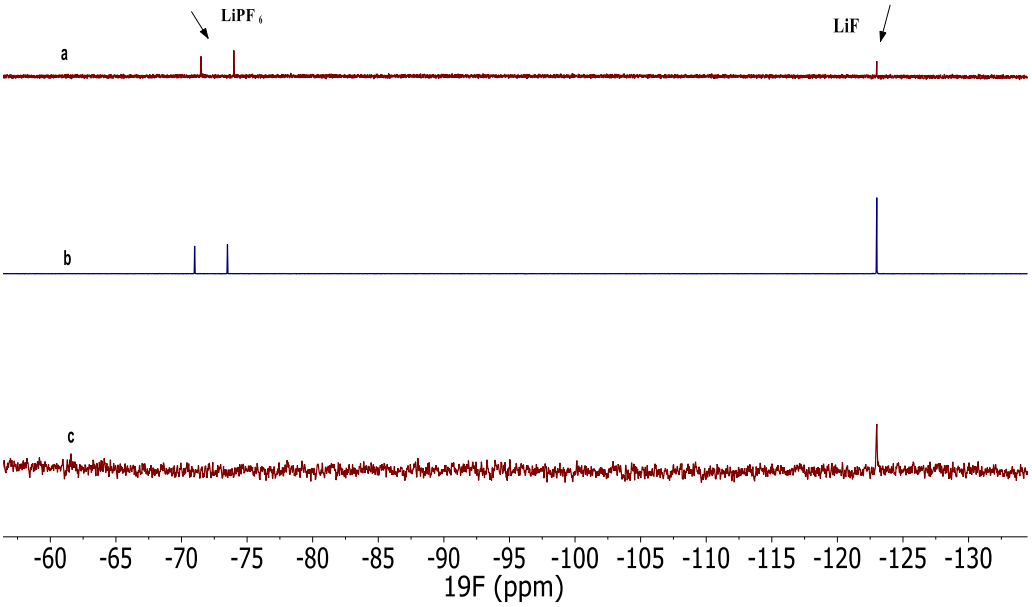

Figure 3-11 (a) ^{19}F NMR spectrum of BF-Si electrode cycled in EC-electrolyte after 20 cycles. (b) ^{19}F NMR spectrum of BF-Si electrode c cycled in FEC-electrolyte after 20 cycles. (c)BF-Si electrodes cycled in 1.2 M $LiClO_4$/FEC electrolyte.

CHAPTER 4

ROLE OF SOLUTION STRUCTURE IN SOLID ELECTROLYTE INTERFACE (SEI) FORMATION ON GRAPHITE WITH $LiPF_6$ IN POPYLENE CARBOANTE (PC)

Mengyun Nie[1], Daniel P. Abraham[2], Daniel M. Seo[1],Yanjing Chen[1], Arijit Bose[1], and Brett L. Lucht[1]

[1]*University of Rhode Island, Kingston, Rhode Island 02881, United States*

[2]*Argonne National Laboratory, Argonne, Illinois 60439, United States*

The following was published in the Journal of the Physical Chemistry C, and is presented here in manuscript format

Introduction:

Since the initial commercialization of lithium ion batteries (LIBs) in 1991, the LIB market has rapidly grown to dominate the portable electronic market and is currently expanding into the electric vehicle market. During this time there have been significant advances in the development of both anode and cathode materials for LIBs.[1] However, advances in the development of electrolytes for LIB has progressed more slowly.[2] One of the most important components of the LIB is the solid electrolyte interphase (SEI) generated on the surface of the graphitic anode during the first few charging cycles via the reductive decomposition of the electrolyte.[3-10] Ideally, the SEI functions as a passivation layer and is lithium ion conducting but electrically insulating allowing lithium ions to intercalate and deintercalate the electrode while preventing electrolyte reduction at the anode surface. While there has been significant research on the structure and properties of the anode SEI,[3-10] there have been few investigations on the role electrolyte solution structure on the SEI formation mechanism.[11-12]

There has recently been increased interest in developing a better understanding of the solution structure of electrolytes for lithium ion batteries. The lithium cation coordination sphere has been investigated by IR, NMR, Raman, DSC, MS, and computational methods.[13-20] In electrolyte solutions with weakly coordinating anions and polar aprotic solvents, including PC, EC, and acetonitrile, the coordination sphere of the Li cation typically contains four solvent molecules, but ion pairing is also frequently observed.[20] The solvated cations have an important role in the reaction mechanism and properties of the SEI. Understanding how solvation influences the

solution structure and reactivity of lithium complexes with weakly coordinating anions at the anode interface is very difficult due to rapid solvent exchange on the lithium cation, the presence of different solvent molecules within common electrolytes resulting in mixed solvation, the possibility of ion pairing, and the inhomogeneous nature of the surface reactions. Developing a better understanding of the role of electrolyte solution structure on SEI formation is critical for the development of superior LIBs.

The difference in cycling performance between EC and PC based electrolytes with graphite anodes has long been a mystery in the field of lithium batteries.[21] Electrolytes containing EC have good cycling performance which is typically attributed to the formation of a stable anode SEI.[5-6] Alternatively, electrolytes containing PC have poor cycling performance due to continuous electrolyte reduction due to the lack of the formation of a stable anode SEI.[22] There have been numerous investigations into the differences in cycling behavior. Most of these investigations attribute the differences to the co-intercalation of PC solvent molecules with the Li cation into the graphite sheets which leads to exfoliation of the graphite.[23-26] Other investigations attribute the differences to the physical properties of the electrolyte reduction products.[27-29] In some cases good cycling performance has been observed with PC containing electrolytes when SEI forming additives.[30-32] In these cases, the additives are preferentially reduced on the anode surface to generate a stable SEI preventing continuous PC reduction. In other investigations, reversible cycling of PC electrolytes has been observed at high concentrations of $LiPF_6$ or low concentrations of PC.[12,33]

We have recently reported on the use of Binder Free (BF) graphite electrodes with integrated TEM grids for characterization of the anode SEI.[34-36] In this manuscript, we report an investigation of the electrochemical properties, solution structure, anode SEI structure, and SEI formation mechanism for electrolytes containing various concentrations of $LiPF_6$ in PC with a BF graphite electrode. The electrochemical properties have been investigated via a combination of cyclic voltammetry and galvanostatic cycling. The solution structure has been investigated via a combination of IR spectroscopy and DOSY Nuclear Magnetic Resonance (NMR) spectroscopy. The anode SEI has been characterized via a combination of Transmission Electron Microscopy (TEM) with Energy Dispersive X-ray Spectroscopy (EDX), NMR spectroscopy of D_2O extracts from cycled anodes, XPS and IR This combination of techniques has provided significant new insights into the role of solution structure in SEI formation mechanisms.

Experimental Sections

Preparation of Binder-Free Electrodes

Binder-free electrodes are made by Electrophoretic Deposition (EPD). In this method, graphite particles (SFG-6, TIMCAL, 5 g/L) are suspended in acetonitrile solution by ultra-sonication followed by the addition of Triethylamine (1mL/L). A copper current collector is immersed in the EPD bath and a DC potential of 50 V is applied for 2 minutes. Graphite particles are deposited evenly on the copper surface to yield a Binder-Free (BF) Graphite Electrode. The electrode is placed in a vacuum oven at ~120 ℃ overnight to dry the electrode then transferred to an argon-filled gloved box.

Preparation of electrolytes coin cells

Propylene Carbonate is used to dissolve various concentrations of $LiPF_6$. Five $PC/LiPF_6$ electrolytes with different concentration were prepared: 1.2 M, 2.4 M, 2.8 M, 3.0 M and 3.5 M $LiPF_6$/PC. Binder-free graphite electrodes were prepared with copper TEM grids integrated into the binder-free graphite electrode.[36] Cell assembly was conducted in an Ar-atmosphere glove box (<1 ppm H_2O,). Cells experience one galvanostatic charge/discharge cycle at C/20 rate from 2.0 V to 0.05 V in by Arbin BT2000 battery cycler at 25 ^oC.

Cyclic voltammetry

Cyclic voltammetry was conducted in two electrode (BF-graphite/Li) CR2032 coin cells with a Princeton Versa STAT 3 at 20 ^oC. The scan rate was 0.05 mV/s from 0.05-2 V. Three scans were conducted for each cell.

IR and DOSY NMR Spectroscopy

Diffusion-ordered Nuclear Magnetic Resonance Spectroscopy (DOSY NMR) and Infrared (IR) spectroscopy was conducted on pure electrolyte samples.

The Simulated Echo pulse sequence (STEBPGP1S) is used for DOSY experiments. According to Stejskal–Tanner equation (Equation 1), upon adjusting the gradient strength (G_i) from 2% to 95%, the attenuated signal strength of peaks (I) on ^7Li and ^{19}F are detected.

$$I=I_0 \exp\left[-D\left(2\pi\gamma G_i\delta\right)^2\left(\Delta-\frac{\delta}{3}\right)\right] \quad \text{Eq 1}$$

Where I is the intensity of monitored peak and γ is gyromagnetic ratio of nucleus under investigation. The length of the gradient pulse (δ) and diffusion time (Δ) have

been optimized for the DOSY measurements. The data has been analyzed by Bruker Topspin software and 32 single spectra with varying gradients strength have been taken to provide 32 points in experimental data plot. Linear fitting of a plot of ln(I) vs.Gi^2 provides the diffusion coefficient of monitored nuclei.

FTIR was measured by Bruker TENSOR 27 spectrometer with an ATR accessory. FTIR bands were deconvoluted with the combination of Gaussian/Lorentzian function. The area of deconvoluted bands were collected and the relative area of uncorrdinated solvent and coordinated solvent were calculated. The concentrations of coordinated and uncoordinated solvent were calculated with the assumption that IR band of uncoordinated and coordinated solvent have equal sensitivity.

TEM Imaging and EDX

Cycled cells were disassembled in an Ar-atmosphere glove box (< 1 ppm H_2O). TEM grids were extracted from cycled coin cells and rinsed with anhydrous dimethyl carbonate (DMC, Acros) then dried overnight. Imaging was conducted using a JEOL JEM-2100F TEM (Peabody, MA) at 160 kV.. Energy-dispersive X-ray spectroscopy or EDX (Model INCAx-act, Oxford Instrument, UK) was used to detect elements on the surface of graphite anode. To detect the element composition at different areas, multiple locations from the edge to the center were probed by EDX during imaging. The diameter of EDX beam was 10 nm. Low-dose imaging was employed to minimize the electron beam induced changes to the organic components of SEI layers.

XPS analysis of electrodes

XPS was conducted on BF-graphite electrodes before and after cycling. After cycling the electrodes were rinsed with DMC and dried overnight in vacuum. The X-

ray photoelectron spectroscopy (XPS) was obtained on a PHI 5500 system using Al, *K-alpha* radiation (hv=1486.6 eV) under ultrahigh vacuum conditions; the XPS data was collected at multiple locations of cycled graphite electrodes. The C 1s, O 1s, F 1s, P 2p spectra were calibrated based on the C1s graphite peak binding energy at 284.5 eV.

NMR analysis of electrodes

Multinuclear and multidimensional NMR analyses were conducted on a Bruker Avance III 300 MHz NMR spectrometer. Electrodes were rinsed with DMC to remove residual electrolyte and dried in vacuum. The graphite electrodes were then extracted in and Ar glove box with high purity D_2O opened from a seal vial and analyzed by ^{1}H, ^{13}C, DEPT-135, HSQC, COSY and DOSY NMR spectroscopy.

Results and discussion

1. Electrochemical cycling performance

The BF graphite/Li coin cells have been cycled with $LiPF_6$/PC electrolyte with five different concentrations of $LiPF_6$. As shown in Figure 1, the potential profiles of the coin cell cycled in 1.2 M $LiPF_6$/PC electrolyte is typical of graphite with PC based electrolytes as reported previously.[12,29] A long plateau is observed at 0.9 V vs. Li, consistent with continuous electrolyte reduction and an absence of lithium intercalation into graphite resulting in very poor columbic efficiency (CE, ~4%). When the concentration is increased to 2.4 M, the cell potential gradually drops from 0.9 V to ~0.4 V, but very little reversible capacity (CE ~ 10 %) is obtained. Significant changes are observed when the concentration of $LiPF_6$ is increased to 2.8 M. The cells cycle with much higher efficiency (66 %), the shoulder characteristic of

electrolyte reduction at ~0.9 V is significantly reduced, and lithium ion intercalation is observed at 0.2 – 0.05 V. The plateau at ~0.9 V is further suppressed in cells cycled with 3.0 and 3.5 M electrolytes, The delithiation capacities were 297 and 273 mAh while the CE was approximately 80% for both concentrations of $LiPF_6$.

2. Cyclic voltammetry

Cyclic voltammetry is a complementary electrochemical method to constant current cycling which provides more detail about the reactions of the electrolyte with the electrode surface. The first three consecutive cyclic voltammograms of $LiPF_6$/PC electrolytes with different concentrations of $LiPF_6$ are provided in Figure 2. The initial cathodic processes are critical to the operation of lithium ion batteries due to the reduction reactions of the electrolyte (2.0 - 0.3 V vs Li) which result in the formation of the solid electrolyte interface (SEI) during the initial lithiation cycles. The SEI formation is then followed by lithium ion intercalation into the graphite (0.3 -0.05 V vs Li). The anodic processes from 0.05-2V are typically characterized by de-intercalation of Li^+ from graphite.

The first cathodic sweep of the BF-graphite electrode with 1.2 M $LiPF_6$/PC contains a strong peak at 0.36 V vs Li (I_{pc}=-4.4 mA) suggesting a significant reductive decomposition of the electrolyte. The onset of the electrolyte reduction begins at ~0.9 V which is consistent with the plateau observed in constant current cycling, as discussed above. This cathodic peak is consistent with the reductive decomposition of PC.[12,29] The anodic sweep contains no observable peaks suggesting that the electrolyte reduction is irreversible and that there is no lithium ion deintercalation from the graphite. The second cathodic scan is similar although the intensity of the electrolyte

reduction peak at 0.33 V has lower current. When the concentration of $LiPF_6$ is increased to 2.4 M two cathodic peaks are observed Epc=0.32 V and Epc=0.1 V, respectively. The first peak is attributed to the reductive decomposition of electrolyte and only exists in first cycle while the second peak is attributed to lithium intercalation. Subsequent CV scans contain the typical reversible peaks, starting from~0.25 V, characteristic of Li+ insertion and de-insertion from graphite:

When the concentration of $LiPF_6$ is further increased to 2.8 M two peaks are still observed during the first cathodic process. However, the current of initial reduction peak is reduced and the peak occurs at higher potential E_{pc}=0.56 V. In addition, the intensity of peaks from lithiation is increased. The anodic scan reveals greater intensity for the peak associated with delithiation and subsequent scans reveal reversible intercalation/deintercalation of lithium. At very high concentrations of $LiPF_6$ (3.0 M and 3.5 M) the initial reduction peak on the first cathodic scan has much weaker intensity (0.12 mA) and is further shifted to higher potential (0.65 V). The shift of the irreversible reduction peak to higher potential at higher concentration of $LiPF_6$ also coincides with an onset of reversible lithium ion intercalation/deintercalation and reversible cycling of lithium ion cells.

3. IR spectra of $LiPF_6$/PC electrolytes

Infrared (IR) spectra were obtained of $LiPF_6$/PC solutions at various concentrations of $LiPF_6$. The IR spectrum of pure PC contains a strong C=O stretching vibration at 1789 cm^{-1} and a weaker band at 1800 cm^{-1}. Addition of 1.2 M $LiPF_6$ to PC results in changes in the IR spectra. The C=O absorptions at 1789 and 1800 cm^{-1} decrease in intensity and new peaks at 1770 and 1752 cm^{-1} characteristic of

C=O absorptions for PC coordinated to Li^+ are observed (Figure 3). In addition, a new absorption characteristic of $LiPF_6$ is observed at 844 cm^{-1}. Further increases in the concentration of $LiPF_6$ result in additional changes to the IR spectra. Upon increasing the concentration of $LiPF_6$ to 2.8 M, the C=O absorptions of uncoordinated PC (1789 and 1800 cm^{-1}) decrease and are replaced by the absorptions at 1770 and 1752 cm^{-1}. Similar changes are observed for the C-O absorption bands. The peak associated with uncoordinated PC (1180 cm^{-1}) is gradually replaced by coordinated PC (1210 cm^{-1}) with increasing concentration of $LiPF_6$ (Figure SI1) The absorption for $LiPF_6$ is also changed. While the peak at 844 cm^{-1} is still present, two new absorptions at 877 and 834 cm^{-1} are observed (Figure 3).

The relative area of the IR bands of the C=O absorptions for coordinated and uncoordinated PC have been modeled (Figure SI2 and SI3). The relative areas of coordinated and uncoordinated PC are used to estimate number of PC molecules coordinated to the Li cation using Equation 2, where $C_{PC\ C}$, $C_{PC\ UC}$, and C_{Li} are the concentrations of coordinated PC, uncorrodinated PC and lithium, respectively, *N* is the average solvation number, and $A_{PC\ C}$ and $A_{PC\ UC}$ are relative areas of the IR bands for coordinated PC and uncoordinated PC, respectively.

$$C_{\mathrm{PC\,C}} = N\,C_{Li}$$

$$C_{\mathrm{PC\,C}} = \frac{A_{\mathrm{PC\,C}}}{A_{\mathrm{PC\,C}} + A_{\mathrm{PC\,UC}}} C_{\mathrm{PC}}$$

$$N = \frac{A_{\mathrm{PC\,C}}}{A_{\mathrm{PC\,C}} + A_{\mathrm{PC\,UC}}} \frac{C_{\mathrm{PC}}}{C_{\mathrm{Li}}}$$

Equation 2

The number of PC molecules coordinated to the lithium cation (solvation number) decreases with increasing concentration of $LiPF_6$ (Figure 4). The decrease in solvation number coincides with the increase in the intensity of the $LiPF_6$ absorptions at 877 and 834 cm^{-1} characteristic of ion pairs.[37] The changes in the IR spectral properties are consistent with a change in solution structure. The predominant structure in solution, at low concentrations of $LiPF_6$ (1.2 M), is a tetra-PC solvated lithium cation with a solvent separated PF_6^- anion. At high concentrations of $LiPF_6$ (3.0 M), the predominant structure in solution is a tri-PC coordinated cation-contact ion pair (Scheme 1).[38] The change in solution structure correlates with a change in the reversibility of the cycling of lithium ion cells.

Scheme 1

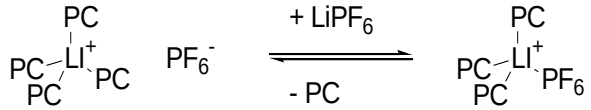

4. TEM and EDX analysis

Binder free-graphite electrodes were prepared with integrated copper TEM grids allowing straightforward TEM analysis without additional treatment. The cells were cycled with five concentrations $LiPF_6$ in PC (1.2 M, 2.4 M, 2.8 M, 3.0 M and 3.5 M). The graphite particles cycled with different concentrations of $LiPF_6$ have significantly different surface films. Graphite particles cycled in the presence of 1.2M $LiPF_6$ in PC are very similar to the fresh graphite particles. There is no significant change in the appearance of the surface. EDX analysis reveals the elemental composition at two points of the graphite particle, the edge and the center (inset of Figure 4 B). A slight

increase in the concentration of O, F and P is observed on the edge of the graphite particle compared to the bulk graphite consistent the presence of low concentrations of electrolyte decomposition products. This is surprising since cells cycled with 1.2 M $LiPF_6$ in PC observe continuous electrolyte reduction at 0.9 V generating a high concentration of electrolyte reduction products. However, it appears that the electrode reduction products of 1.2 M $LiPF_6$ in PC either do not adhere strongly to the surface of the graphite particles or are readily dissolved during the DMC rinsing of the electrodes.[29,40] In either case, the electrolyte decomposition products do not passivate the surface of the graphite electrode resulting in consistent electrolyte reduction.

As the concentration of $LiPF_6$ is increased the presences of electrolyte decomposition products on the surface of the graphite particles become more apparent. Upon increasing the concentration to 2.4 M, a thin and uniform film is observed on edge of graphite particles. The thickness of the film is approximately 5 nm and has an increased concentration of F and O, 3.5 and 1.2%, respectively. A further increase the concentration of $LiPF_6$ to 2.8 M results in the generation of a thicker surface film on the graphite particle. In addition, the concentration of F and O are increased to 6.6 and 2.1 %, respectively. The presences of higher concentrations of F and O on the graphite surface coincides with the onset of reversible cycling, as described above, and are characteristic of the formation of a passivating SEI.[36] At 3.5 M, a grainy thin film (~50 nm) is observed coating the entire graphite particle and the concentration F and O at the surface are further increased 13.8 and 3.5, respectively. Interestingly, the ratio of F to O is relatively constant ~3:1 for all of the surface films which suggests

that the F content is much higher than for the SEI generated for 1.2 M $LiPF_6$ in EC which contained an SEI with a 1:1 ratio of F to O.[36]

5. D_2O NMR extraction and HRLC-Mass of BF-graphite electrodes cycled in various concentrations $LiPF_6$/PC

In an effort to characterize the components of the SEI on BF-graphite electrolytes cycled with $LiPF_6$ in PC, the cycled electrodes were extracted from the cells, rinsed with DMC to remove residual electrolyte and then extracted with D_2O to dissolve the SEI components. The D_2O extracts were analyzed by ^1H, ^{13}C, and ^{19}F NMR spectroscopy (Figure 5). The ^1H NMR spectra of the D_2O extract from a BF-graphite anode cycled with 1.2 M $LiPF_6$ in PC contains a single set of resonances at 1.10 ppm (d, 6.4 Hz), 3.35 ppm (dd, 11.6, 6.8 Hz), 3.45 ppm (dd, 11.6, 4.1 Hz) and 3.81 ppm (mult). The ^{13}C and DEPT—135 NMR spectra of the sample revealed four resonances at 17.96 ppm (methyl), 66.57 ppm (methylene), 67.91 ppm (methine), and 162.25 ppm (carbonyl) (Figure SI7). In addition, there is no evidence for the presence of significant concentrations of Li_2CO_3 (168.21 ppm) by ^{13}C NMR spectroscopy. The chemical shifts and the coupling constants are identical to the previously reported spectra for lithium propylene dicarbonate (LPDC) while COSY and HSQC NMR spectroscopy provide additional support (Figure SI7).[41] Thus the predominant organic electrolyte decomposition product is LPDC. The ^{19}F NMR spectra reveal a doublet at -73.4 ppm and a singlet at -123 ppm characteristic of residual $LiPF_6$ and LiF. The ^1H, ^{13}C, and ^{19}F NMR spectra of the D_2O extract of the BF-graphite anode cycled with 3.5 M $LiPF_6$ are very similar, but the relative concentrations of the species are dramatically different. The ^1H NMR spectra reveal much lower concentrations of

LPDC while the ^{19}F NMR spectra reveal much higher concentrations of LiF, compared to the extract of the electrode cycled with 1.2 M $LiPF_6$ in PC. This suggests that at low concentrations of $LiPF_6$ the predominant reduction product of the electrolyte is LPDC while at high concentrations of $LiPF_6$ the predominant reduction product is LiF. Further confirmation of the presence of LPDC was obtained via direct injection of the D_2O extract of the electrode cycled with 1.2 M $LiPF_6$ into a high resolution electrospray ionization mass spectrometer (Table SI1 and Figures SI6-SI7). The absolute mass of the parent ion under positive ion mode is consistent with the presence propylene dicarbonic acid (Exact: 164.0321, Found 164.0329) confirming the presence of LPDC on the surface of the cycled anode.

The TEM images were also acquired on cycled graphite anode after D_2O extraction to remove the SEI to confirm quantitative removal. A TEM image of an anode cycled with 3.5 M electrolyte after D_2O extraction is depicted in Figure SI8 and the elemental concentrations as determined by EDX are provided within the inset. The image and the elemental concentrations are very similar to un-cycled graphite element suggesting that the D_2O extraction removes all of the SEI components which can be subsequently characterized by solution NMR spectroscopy.

6. DOSY NMR analysis of multinuclear diffusion in various concentrations of $LiPF_6$/PC electrolytes

In an effort to better understand the solution structure of $LiPF_6$/PC electrolytes and the interactions between the Li^+ cation and the PF_6^- anion, diffusion rates were monitored as a function of [$LiPF_6$]. The diffusion coefficients (D) of Li^+ and PF^-_6 in electrolytes have been determined by ^7Li and ^{19}F DOSY NMR, via linear fitting of

plots of ln(I) vs.Gi^2. A representative data set is provided in supporting information (Figure SI4). The diffusion coefficients of Li^+ and PF_6^- at three different concentrations of $LiPF_6$ in PC are provided in Table 1. Both Li^+ and PF_6^- diffuse at slower rates at higher salt concentrations which is not surprising due to the increased viscosity of electrolytes with high salt content.[39]

However, it is more informative to compare the diffusion coefficients of Li^+ and PF_6^- at the same concentration of salt. For 1.2 M $LiPF_6$ in PC, the diffusion coefficient of Li^+ cation is 6.68^{-11} m^2/s which is about half of the ^{19}F diffusion coefficient 1.20^{-10} m^2/s of the PF_6^- anion, suggesting that transport of the Li^+ cation is slower than the transport of PF_6^- anion. This is consistent with lithium ion solvation in the presence of weakly coordinating anions since the Li^+ cation is typically strongly coordinated by four solvent molecules (PC) while the PF_6^- has weaker interactions with the solvent molecules. Thus, the larger coordinated Li^+ cation diffuses slower than the smaller uncoordinated PF_6^- anion. The difference of the diffusion coefficients for the Li^+ cation and the PF_6^- become smaller as the concentration of $LiPF_6$ is increased. Upon increasing the concentration of $LiPF_6$ to 2.4 M in PC the diffusion constants of the Li^+ cation and the PF_6^- anion are 1.23^{-11} m^2/s and $1.95^{-11}m^2/s$, respectively while further increasing the concentration of $LiPF_6$ to 3.5 M in PC the diffusion constants of the Li^+ cation and the PF_6^- anion are 5.12^{-12} and 7.69^{-12} m^2/s. The ratio of the diffusion constant of Li^+ cation to the PF_6^- anion changes from 1:1.8 to 1:1.5 upon increasing the $LiPF_6$ concentration from 1.2 M to 3.5 M. The changes in diffusion rates are consistent with a change in solution structure from solvent separated ion pairs to contact ion pairs upon increasing the concentration of $LiPF_6$.

7. Surface analysis of cycled BF-graphite electrodes by XPS

The surface of extracted BF-graphite electrodes was analyzed by XPS after cycling with 1.2, 2.4, 2.8, 3.0 and 3.5 M $LiPF_6$ in PC. The XPS spectra are presented in Figure 7 and the elemental concentrations are summarized in Table 2. The absence of binder in the BF-graphite electrodes allows a more accurate measurement of the surface element concentrations and avoids spectral overlap with binder. The C1s spectrum of the fresh BF-graphite electrode is dominated by the peak of graphite at 284.5 eV but also contains a low concentration of a peak at 286 eV consistent with surface oxidation of the graphite. A weak peak characteristic of C-O containing species is observed in the O1s spectrum at 533.8 eV characteristic of surface oxidation of the graphite.[42] Upon cycling with 1.2 M $LiPF_6$ in PC electrolyte, the XPS spectra change significantly. The concentrations of C are decreased while the concentrations of O, F, and P are increased (Table 2). The C1s spectrum contains new peaks at ~287 eV and 290 eV characteristic of C-O and C=O containing species. This is further supported by the O1s spectrum which has a new strong peak at 532-533 eV, consistent with the presence of C-O (533 eV) and C=O (532 eV) containing species supporting the presence of LPDC, as observed by NMR spectroscopy described above.[43] In addition, a significant peak associated with graphite is observed at 284.5 eV consistent with the exposed graphite surface observed by TEM. This suggests that the reduction of PC is occurring at the BF-graphite electrode, however the LPDC being generated is not adhering to the surface of the graphite particles and is instead being trapped in the pores of the electrode. The F1s spectrum contains a strong peak characteristic of LiF

at 685 eV along with a weak shoulder at 687 eV characteristic of residual $LiPF_6$. The corresponding P2p peak for residual $LiPF_6$ is also observed at 138 eV.

Upon steadily increasing the concentration of $LiPF_6$ from 1.2 to 3.5 M the concentrations of C and O systematically decrease while the concentrations of F and P increase. The C1s spectra of electrodes cycled with 2.4 - 3.5 M $LiPF_6$ in PC remain dominated by the C=O, C-O and graphite peaks at 290, 287, and 284.5 eV, respectively. Likewise the O1s spectra of electrodes cycled with 2.4 - 3.5 M $LiPF_6$ are dominated by the C-O and C=O peaks at 533 and 532 eV respectively. This is consistent with the C and O containing species being predominantly LPDC and graphite which is in agreement with the NMR and TEM data. In addition, the decrease in concentration of C and O on the surface of the electrodes correlates with ^1H NMR spectra of the D_2O extracts which indicate that the concentration of LPDC decreases upon increasing the concentration of $LiPF_6$. While the presence of C-O and C=O species could also support the presence of Li_2CO_3 on the surface of the BF graphite electrodes, there is not clear support for the presence of significant concentrations of Li_2CO_3 by ^{13}C NMR, as discussed above. The F1s spectra of electrodes cycled with 2.4 - 3.5 M $LiPF_6$ contain a strong peak at 685 eV characteristic of LiF and a shoulder at 687 eV characteristic of $LiPF_6$ or $Li_xPF_yO_z$. Weak peaks are also observed in the P2p spectra consistent with low concentrations of $Li_xPO_yF_z$ (135 eV) and residual $LiPF_6$ (138 eV). The increase in concentration of F from 21.8 to 42.5 % as observed by XPS upon increasing the concentration of $LiPF_6$ in PC from 1.2 M to 3.5 M is consistent with the increased concentrations of LiF observed by NMR spectroscopy. The large increase of fluorine in SEI is consistent with more

decomposition of $LiPF_6$ for cells cycled with electrolytes containing higher concentrations of $LiPF_6$. Thus the XPS data is consistent with the results observed by TEM-EDX and NMR suggesting that SEI on the BF-graphite electrodes is primarily composed of LPDC and LiF. However, when the cells cycle reversibly, at high concentrations of $LiPF_6$, the SEI is dominated by LiF with low concentrations of LPDC. When the cells do not cycle reversibly and experience continuous electrolyte reduction, at low concentrations of $LiPF_6$, the dominate reduction product is LPDC with a low concentration of LiF which does not passivate the graphite surface.

Summary and Conclusions

The cycling performance of $LiPF_6$/PC electrolytes with graphite electrodes changes as a function of the $LiPF_6$ concentration. At low $LiPF_6$ concentrations continuous electrolyte reduction is observed at ~0.9 V vs Li and lithiation of the graphitic anode does not occur. At high concentrations of $LiPF_6$ a shoulder is observed at 0.8 V vs Li consistent with SEI formation and a plateau is observed from 0.3 to 0.05 V vs Li consistent with reversible lithiation/delithiation of graphite. Cyclic voltammetry provides analogous results supporting reversible lithiation/delithiation only at high concentrations of $LiPF_6$. IR spectroscopy of $LiPF_6$/PC electrolytes reveals the presence of both PC coordinated to the Li^+ and uncoordinated PC. Modeling of the C=O stretching region provides an estimate of the number of PC molecules coordinated to each Li^+. As the concentration of $LiPF_6$ is gradually increased from 1.2 to 3.0 M the PC solvation number gradually decreases from 4 to 3. In addition, the absorptions characteristic of PF_6^- are consistent with a contact ion pair. A shift from solvent separated ion-pair at low $LiPF_6$ concentration to a contact ion pair

at high $LiPF_6$ concentration is also supported by DOSY NMR spectroscopy. Thus the change in cycling behavior clearly correlates with the change in solution structure.

In order to better understand why the change in solution structure alters the cycling performance, ex-situ surface analysis of the cycled electrodes has been conducted. At low concentrations of $LiPF_6$, the individual graphite particles contain a very thin surface film (~5 nm) as determined by TEM with EDX. However, the bulk electrode contains a high concentration of lithium propylene dicarbonate (LPDC) as determined by a combination of XPS and solution NMR spectroscopy of the D_2O extracts of the electrode. Continuous electrolyte reduction generates LPDC as the dominant product, but the LPDC does not adhere well to the graphite surface and thus does not passivate the surface and subsequently inhibit further electrolyte reduction. At high concentrations of $LiPF_6$ the surface analysis provides very different results. The individual graphite particles contain a thick surface film (~50 nm) with a high concentration of F as determined by TEM with EDX. The SEI contains a high concentration of LiF and a low concentration of LEPC as determined by XPS and solution NMR spectroscopy of the D_2O extracts of electrode. Thus at high concentrations of $LiPF_6$ the predominant reduction product of the electrolyte is LiF which adheres well to the surface of the graphite particles forming a stable SEI which inhibits further electrolyte reduction.

Scheme 2

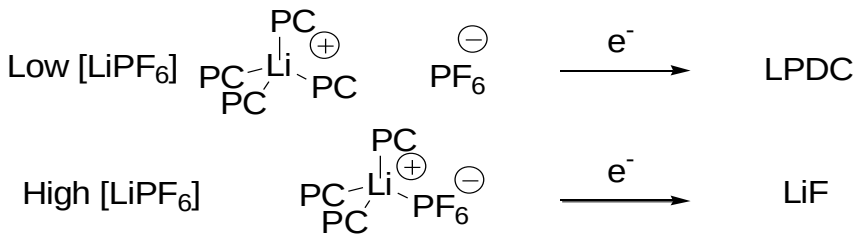

The results are summarized in Scheme 2. At low concentrations of $LiPF_6$ the predominant solution structure is the solvent separated ion pair. Upon charging the cell, the principal reduction product of the solvent separated ion pair is LPDC which does not passivate the electrode surface and the electrolyte is continuously reduced. At high concentrations of $LiPF_6$ the predominant structure is the contact ion pair. Upon charging the cell the principal reduction product of the contact ion pair is LiF, with a low concentration of LPDC to enhance the Li ion conduction, which passivates the electrode surface allowing efficient lithiation/delithiation of the graphite electrode.

Reference

(1) Goodenough *Acc. Chem. Res.*, 2013, *46*, pp 1053–1061

(2) Xu, K. *Chem. Rev.* 2004,*104*, 4304-4417.

(3) Verma, P.; Maire, P.; Novák, P. *Electrochim. Acta*. 2010, *55*, 6332-6341.

(4) Peled, E. *J. Electrochem. Soc.* 1979, *126*, 2047-2051.

(5) Aurbach, D. *J. Power Sources.* 2000, *89*, 206-218.

(6) Xu, K.; von Cresce, A. *J. Mat. Chem*. 2011, *21*, 9849-9864.

(7) Niehoff, P.; Passerini, S.; Winter, M. *Langmuir* 2013, *29*, 5806-5816.

(8) J.O. Besenhard, M. Winter, J. Yang, W. Biberacher, *J. Power Sources.* 1995,*54* , 228-231

(9) A. Schechter, D. Aurbach and H. Cohen, *Langmuir*. 1999, *15*, 3334-3342.

(10) M. Winter, *Z. Phy. Chem.* 2009, *223*, 1395-1406.

(11) von Cresce, A.; Xu, K. *Electrochem. Solid-State Lett.* 2011, *14*, A154-A156.

(12) Yamada, Y.; Koyama, Y.; Abe, T.; Ogumi, Z. *J. Phys. Chem. C* 2009, *113*, 8948-8953.

(13) Barthel, J.; Deser, R. *J Solution Chem.* 1994, *23*, 1133-1146.

(14) Cazzanelli, E.; Croce, F.; Appetecchi, G. B.; Benevelli, F.; Mustarelli, P. *J. Chem. Phys.* 1997, *107*, 5740-5747.

(15) Barthel, J.; Buchner, R.; Wismeth, E. *J Solution Chem.* 2000, *29*, 937-954.

(16) Alía, J. M.; Edwards, H. G. M. *Vib. Spectrosc*. 2000, *24*, 185-200.

(17) Tasaki, K.; Goldberg, A.; Liang, J.; Winter, M. *J. Electrochem. Soc.* 2011, *33*, 59-69.

(18) von Wald Cresce, A.; Borodin, O.; Xu, K. *J. Phys. Chem. C* 2012, *116*, 26111-26117.

(19) Yang, L.; Xiao, A.; Lucht, B. L. *J. Mol. Liq.* 2010, *154*, 131-133

(20) Seo, D. M.; Borodin, O.; Han, S.-D.; Ly, Q.; Boyle, P. D.; Henderson, W. A. *J. Electrochem. Soc.* 2012, *159*, A553−A565.

(21) R. Fong, U. von Sacken, and J. R. Dahn, *J. Electrochem. Soc.* 1990, 137, 2009 - 2013

(22) Herstedt, M.; Andersson, A. M.; Rensmo, H.; Siegbahn, H.; Edström, K. *Electrochim. Acta* 2004, *49*, 4939-4947.

(23) Inaba, M.; Siroma, Z.; Kawatate, Y.; Funabiki, A.; Ogumi, Z. *J. Power Sources* 1997, *68*, 221-226.

(24) Jeong, S.-K.; Inaba, M.; Iriyama, Y.; Abe, T.; Ogumi, Z. *J. Power Sources* 2003, *119–121*, 555-560.

(25) Chung, G. C.; Kim, H. J.; Yu, S. I.; Jun, S. H.; Choi, J. w.; Kim, M. H. *J. Electrochem. Soc.* 2000, *147*, 4391-4398.

(26) Wang,J.; Manga, K. K.; Bao, Q.; Loh, K. P. *J. Am. Chem. Soc.* 2011, *133*, 8888-8891

(27) Tasaki, K. *J. Phys. Chem. B* 2005, *109*, 2920-2933

(28) Aurbach, D.; Daroux, M. L.; Faguy, P. W.; Yeager, E. *J. Electrochem. Soc.* 1987, *134*, 1611-1620.

(29) Xu, K.. *J. Electrochem. Soc.* 2009, *156*, A751-A755.

(30) Abe, K.; Yoshitake, H.; Kitakura, T.; Hattori, T.; Wang, H.; Yoshio, M. *Electrochim. Acta* 2004, *49*, 4613-4622.

(31) Aurbach, D.; Gamolsky, K.; Markovsky, B.; Gofer, Y.; Schmidt, M.; Heider, U. *Electrochim. Acta* 2002, *47*, 1423-1439.

(32) Zhuang, G. V.; Xu, K.; Jow, T.R.; Ross Jr, P. N. *Electrochem. Solid-State Lett.* 2004, *7*, A224-A227.

(33) Jeong, S.-K.; Inaba, M.; Iriyama,Y.; Abe,T.; Ogumi.Z.; *J. Power Sources,* 2008,*175*, 540-546

(34) Kang, S. H.; Abraham, D. P.; Xiao, A.; Lucht, B. L. *J. Power Sources* 2008, *175*, 526-532.

(35) Xiao, A.; Yang, L.; Lucht, B. L.; Kang, S.-H.; Abraham, D. P. *J. Electrochem. Soc.* 2009, *156*, A318-A327.

(36) Nie, M.; Chalasani, D.; Abraham, D. P.; Chen, Y.; Bose, A.; Lucht, B. L. *J. Phys. Chem. C* 2013, *117*, 1257-1267.

(37) Aroca, R.; Nazri, M.; Nazri, G. A.; Camargo, A. J.; Trsic, M. *J Solution Chem* 2000, *29*, 1047-1060.

(38) Umebayashi, Y.; Mitsugi, T.; Fukuda, S.; Fujimori, T.; Fujii, K.; Kanzaki, R.; Takeuchi, M.; Ishiguro, S.-I. *J. Phys. Chem. B* 2007, *111*, 13028-13032.

(39) Lencka, M. M.; Anderko, A.; Sanders, S. J.; Young, R. D. *Int. J. Thermophys.* 1998, *19*, 367-378.

(40) Ein‐Eli, Y. *Electrochem. Solid-State Lett.* 1999, *2*, 212-214.

(41) Xu, K.; Zhuang, G. R. V.; Allen, J. L.; Lee, U.; Zhang, S. S.; Ross, P. N.; Jow, T. R. *J. Phys. Chem. B* 2006, *110*, 7708-7719.

(42) Andersson, A.; Abraham, D.; Haasch, R.; MacLaren, S.; Liu, J.; Amine, K. *J. Electrochem. Soc.* 2002, *149*, A1358-A1369.

(43) Dedryvere, R.; Gireaud, L.; Grugeon, S.; Laruelle, S.; Tarascon, J. M.; Gonbeau, D. *J. Phys. Chem. B* 2005, *109*, 15868-15875

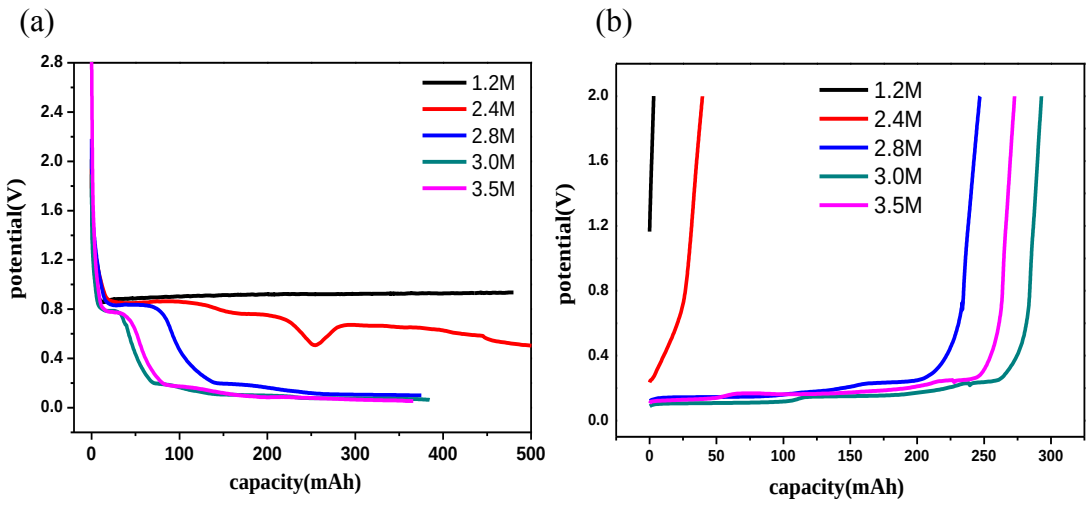

Figure 4-1. Potential vs. capacity curves for BF-graphite/Li cells cycled with five concentrations of $LiPF_6$/PC electrolytes: (a) lithium intercalation profiles (b) lithium de-intercalation profiles.

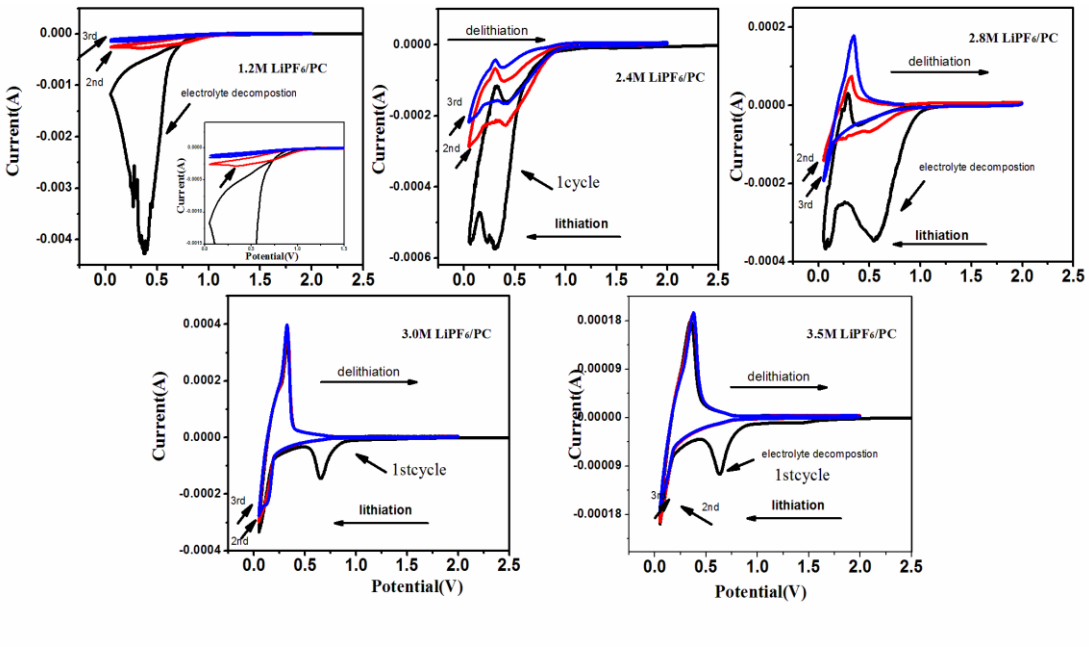

Figure 4-2: Cyclic voltammograms of BF-graphite/Li system in five concentrations $LiPF_6$/PC electrolytes cycled between 2-0.05V with 0.05mV/s.

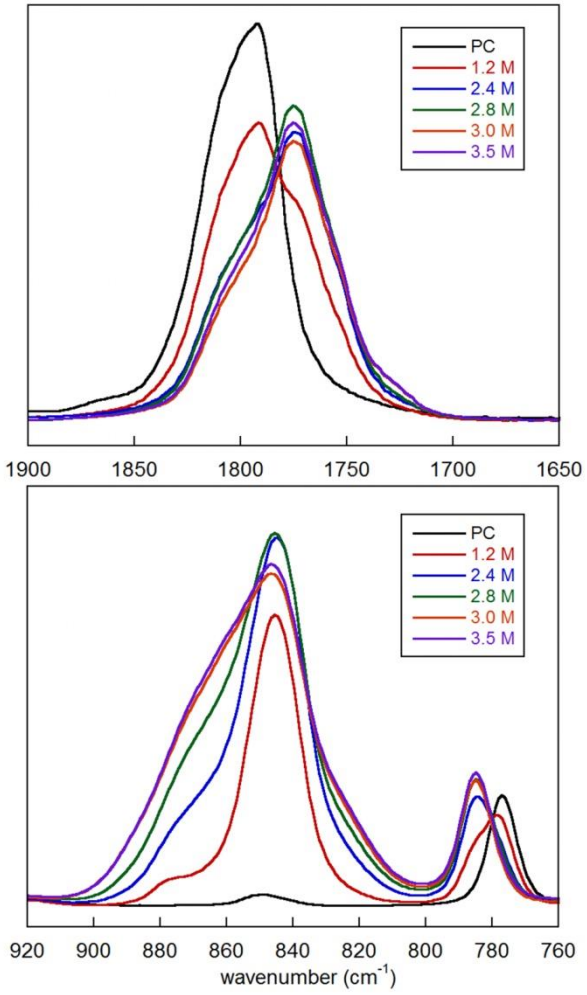

Figure 4-3: FTIR spectra of five concentrations $LiPF_6$/PC electrolytes at selected ranges.

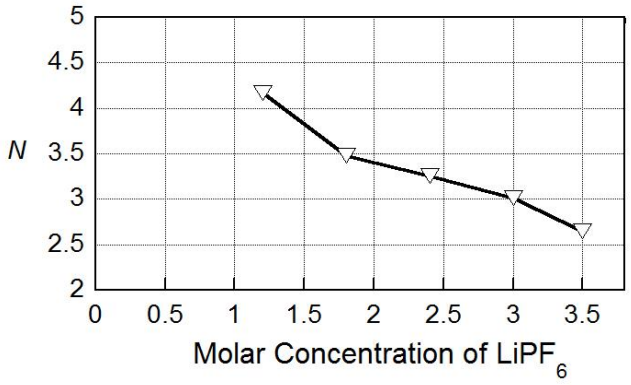

Figure 4-4.Number of PC molecules (N) coordinated to the Li cation at different $LiPF_6$ concentrations.

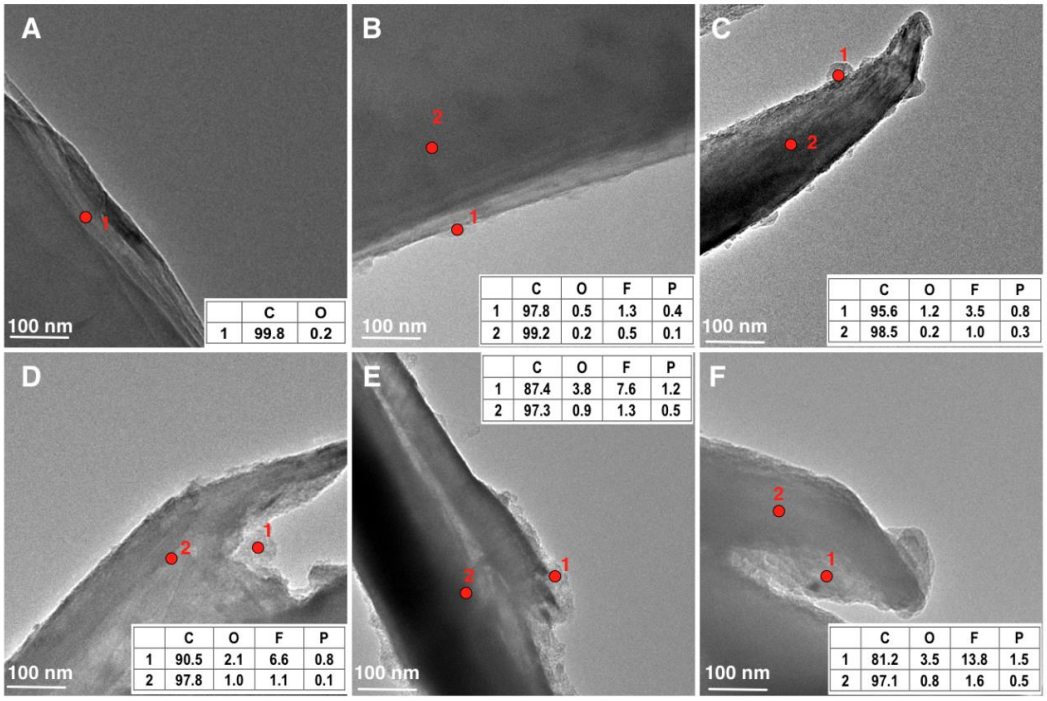

Figure 4-5. TEM bright-field images of fresh graphite and graphite anodes cycled with five concentrations $LiPF_6$/PC electrolytes. (A) Fresh graphite electrode, (B) 1.2 M, (C) 2.4 M (D), 2.8 M (E) 3.0 M and (F) 3.5 M. The inset indicates the element composition detected by EDX. The red spots indicate locations probed by EDX

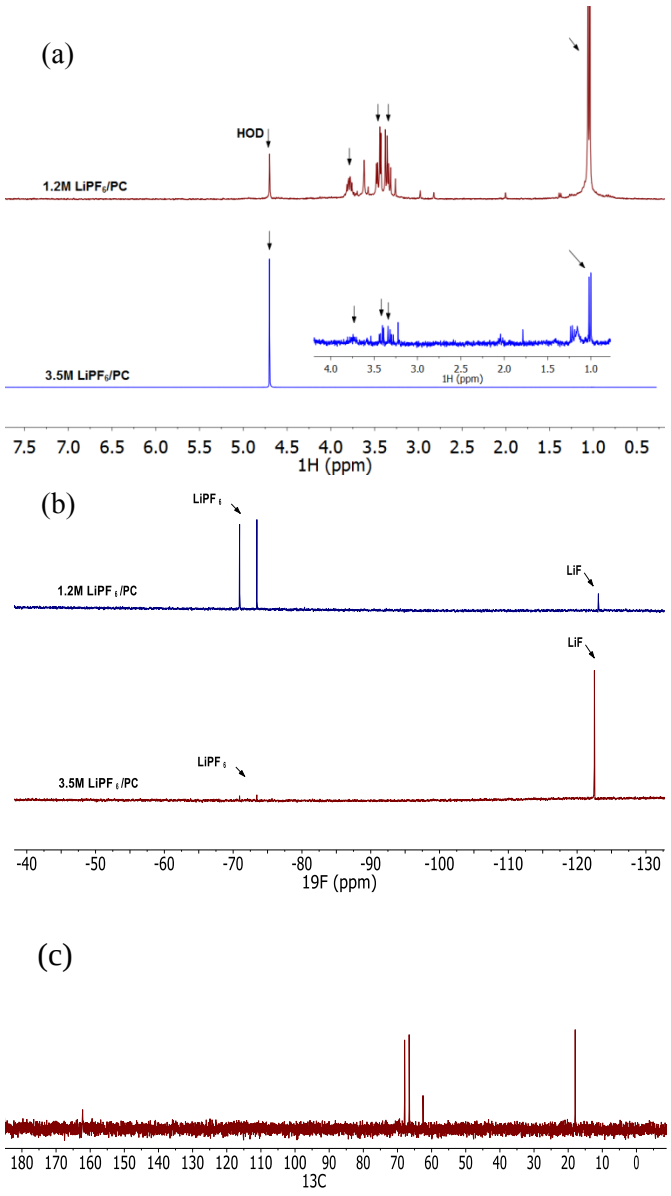

Figure 4-6. (a) ^{1}H NMR spectra (b) ^{19}F NMR spectra of anodes extracted from 1.2 M and 3.5 M $LiPF_6$/PC electrolytes. (c) ^{13}C NMR spectrum of sample extracted from 1.2 M $LiPF_6$/PC electrolyte.

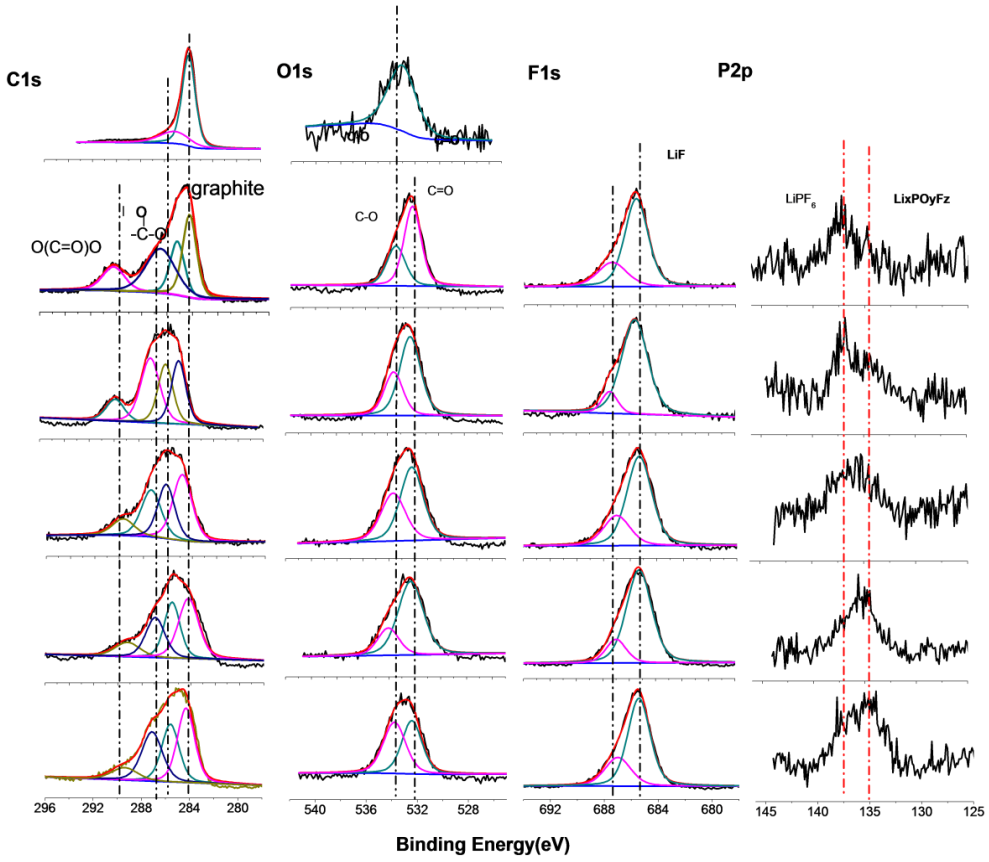

Figure 4-7. XPS spectra of Fresh BF-electrodes and BF-anodes extracted from coin cells cycled to five concentrations $LiPF_6$/PC electrolytes from top are: fresh BF-graphite electrode, 1.2M, 2.4M, 2.8M, 3.0M and 3.5M $LiPF_6$/PC electrolytes.

	C%	O%	F%	P%
Fresh	**95.5**	**4.5**	**..**	**..**
1.2 M $LiPF_6$/PC	**48.7**	**28.3**	**21.8**	**1.1**
2.4 M $LiPF_6$/PC	**47.1**	**27.6**	**23.7**	**1.3**
2.8 M $LiPF_6$/PC	**38.5**	**24.4**	**35.0**	**2.0**
3.0 M $LiPF_6$/PC	**37.5**	**19.5**	**40.8**	**2.1**
3.5 M $LiPF_6$/PC	**37.2**	**19.3**	**41.5**	**2.3**

Table 4-1. Element percentage from BF-anodes cycled with five concentration $LiPF_6$/PC electrolytes

CHAPTER 5

SPECTROSCOPIC STUDY ON VARIOUS SALTS ON SEI FORMATION ON BINDER FREE GRAPHITE ELECTRODES IN LITHIUM ION BATTERY

Mengyun Nie[1] and Brett L. Lucht[1]

[1]*University of Rhode Island, Kingston, Rhode Island 02881, United States*

The following is in preparation for submission to the Journal of the Electrochemical Society, and is presented here in manuscript format

Introduction

The development of application, storage and renewable energy is one of most important issues in nowadays. Since the lithium ion battery achieved great success in global business market, the large scale applications such as plug in electric vehicles are coming to daily life. Face to the energy crisis, lithium ion battery is a very promising technique which has attractive advantages: high energy density, small volumetric size and relative long life. In lithium ion battery, the capacity and efficiency are highly dependent on how much Li ions are transport between cathode and anode, thus lithium salts which used to make electrolytes are play an important role in working of lithium ion battery. During the past two decades, $LiAsF_6$, $LiClO_4$, $LiBF_4$ and $LiPF_6$ are quite common used in researches, but due to good solubility in carbonates-based electrolytes, high ionic conductivity and relative low price, etc.[1,2] Only LPF_6 are successfully launched into markets since now. However, the study of optimizing new Li ion salts is never stopped. Now, several ideas are emphasized in designing new salts, such as ionic conductivity, related SEI formation on carbonaceous electrodes, thermal stability and the effect of anions on the aluminum current collector. Recently, there is a rapidly growing interest for bis(fluorosulfonyl) imide,$Li[(FSO_2)_2N]$ (LiFSI) to be used in ionic-liquid electrolyte due to promising properties such as decreased of release of HF, relative high conductivity, high-rate and good low temperature performances[3,4]. However, not too much study was focused on the effect of different anions on SEI formation, including the influence of SEI component and morphology.[5,6] We have developed novel binder free graphite electrodes and investigated the cycling performance in $LiPF_6$, $LiBF_4$, LiTFSI, LiFSI, LiDFOB and LiBOB with EC composed electrolytes. The absence of binder and

presence of a single solvent electrolyte simplifies the analysis of the SEI components. After cycling, ex-situ analysis of the electrodes has been conducted via a combination of TEM, solution NMR spectroscopy of electrode extracts, FT-IR, and XPS. The specially designed TEM experiment allows to direct image of the graphite particles after cycling, while analysis of the D_2O extracts provides the molecular structure of the SEI components. The analysis provides information about the change of SEI composition resulted from multiple anions and insights into the relationship of irreversible capacity loss on first lithiaition with the lithium salts during SEI formation.

Experimental Sections

Preparation of Binder-free Graphite Electrode and Coin Cells Fabrication

Binder free graphite (BF-G) electrodes were prepared by Electrophoretic Deposition (EPD) method in the same manner to our previously reported preparation of binder free graphite electrodes[7] The EPD bath was prepared with SFG graphite particles (~5um, Timex) dissolved in acetonitrile with additional 0.1% v/v trimethylamine (anhydrous, Fisher, Co). Utilizing this method, results in the preparation of electrodes without polymer binders (PVDF) or conductive carbon. The electrode is composed exclusively SFG 6 graphite particles with a theoretical capacity ~372mAh/g. The BF-graphite electrodes were vacuum dried for 24 h at 120 ^{o}C. Coin cells (CR2032) were fabricated with BF-graphite electrodes, polypropylene separator (celgard 3501), and lithium foil in high purity Ar-filled glove box. Six different lithium salts ahve been investigated which fall into three categories: 1) $LiPF_6$ and $LiBF_4$ 2) LiBOB and LiDFOB, 3) LiTFSI and LiFSI. Ethylene carbonate (BASF) as

the only solvent used to prepare 1mol/L electrolytes with the different lithium salts. Each coin cell contains 30 uL of electrolyte.

Special coin cells were assembled containing binder-free graphite electrodes with copper TEM grids (Figures 1-2). Graphite particles were removed from the center of the BF graphite electrode to allow placement of the copper TEM grid. During cell construction some of the particles shift from the BF graphite electrode and adher to the copper TEM grid. Cell assembly was conducted in an Ar-atmosphere glove box (<1 ppm H_2O).

Electrochemical cycling:

Coin cells undergo a constant-current charge and discharge between 2.0 to 0.05 V on an ARBIN BT 2000 cycler with a current density of ~50uA/cm^2 which is approximately a C/20 rate at 25 ^oC. The cells were stopped after the first lithiation and delithation.

TEM Imaging and EDX

Cycled cells were disassembled in an Ar-atmosphere glove box (< 1 ppm H_2O). TEM grids were extracted from cycled coin cells and rinsed with anhydrous dimethyl carbonate (DMC, Acros) to remove residual electrolyte and dried overnight in a vacuum. The TEM grids were quickly transferred into the TEM chanber. Imaging was conducted using a JEOL JEM-2100F TEM (Peabody, MA) at 160 kV. Size analysis was performed using Image J software. Energy-dispersive X-ray spectroscopy or EDX (Model INCAx-act, Oxford Instrument, UK) was used to detect the element composition at various points in the SEI as well as on the anode; three spots from the edge to the center of particles were examined by EDX during imaging. The diameter

of beam was 5 nm and low-dose imaging was employed to minimize the electron beam induced changes to the organic components of SEI layers.

XPS, FTIR and NMR samples preparation

X-ray photoelectron spectroscopy of BF-graphite electrodes cycled with different electrolytes was conducted on a PHI 5500 system using Al Ka radiation source (hv=1486 eV) under ultrahigh vacuum. The binding energies of all elements were based on calibrated C-H bonding energy at 285 eV. The spectra were analyzed and fitted by Multipack 6.1 and XPS peak software (version 4.1). Line syntheses of elemental spectra were conducted using Gaussian–Lorentzian (70:30) curve fitting. Element concentration was calculated based on the equation: $C_x = (I_x/S_x)/(\sum I_i/S_i)$, where I_x is the intensity of the relative element, and S_i is the sensitivity number of the element.[9] FTIR was measured by Bruker TENSOR 27 spectrometer with a Ge crystal and ATR accessory. Samples are protected under Ar-purge during the measurements. All NMR samples were prepared via extraction of cycled BF-graphite electrodes with D_2O in an Ar filled glove box. Before extraction, the BF-graphite electrodes were rinsed with anhydrous DMC to remove residual electrolyte and dried overnight under vacuum. Multinuclear NMR analyses were conducted on a Bruker Avance III 300 MHz NMR spectrometer.

Results and Discussion

Electrochemical cycling behavior

The charge - discharge plots for coin cells containing electrolytes with six different lithium salts are presented in Figure 5-1. The irreversible capacity lost is significant different with various lithium salts. 1mol LiBOB/EC has the worst first

cycle efficiency, containing a long plateau at ~1.8 V which consumes almost 50% of the capacity during the first cycle. Correspondingly, the delithiation capacity for the cell containing LiBOB is the lowest for all of the electrolytes investigated, 38%. The cell containing the LiDFOB/EC electrolyte has similar performance to the LiBOB electrolyte, with a long plateau at 1.8 V. It is necessary to mention that the long plateau at 1.8V is diminished upon additional cycling. The cell containing the LiDFOB electrolyte has more reversible capacity, 190 mAh/g, and better efficiency, 61%, than the cell with the LiBOB electrolyte. The cells containing $LiBF_4$ and $LiPF_6$ electrolytes have similar lithiation curves, with a plateau at 0.7 V. However, the cell with $LiPF_6$ has more delithiation capacity 309 mAh/g and better efficiency, 80%. The third group salts are LiTFSI and LiFSI which have nearly identical cycling behaviors in both lithiation and delithiation. The cycling capacities and efficiency are comparable to the $LiPF_6$ electrolyte suggesting that LiTFSI/LiFSI electrolytes provide good reversible capacity and undergo similar capacity loss in SEI formation to $LiPF_6$.

Surface analysis of cycled BF-graphite electrodes

TEM images——The TEM images are from cells with TEM grids imbedded in BF-graphite/Li coin cells. After cycling the electrodes are washed with DMC to remove residual electrolytes, then the graphite particles adhered to the copper TEM grids are directly imaged. Although the cycling behaviors are similar for the $LiBF_4$ and $LiPF_6$ electrolytes, the TEM images reveal significantly different morphology on the surface of the graphite particles. A continuous amorphous film was observed on $LiPF_6$/EC cycled graphite as previously reported.[10] However, the graphite particle cycled with $LiBF_4$ electrolyte has a grainy and dense film on the particle surface.

EDX analysis has been conducted at the each edge of particles where the SEI is present. The EDX indicated a dramatically higher F concentration as 43% on the chunk particles after cycled by $LiBF_4$ cycled graphite, similar with early reported by Edstrom,etc. $LiPF_6$ still shows 1:1 ratio O to F as 4% and 4%, respectively. Thus F-rich species resulted in a dramatically different SEI layer attached on edge of graphite particles. LiBOB and LiDFOB don't show the thin film around the edge of graphite. But graphite cycled with LiDFOB has slightly covered with grainy thick layers similar with the one found in $LiBF_4$ cycled particles. Although they have very similar functional group, a high concentration of F is still found at LiDFOB cycled particles.

XPS spectra—— In order to better understand the composition of the anode SEI generated in the presence of different electrolytes, XPS spectra were acquired of BF-graphite electrodes extracted from cycled cells. The elemental concentrations are provided in Table 1 while the element spectra are provided in Figure 5-3. Based on the electrolytes used, C, O, and F are present on all electrodes except for electrodes cycled with LiBOB. S is present on electrodes cycled with LiTFSI/LiFSI while B is present on electrodes cycled with LiBOB/LiDFOB. The Fresh BF-graphite electrode contains about 95% C and 5% O from oxygenated impurities on the surface of the graphite. After cycling at 25 ^{o}C, for all electrolytes the concentration of C is decreased while the concentrations of all of the other elements are increased. Electrodes cycled with LiDFOB and LiBOB have the highest concentrations of O, 31.4% and 48.2%, respectively, while the $LiBF_4$ electrode has the highest concentration of on the surface, 31.3%. The concentration of O: F is close to 1:1 on surface of the electrodes cycled with $LiPF_6$, LiTFSI, LiFSI salts.

The relative intensity of the graphite peak at 284.5 eV is decreased after cycling suggesting that most of the surface is covered by the SEI components. The C1s spectra contain a dominant peak at 285.5eV consistent with C-H containing species from electrolyte decomposition and hydrocarbon contamination. Electrodes cycled with $LiPF_6$, $LiBF_4$, LiTFSI and LiFSI are similar with additional peaks at 287.5 and 290 eV, characteristic of CH_2-O, and O-(C=O)-O containing species, such a lithium alkyl carbonates. The C1s peak at 290 eV characteristic of O(C=O)O has strong intensity electrodes cycled with LiDFOB and LiBOB electrodes resulting for the generation lithium oxalate or other oxalates containing species.[11] The corresponding peaks of C-O and C=O are also found on O1s spectra with 533.5 and 531.5eV. A single dominant peak is observed in the F1s spectra at 685.5 eV for all F containing salts characteristic of LiF. In addition, there is evidence for the presence of other elements from decomposition of the different anions. Electrodes cycled contain a weak P2p peak at 135.5eV characteristic of $Li_xPF_yO_z$ while cells cycled with LiTFSI and LiFSI contain weak broad peaks at S 2p spectrum, at 168.5 to 170.0 eV is attributable to CF_3SO_2− group or oxidized S-containing species, probably Li_2SO4[12]. Also there are evidences for the presence of B on the surface of electrodes cycled with LiDFOB, LiBOB and $LiBF_4$. The peaks observed on the B1s spectra around 193.0 and 192.0eV are characteristic of B-O and B-F containing species and both can be attributed to residue salts or decomposition products from BOB and DFOB anions.

FTIR analysis---FTIR spectra of BF-graphite electrodes and electrodes extracted from cells cycled with different salt/EC electrolytes are depicted in Figure 5-4. In this work, the fresh graphite powder used contains a strong peak 866 fresh cm^{-1} and shows

up at all spectra. Absorptions characteristic of lithium ethylene dicarbonate (LEDC) are observed at 832, 1043, 1185, 1303, 1413 and 1656 cm^{-1}, as previously reported, for electrodes cycled with $LiPF_6$, $LiBF_4$, LiTFSI and LiFSI electrolytes. In addition, absorptions are observed at 866 and 1420 cm^{-1} characteristic of Li_2CO_3. However, these peaks overlap with other absorptions consistent with a low concentration of Li_2CO_3 on electrode surface. However, the IR spectra of the electrodes cycled with LiBOB and LiDFOB electrolyte are dominated peak at 1620 and 1320 cm^{-1} of lithium oxalate or other oxalate containing species.[11] Another strong peak is observed at 1760-1800 cm^{-1} which is characteristic of alkyl carbonates, possibly from poly or oligo ethylene carbonate. Additional peaks characteristic of lower concentrations of LEDC are also present. The differences in surface species for electrodes cycled with LiBOB and LiDFOB are likely due to the decomposition of the oxalate groups on boron.

NMR multinuclear analysis of BF-graphite electrodes extracted with D_2O

In order to further characterize the structure of the SEI formed from different lithium salts on BF-graphite anodes after the first cycle, ^{1}H, ^{13}C, ^{19}F NMR spectroscopy of D_2O extracts of the BF-graphite electrodes has been conducted. The ^{1}H NMR spectra are provided in Figure 5-5. The ^{1}H NMR spectra of all of the D_2O extracts contain a single peak at 3.51 ppm (s) consistent with the presence of lithium ethylene dicarbonate (LEDC) (Figure 5a)[12]. However, the spectra of the D_2O extracts of electrodes cycled with LiBOB and LiFOB electrolytes contain a second singlet at 3.63 ppm with slightly lower intensity. In order to additional structural, ^{13}C spectra were acquired. All of the electrodes which contain LEDC have two ^{13}C peaks at 62.5

and 160.5 ppm characteristic of LEDC[12]. The ^{1}H spectrum of the D_2O extract of the electrode cycled with LiBOB electrolyte contains a strong resonance at 172.9 ppm characteristic of $Li_2C_2O_4$. There are three other additional ^{13}C resonances which are easily describable at 55.2, 174.2, and 176.5 ppm consistent with the presence of additional C=O and C-O containing species, although other resonances with intensity comparable to the noise may be observable in the C=O region (160 - 180 ppm). Due to the NOE enhancement of the C-O peak due to the presence of C-H bonds, the peak at 55.2 ppm is most likely not correlated with either of observed C=O peaks at 174.2 or 176.5 ppm. However, another weaker intensity C=O peak may be present and correlated to the C-O peak at 55.2 ppm. Thus the two C=O peaks at 174.2 and 176.5 ppm are most likely oxalate derivatives of boron such as $FB(C_2O_4)$, $LiOB(C_2O_4)$ or related species while the peak at 55.2 ppm is a symmetrical $-CH_2O-$ species. The ^{13}C NMR spectrum of extract of the electrode cycled with LiDFOB electrolyte has similar peaks to those observed for the electrode cycled with LiBOB, but the concentrations are much lower.

The D_2O extractions of electrodes cycled with F-containing salts were also analyzed by ^{19}F NMR spectroscopy. All of the ^{19}F spectra contain a singlet at -123.0 ppm characteristic of LiF. A general trend in LiF concentration can be observed from the different signal to noise ratios of the different samples. The relative intensity of the LiF peak was greatest for the electrodes cycled with $LiBF_4$ and LiDFOB electrolyte while the intensity was lowest for electrodes cycled with LiTFSI, as expected due to the stability C-F bond.[13] In additional, residual salts were observed in the D_2O extracts of electrodes cycled with for all fluorinated salts except LiFSI. A

doublet is observed at -72.2 ppm, characteristic as residual $LiPF_6$ for electrodes cycled with $LiPF_6$ electrolyte while a singlet is observed at -80.2 ppm characteristic of LiTFSI for electrodes cycled with LiTFSI electrolyte. Interestingly, the D_2O extract of electrodes cycled with both $LiBF_4$ and LiDFOB have the same singlet at -150.5 ppm characteristic of $LiBF_4$ suggesting that LiDFOB undergoes a disporportionation reaction with $LiPF_6$ to generate $LiBF_4$. No other significant peaks were observed by ^{1}H, ^{13}C, ^{19}F NMR spectroscopy suggesting that LEDC and LiF are the primary components of the anode SEI generated with $LiPF_6$, $LiBF_4$, LiTFSI and LiFSI/EC electrolytes. However, a more complex SEI is generated with LiBOB and LiDFOB electrolytes which contains high concentrations of lithium oxalate, boron oxalates, and related species along with LEDC and LiF.

Summary and Conclusion

The effect of different lithium salts on the structure of the solid electrolyte interphase (SEI) on graphite anodes for lithium ion batteries has been investigated via a combination of electrochemical cycling, TEM, XPS, FTIR and NMR analysis, the change of the cycling behaviors resulted from the different electrochemical reactions. The first charging cycle has different electrochemical features for the different salts suggesting the generation of different species in the SEI. Electrolytes based on $LiPF_6$, $LiBF_4$, LiFSI, and LiTFSI have a similar shoulder at ~ 0.8 V, although the magnitude of the shoulder differs for different salts. Electrolytes containing LiBOB or LiDFOB have a shoulder at ~1.8 V consistent with the reduction of the oxalate ligand as previously reported. The surface analysis reveals thin SEI films on all electrodes (10 -50 nm). However, the films are smooth and uniform for electrodes cycled with $LiPF_6$,

LiBOB, LiTFSI and LiFSI, while the films are grainy for $LiBF_4$ and LiDFOB, due to the high LiF content. The composition of the electrode surface films also varies as a function of salt suggesting the the salt reduction products are an important component of the SEI. All of the SEIs contain LEDC, the reduction product of EC, and all of the SEI's except for the one generated from LiBOB contain LiF. However, the ratio of LEDC to LiF differs for the different salts. The concentration of LiF is highest for $LiBF_4$ and is comparable for $LiPF_6$, LiDFOB, LITFSI, and LiFSI. The higher concentration of LiF in the presence of $LiBF_4$ is likely related to the stronger association of BF_4^- to the lithium cation and more reductive decomposition of the anion. In addition, the electrodes cycled with LBOB and LIDFOB contain additional components related to the decomposition products of the oxalate species including lithium oxalates, boron oxalates, and some other uncharacterized species containing -CH_2O- fragments.

Reference

(1) Lucht B. L., Xiao.A; *J Electrochem Soc* **2009**, *156*, A318.

(2) Aravindan, V.; Gnanaraj, J.; Madhavi, S.; Liu, H.-K. *Chemistry – A European Journal* **2011**, *17*, 14326.

(3) Han, H.-B.; Zhou, S.-S.; Zhang, D.-J.; Feng, S.-W.; Li, L.-F.; Liu, K.; Feng, W.-F.; Nie, J.; Li, H.; Huang, X.-J.; Armand, M.; Zhou, Z.-B. *J. Power Sources* **2011**, *196*, 3623.

(4) Ishikawa, M.; Sugimoto, T.; Kikuta, M.; Ishiko, E.; Kono, M. *J. Power Sources* **2006**, *162*, 658.

(5) Xiao, A.; Yang, L.; Lucht, B. L.; Kang, S.-H.; Abraham, D. P. *Journal of the Electrochemical Society* **2009**, *156*, A318.

(6) Andersson, A. M.; Edström, K. *Journal of the Electrochemical Society* **2001**, *148*, A1100.

(7) Xu, K.; Lee, U.; Zhang, S.; Wood, M.; Jow, T. R. *Electrochem. Solid-State Lett.* **2003**, *6*, A144.

(8) Zhuang, G. V.; Xu, K.; Jow, T. R.; Ross, P. N. *Electrochem. Solid-State Lett.* **2004**, *7*, A224.

(9) Benoit, R.,Vide-Sci. Techn. Appl. 2003, 58 (308), 219-+.

(10) Nie, M.; Chalasani, D. ; Abraham, D. P.; Chen, Y.; Bose, A.; Lucht, B. L.,J.Phys.Chem.C 2013, 117 (3), 1257-1267.

(11) Shui Zhang, S. *Electrochemistry Communications* **2006**, *8*, 1423.

(12) Xu, K.; Zhuang, G. R. V.; Allen, J. L.; Lee, U.; Zhang, S. S.; Ross, P. N.; Jow, T. R. *J. Phys. Chem. B* 2006, *110*, 7708-7719.

(13) Ensling, D.; Stjerndahl,M.; Nyten,A.; Gustafsson, T.; and Thomas,J.O. *J. Mater. Chem.***2009,** *19,* 82-88.

(a)

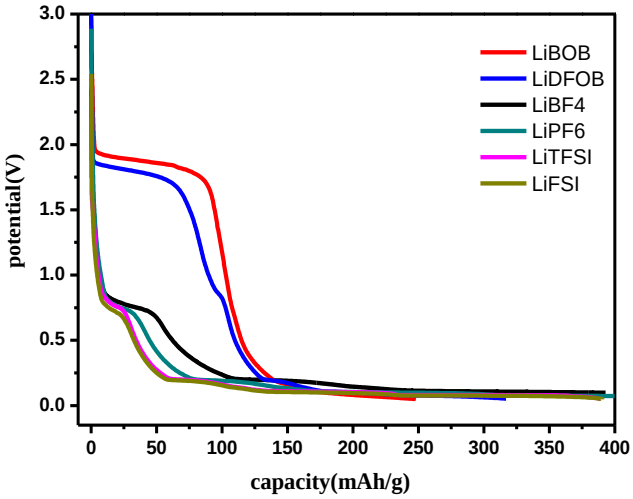

(b)

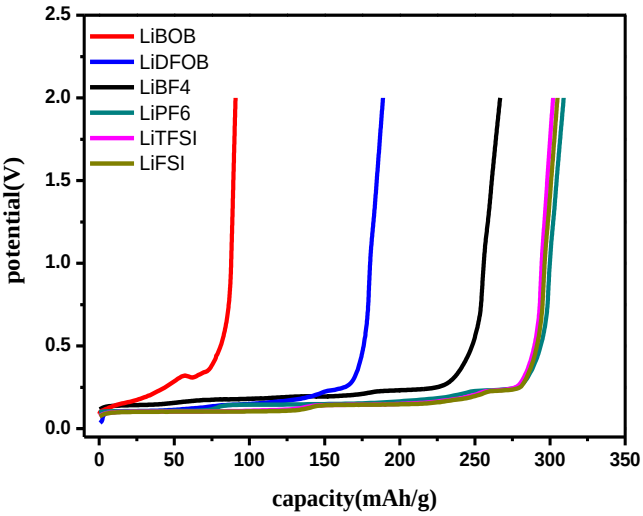

Figure 5-1. Potential vs. capacity curves for BF-graphite/Li cells cycled with six different lithium salts/EC electrolytes: 1M $LiPF_6$/EC, 1M $LiBF_4$/EC, 1M LiTFSI/EC, 1M LiFSI/EC, 1M LiBOB/EC and 1M LiDFOB/EC. (a) lithium intercalation profiles (b) lithium de-intercalation profiles.

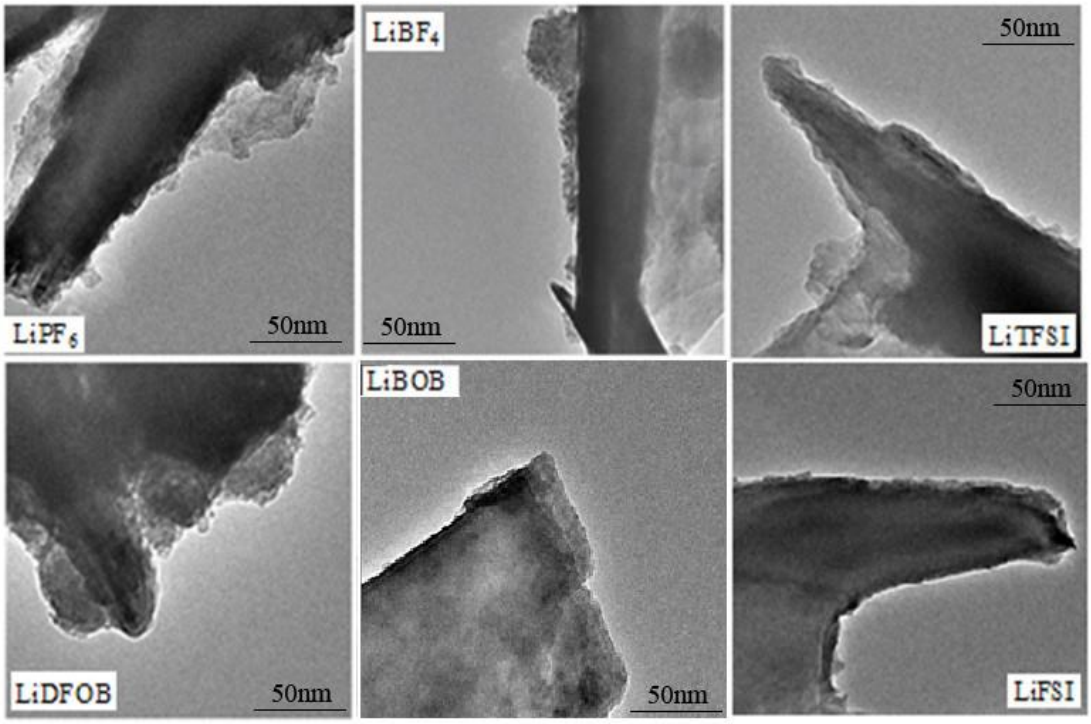

Figure 5-2. TEM images of graphite particles extracted from BF-graphite/Li cells cycled with six different lithium salts/EC electrolytes: 1M $LiPF_6$/EC, 1M $LiBF_4$/EC, 1M LiTFSI/EC, 1M LiFSI/EC, 1M LiBOB/EC and 1M LiDFOB/EC. LiFSI

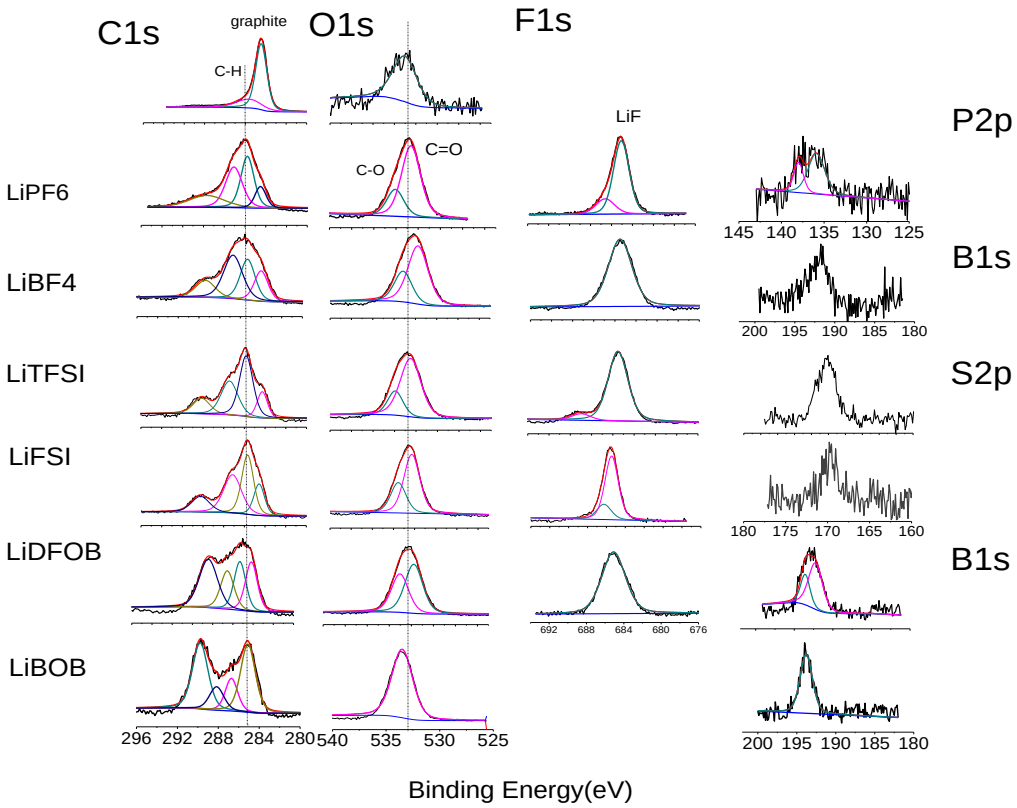

Figure 5-3. XPS spectra of BF-electrodes extracted from BF-graphite/Li cells cycled with six different lithium salts/EC electrolytes: 1M $LiPF_6$/EC, 1M $LiBF_4$/EC, 1M LiTFSI/EC, 1M LiFSI/EC, 1M LiBOB/EC and 1M LiDFOB/EC.

	LiPF6	LiBF4	LiDFOB	LiBOB	LiTFSI	LiFSI	Fresh
C	46.3	44.2	32.5	45.1	46.7	45.7	
O	26.8	22.7	31.4	48.2	29.2	29.6	
F	24.6	31.3	26.4	..	23.5	22.7	
B	..	1.9	9.7	6.7	..	..	
S	..	..	..	..	0.6	2.0	
P	2.2	..	..	..			

Table 5-1 Element percentage from BF-anodes cycled with six salts/EC electrolytes

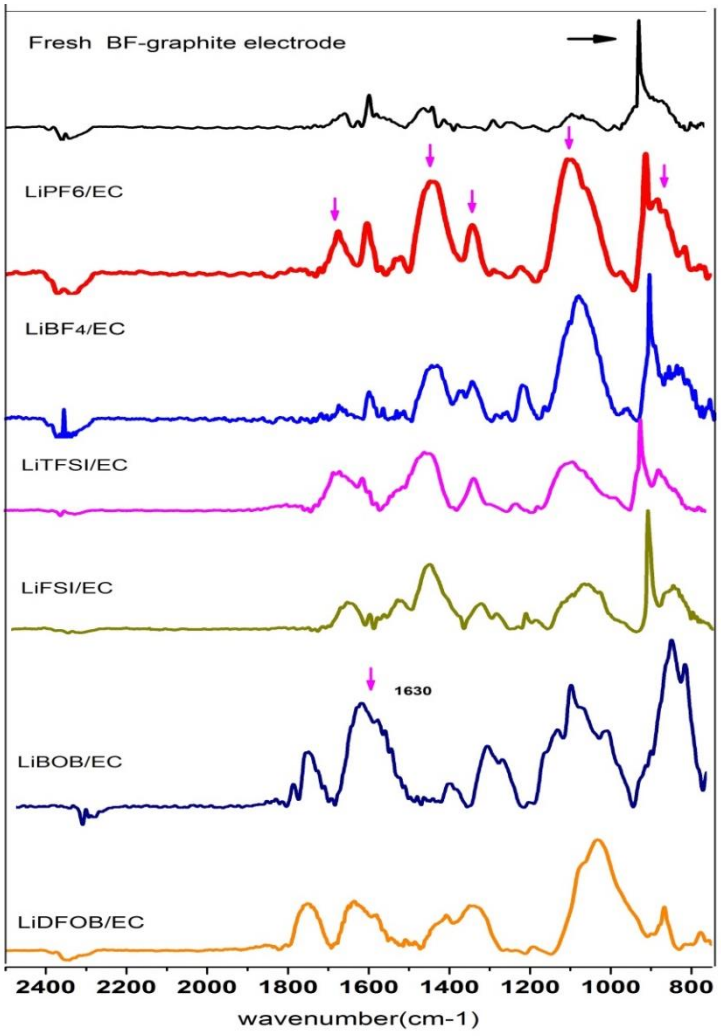

Figure 5-4. IR spectra of 1M various salts/EC cycled BF graphite anodes. Top spectrum is fresh graphite electrode

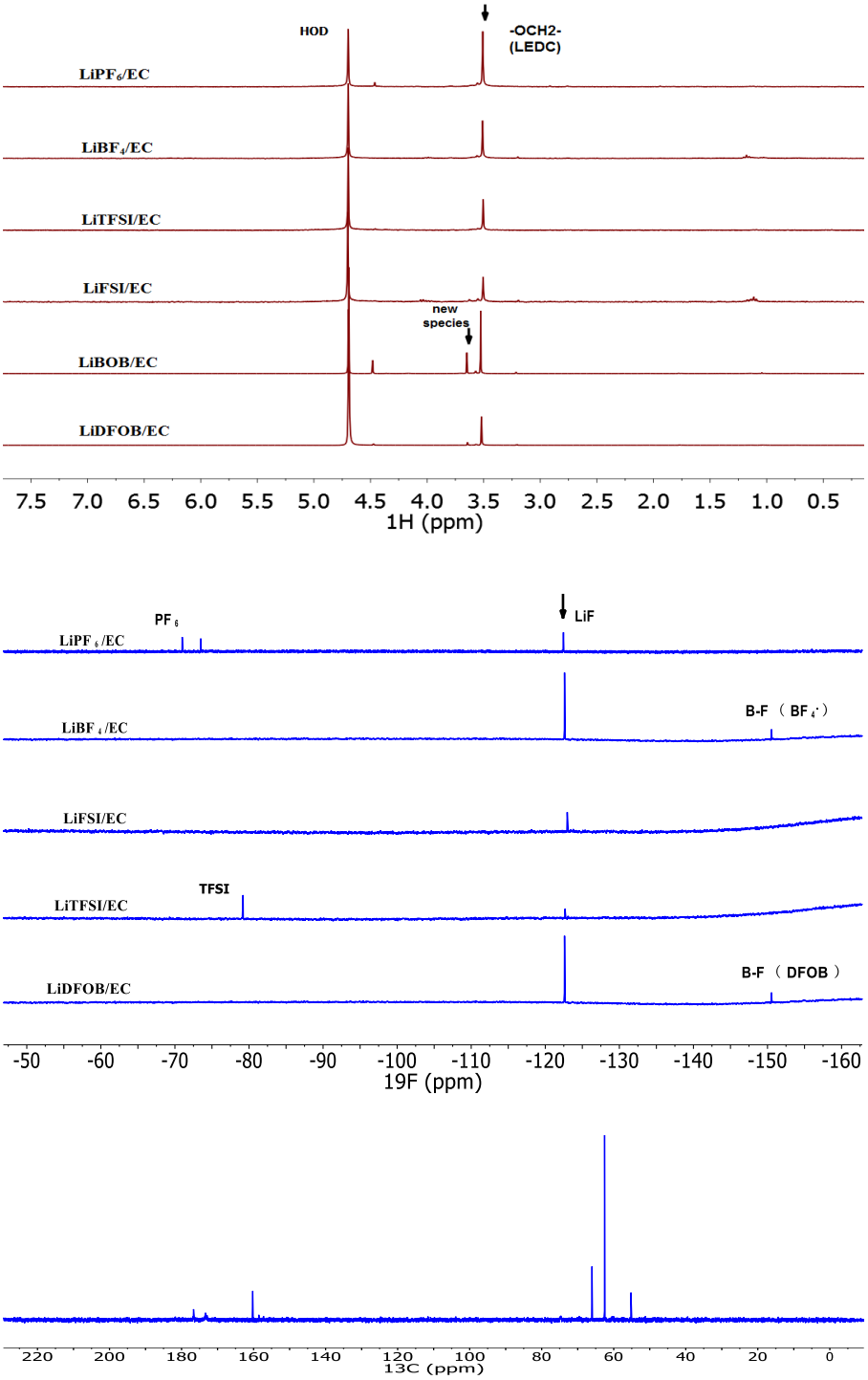

Figure 5-5. (a) ^{1}H NMR spectra, (b) ^{19}F NMR spectra of the D_2O extract of graphite anode cycled with various salts, and (c) ^{13}CNMR spectrum of 1 M LiBOB/EC cycled electrode.